ISSN 0915-6364

NATIONAL INSTITUTE FOR FUSION SCIENCE

Atomic Processes Relevant to Polarization Plasma Spectroscopy

T. Fujimoto, F. Koike, K. Sakimoto, R. Okasaka, K. Kawasaki,
K. Takiyama, T. Oda and T. Kato

(Received — Mar. 2, 1992)

NIFS-DATA-16 Apr. 1992

RESEARCH REPORT
NIFS-DATA Series

NAGOYA, JAPAN

Atomic Processes Relevant to Polarization Plasma Spectroscopy

T. Fujimoto[1], F. Koike[2], K. Sakimoto[3], R. Okasaka[1],
K. Kawasaki[4], K. Takiyama[5], T. Oda[5] and T. Kato

National Institute for Fusion Science, Nagoya 464-01, Japan

Permanent address

1) Department of Engineering Science, Faculty of Engineering, Kyoto University, Kyoto 606-01
2) School of Medicine, Kitasato University, Kitasato 1-15-1, Sagamihara, Kanagawa 228
3) The Institute of Space and Astronautical Science, Sagamihara, Kanagawa 229
4) Physics Department, Faculty of Education, Okayama University, Okayama 700
5) Department of Applied Physics and Chemistry, Faculty of Engineering, Hiroshima University, Higashihiroshima 724

Abstract

When atoms (ions) are excited anisotropically, polarized excited atoms are produced and the radiation emitted by these atoms is polarized. From the standpoint of plasma spectroscopy research, we review the existing data for various atomic processes that are related to the polarization phenomena. These processes are: electron impact excitation, excitation by atomic and ionic collisions, photoexcitation, radiative recombination and bremsstrahlung. Collisional and radiative relaxation processes of atomic polarization follow. Other topics included are: electric-field measurement, self alignment, Lyman doublet intensity ratio, and magnetic-field measurement of the solar prominence.

Key words

spectroscopy, diagnostics, collision, laser-induced-fluorescence spectroscopy, excitation, recombination, polarization, anisotropy, alignment, denstiy matrix, relaxation, magic angle, angular momentum, electric field, Hanle effect

Preface

As an attribute of light, polarization has been well known for a long time, almost as long as dispersion and diffraction. Reflection of light by a surface of water, scattering of the sun light by the atmosphere ----- the blue sky, transmission of light through calcite, and so on; all these create polarized light. However, until recently people working in the field of plasma tended to believe rather naively that the light was unpolarized and that the light intensity they observed was simply given by the famous Einstein relationship, i.e., the intensity is proportional to the upper-level population and the spontaneous transition probability. This situation is changing now.

Some years ago, one of the authors of this review began to feel the necessity of reviewing the present status of our knowledge about the atomic processes concerning polarization of light emitted from plasma and collecting the existing atomic data. He found several colleagues who found this project exciting and worth committing to. They agreed to organize a workshop under auspice of the Institute of Plasma Physics, Nagoya University. Since then several years have passed and their study has made some progress. During this period the Institute changed itself to become the National Institute for Fusion Science, but its support to this endeavor did not change.

At this point we have decided to publish this review because we felt that our efforts on the subject matter have matured to a certain level. We hope this review finds many interested researchers and contributes to a progress of plasma spectroscopy expanding into a new area.

In future, we may have a chance to amend this review; apart from revisions of the present version we would include: magnetic-dipole and electric-quadrupole transitions, multiphoton excitation, Zeeman and Stark effects, Faraday rotation, polarized atoms under electric or magnetic field, and Rayleigh scattering.

Summer, 1991

CONTENTS

List of Authors

II. F. Koike

III. K. Sakimoto

IV. F. Koike, R. Okasaka

V. T. Fujimoto

VI. T. Fujimoto, K. Sakimoto

VII. T. Fujimoto

VIII.

1. K. Kawasaki, K. Takiyama, T. Oda
2. T. Fujimoto
3. T. Fujimoto
4. T. Kato

I. INTRODUCTION

The importance of polarization of optical radiation is being recognized recently by workers in the field of plasma spectroscopy. This interest stems from the two factors; the first is that polarization of emission radiation and related phenomena are being observed more often in recent plasma spectroscopy experiment. This is due to the progress in techniques of producing and heating plasmas and also to the progress in diagnostics techniques, including those adopting the laser excitation. The second is, there appears to be a common understanding that the polarization phenomena would give us information about the finer details of the plasma. Thus the phenomena are considered to be a candidate for the subject of future plasma diagnostics. In fact, from the observation of the polarized components of the motional Stark split line, or from the circular polarization of the emission line, the local magnetic field has been determined in tokamak plasma. The anisotropic velocity distribution of electrons such as suprathermal electrons, the existence of electric and magnetic fields in the plasma, the interaction of the plasma with a particle beam; all these anisotropic or non-thermal properties of the plasma should be reflected in the polarization characteristics of radiation emitted by the plasma particles or even by the beam particles. By employing the laser-induced-fluorescence (LIFS or LIF) technique combined with the polarization analysis we may obtain various information on the plasma, e.g., the electron, ion, and atom densities and the local electric and magnetic fields. Thus, these prospects suggest that polarization plasma spectroscopy can be a promising new diagnostic technique. This volume is intended to review various atomic processes relevant to the polarization phenomena in plasma.

It is a well known fact that, when atoms (or ions; from now on we simply use the word 'atoms' to indicate the both.) are photo-excited by polarized light, fluorescence light is polarized. This is because these atoms have population imbalance among the magnetic sublevels in the upper-level. Whenever excitation is spatially ansiotropic, like the above example of photo-excitation, population imbalance is created in a group of atoms. Such atoms constitutes a class of atomic ensembles called the polarized atoms. The radiation emitted by these atoms is polarized and has a spatially anisotropic intensity distribution. In order to understand the polarization characteristics of the emitted radiation we have to understand how anisotropic excitation produces polarized atoms and how these atoms emit anisotropic radiation. Besides the photo-excitation, population imbalance can be created by collisional excitation and by recombination. In the following several chapters we discuss the present status of our knowledge about anisotropic collisional excitation, anisotropic radiative excitation and recombination. Unfortunately, these fields have been developed rather independently by different workers, and different standard descriptions have been establised. In our present review, we follow the standard practice according to each subject.

Chapter 2 outlines the framework in which polarized atoms produced by anisotropic collisions are described, and several standard descriptions are compared. Relationship is given between the excitation anisotropy and the polarization characteristics of the emission lines. Chapter 3 deals with the electron impact excitation; some general characteristics of the excitation anisotropy are given, and detailes follow; i.e., the threshold behavior, high energy limit, the principal quantum number dependence and so on. Chapter 4 is devoted to the ion and atom collisions. Excitation by the electron capture process and that by the direct excitation process are discussed. As an example, the case of neutral helium is given in detail. Chapter 5 describes the photo-excitation; the density matrix formalism is introduced and the polarization characteristics of the emission lines are given in a closed form. Chapter 6 deals with the recombination processes.

The population imbalance among the magnetic sublevels in the atomic ensemble may be destroyed in plasma. We call the decrease in the degree of the population imbalance relaxation. The relaxation is caused by atomic or electronic collisions, and by radiation reabsorption. These phenomena are reviewed in chapter 7.

Besides the phenomena introduced above there are several polarization phenomena which are, or will be in future, of interest in plasma spectroscopy. The last chapter is devoted to these subjects.

II. ANISOTROPIC EXCITATION BY ELECTRONIC AND ATOMIC COLLISIONS

2.1. Introduction

Polarization of the atomic excited states can be created, on one hand, through electron impact excitation of atoms (Heddle, 1989) and on the other hand, through electron- capture or direct-excitation processes in collisions of ions and atoms (Janev, 1985, Andersen, 1988). We could observe the polarizations of optical radiation in plasma when there exists any spatial anisotropy in the velocity distribution of the colliding electrons, ions or atoms. Furthermore, we can expect the polarization of the atomic excited states in active plasma diagnostics using particle beam injection. We could also observe the polarization, in this case, with respect to the injected particle beam axis in the optical radiation of the plasma or the injected beam particles. In the present chapter, we discuss general property of the atomic polarization effects which are common to both the electronic and ionic and atomic impact on ions and atoms. Both the subjects which are specific for the electron impact excitation or the heavy particle collisions are rendered to the discussions given in the following separate chapters.

2.2. Density matrix of the atomic excited states

The coherence and the anisotropy of the atomic sub- states are represented by the density matrix (Fano, 1957). The unnormalized density matrix $\rho^{\rm un}$ relevant to the present electron capture or direct excitation processes is defined by (Blum, 1981)

$$<J'\,M'\,|\rho^{\rm un}|\,JM> = <a^{(q)}_{J'M'}\,a^{(q)\,*}_{JM}>, \tag{2.1}$$

where $a^{(q)}_{JM}$ is the amplitude for the transition, J and M are the total angular momentum quantum number and its magnetic component of the excited atomic states, respectively, q denotes the set of extra quantum numbers which specifies the atomic excited state, the notation $*$ denotes the complex conjugation, and furthermore the set of braces $<$ and $>$ in the right hand side denotes the statistical average over the incoherent parameters of the collision system such as the impact parameter or the kinetic energy of the colliding particles. The density matrix describes completely the excited product ionic or atomic state. Its diagonal matrix elements $\sigma_{JM} \equiv <JM|\rho^{\rm un}|JM>$ describe the population of the sub-states of the product ions or atoms. And the sum over M of them, i.e., the trace of the density matrix $\rho^{\rm un}$:

$$\sigma_J \equiv \sum_M \sigma_{JM} = {\rm Tr}\rho^{\rm un} = \sum_M <JM|\rho^{\rm un}|JM> \tag{2.2}$$

gives the total population of the excited states with the quantum number J. For the particle impact excitation or electron-capture processes, the quantity σ_J can be the

corresponding scattering cross section, and σ_{JM} the scattering cross sections for the M - sublevel excitations. Sometimes, it happens that we need only the relative intensities of the optical radiation. In that case, it is convenient if the density matrix ρ is normalized to give $\mathrm{Tr}\rho = 1$. We can define the normalized density matrix ρ by

$$\rho \equiv \rho^{\mathrm{un}}/\mathrm{Tr}\rho^{\mathrm{un}} = \frac{\rho^{\mathrm{un}}}{\sigma_J} \tag{2.3}$$

for this purpose. According to the conventional terminology (Fano, 1957), the term "density matrix" with no further clarification indicates a **normalized** density matrix. We follow this convention throughout this chapter, and we use $\sigma_J\rho$ or $\rho\mathrm{Tr}\rho^{\mathrm{un}}$ when we refer to the unnormalized density matrix. But we must note here that not all the papers found in the literature obey this convention. For example, Blum calls his unnormalized density matrix simply a density matrix in one of his papers (Blum, 1981).

The difference in the populations between the different M-substates gives the anisotropy of the atomic system. By measuring the polarization of the radiation emitted from plasma, we could gain information about the anisotropy of the system (Berezhko, 1977). The off-diagonal elements of the density matrix ρ describe the coherence between different M-substates; we recognize the magnetic sublevels being coherently excited when and only when we have non-zero off-diagonal elements of ρ. For instance, the matrix elements $<JM'|\rho|JM>$ with $M' \neq M$ describe the coherence between the $|JM>$ and $|JM'>$ sub-levels of the product ions or atoms and they also are related to the polarization of emitted radiation. Furthermore, the matrix elements $<J'M'|\rho|JM>$ with $J' \neq J$ describe the coherence between the energetically split sub-states, and this coherence can be observed under certain circumstances as quantum beats (Sellin, 1979) in the optical radiation.

In the next section 2.3, we consider the general property of the polarization tensor and the related quantities. In section 2.4, we shall concentrate ourselves on the anisotropy between the magnetic sub-states. Considering the current status of the polarization plasma spectroscopy and diagnostics, we should study this quantity in detail on the highest priority.

2.3. Polarization tensor and polarization parameters

The anisotropy and the coherence of the magnetic sublevels are characterized by the polarization tensor, of which components $\pi_{\Lambda,\mu}(J',J)$ are given by (Ferguson, 1965)

$$\pi_{\Lambda,\mu}(J',J) = \sum_{M'M} (-1)^{J-M} C(J'J\Lambda;M',-M,\mu) <J'M'|\rho|JM>, \tag{2.4}$$

where $C(J'J\Lambda;M',-M,\mu)$ is the Clebsch-Gordan coefficient (Rose, 1957). The polarization tensor $\pi_{\Lambda,\mu}(J',J)$ is the same as the "state multipole" $<t(J',J)^+>_{KQ}$ with $K = \Lambda$ and $Q = -\mu$ used by Anderson et al (Andersen, 1988). And, if $J' = J$,

the polarization tensor $\pi_{\Lambda,\mu}(J',J)$ is also the same as the state multipole $<T(L)^{\dagger}_{KQ}>$ with $L = J$, $K = \Lambda$ and $Q = +\mu$ given by Blum (Blum, 1981). Note that he has used the upper case "T " in place of the Andersen et al's notation " t " in $<t(J,J)^{+}>_{KQ}$. And also note that the sign of the index Q has been reversed in Andersen et al's paper compared with the Q in Blum's paper, i. e., Blum's $<T(L)^{\dagger}_{KQ}>$ is equal to Andersen et al's $<t(J,J)^{+}>_{K,-Q}$. Furthermore, Andersen et al are using the upper case "T" to introduce the moments of the state multipoles. We follow the Andersen et al's notation to represent the the moments of the state multipoles, as found in the rest of this section.

As far as we are concerned with the emission of the dipole radiation of light, we need only the elements of the polarization tensor with $\Lambda = 0$, 1, 2 and $\mu = 0, \pm1, \pm2$ for the spectral analysis. For convenience we illustrate below the concrete forms of eq.(2.2) for several combinations of J, J', Λ and μ.

For $J' = J$, we have

$$\pi_{0,0}(J,J) = \frac{\sum_M <JM|\rho|JM>}{\sqrt{2J+1}} = \frac{1}{\sqrt{2J+1}}, \tag{2.5a}$$

$$\pi_{1,0}(J,J) = \frac{\sqrt{3}\sum_M M<JM|\rho|JM>}{\sqrt{J(J+1)(2J+1)}}, \tag{2.5b}$$

$$\pi_{1,1}(J,J) = -\frac{\sqrt{3}\sum_M \sqrt{(J+M+1)(J-M)}<J,M+1|\rho|JM>}{\sqrt{2J(J+1)(2J+1)}}, \tag{2.5c}$$

$$\pi_{1,-1}(J,J) = \frac{\sqrt{3}\sum_M \sqrt{(J-M+1)(J+M)}<J,M-1|\rho|JM>}{\sqrt{2J(J+1)(2J+1)}}, \tag{2.5d}$$

$$\pi_{2,0}(J,J) = -\frac{\sqrt{5}\sum_M [J(J+1)-3M^2]<JM|\rho|JM>}{\sqrt{J(J+1)(2J+1)(2J+3)(2J-1)}}, \tag{2.5e}$$

$$\pi_{2,1}(J,J) = -\frac{\sqrt{15}\sum_M (2M+1)\sqrt{(J+M+1)(J-M)}<J,M+1|\rho|JM>}{\sqrt{2J(J+1)(2J+1)(2J+3)(2J-1)}}, \tag{2.5f}$$

$$\pi_{2,-1}(J,J) = \frac{\sqrt{15}\sum_M (2M-1)\sqrt{(J-M+1)(J+M)}<J,M-1|\rho|JM>}{\sqrt{2J(J+1)(2J+1)(2J+3)(2J-1)}}, \tag{2.5g}$$

$$\pi_{2,2}(J,J) = \frac{\sqrt{15}\sum_M \sqrt{(J+M+1)(J+M+2)(J-M)(J-M-1)}\langle J,M+2|\rho|JM\rangle}{\sqrt{2J(J+1)(2J+1)(2J+3)(2J-1)}} \quad (2.5h)$$

and

$$\pi_{2,-2}(J,J) = \frac{\sqrt{15}\sum_M \sqrt{(J-M+1)(J-M+2)(J+M)(J+M-1)}\langle J,M-2|\rho|JM\rangle}{\sqrt{2J(J+1)(2J+1)(2J+3)(2J-1)}}. \quad (2.5i)$$

For $J' = J+1$, we have

$$\pi_{1,0}(J+1,J) = \frac{\sqrt{3}\sum_M \sqrt{(J+M+1)(J-M+1)}\langle J+1,M|\rho|JM\rangle}{\sqrt{(J+1)(2J+1)(2J+3)}}, \quad (2.5j)$$

$$\pi_{1,1}(J+1,J) = \frac{\sqrt{3}\sum_M \sqrt{(J+M+1)(J+M+2)}\langle J+1,M+1|\rho|JM\rangle}{\sqrt{2(J+1)(2J+1)(2J+3)}}, \quad (2.5k)$$

$$\pi_{1,-1}(J+1,J) = \frac{\sqrt{3}\sum_M \sqrt{(J-M+1)(J-M+2)}\langle J+1,M-1|\rho|JM\rangle}{\sqrt{2(J+1)(2J+1)(2J+3)}}, \quad (2.5l)$$

$$\pi_{2,0}(J+1,J) = \frac{\sqrt{15}\sum_M M\sqrt{(J+M+1)(J-M+1)}\langle J+1,M|\rho|JM\rangle}{\sqrt{J(J+1)(J+2)(2J+1)(2J+3)}}, \quad (2.5m)$$

$$\pi_{2,1}(J+1,J) = -\frac{\sqrt{5}\sum_M (J-2M)\sqrt{(J+M+1)(J+M+2)}\langle J+1,M+1|\rho|JM\rangle}{\sqrt{2J(J+1)(J+2)(2J+1)(2J+3)}}, \quad (2.5n)$$

$$\pi_{2,-1}(J+1,J) = \frac{\sqrt{5}\sum_M (J+2M)\sqrt{(J-M+1)(J-M+2)}\langle J+1,M-1|\rho|JM\rangle}{\sqrt{2J(J+1)(J+2)(2J+1)(2J+3)}}, \quad (2.5o)$$

$$\pi_{2,2}(J+1,J) = -\frac{\sqrt{5}\sum_M \sqrt{(J+M+1)(J+M+2)(J+M+3)(J-M)}\langle J+1,M+2|\rho|JM\rangle}{\sqrt{2J(J+1)(J+2)(2J+1)(2J+3)}} \quad (2.5p)$$

and

$$\pi_{2,-2}(J+1,J) = \frac{\sqrt{5}\sum_M \sqrt{(J-M+1)(J-M+2)(J-M+3)(J+M)}\langle J+1,M-2|\rho|JM\rangle}{\sqrt{2J(J+1)(J+2)(2J+1)(2J+3)}}. \quad (2.5q)$$

For $J' = J+2$, we have

$$\pi_{2,0}(J+2,J) = \frac{\sqrt{15}\sum_M \sqrt{(J+M+1)(J+M+2)(J-M+1)(J-M+2)}<J+2,M|\rho|JM>}{\sqrt{2(J+1)(J+2)(2J+1)(2J+3)(2J+5)}}, \tag{2.5r}$$

$$\pi_{2,1}(J+2,J) = \frac{\sqrt{5}\sum_M \sqrt{(J+M+1)(J+M+2)(J+M+3)(J-M+1)}<J+2,M+1|\rho|JM>}{\sqrt{(J+1)(J+2)(2J+1)(2J+3)(2J+5)}}, \tag{2.5s}$$

$$\pi_{2,-1}(J+2,J) = \frac{\sqrt{5}\sum_M \sqrt{(J-M+1)(J-M+2)(J-M+3)(J+M+1)}<J+2,M-1|\rho|JM>}{\sqrt{(J+1)(J+2)(2J+1)(2J+3)(2J+5)}}, \tag{2.5t}$$

$$\pi_{2,2}(J+2,J) = \frac{\sqrt{5}\sum_M \sqrt{(J+M+1)(J+M+2)(J+M+3)(J+M+4)}<J+2,M+2|\rho|JM>}{2\sqrt{(J+1)(J+2)(2J+1)(2J+3)(2J+5)}} \tag{2.5u}$$

and

$$\pi_{2,-2}(J+2,J) = \frac{\sqrt{5}\sum_M \sqrt{(J-M+1)(J-M+2)(J-M+3)(J-M+4)}<J+2,M-2|\rho|JM>}{2\sqrt{(J+1)(J+2)(2J+1)(2J+3)(2J+5)}}. \tag{2.5v}$$

And, further, to obtain the polarization tensors for the cases of $J' = J-1$, or $J' = J-2$, we can use the following relation that

$$\pi_{\Lambda,\mu}(J,J') = (-)^{J'-J}(-)^{\mu}\pi_{\Lambda,-\mu}(J',J)^*. \tag{2.5w}$$

The elements of the polarization tensor with $J' = J$, $\pi_{\Lambda,\mu}(J,J)$ has a relation to the moments of excited state multipole $<T(J)_{\Lambda\mu\pm}>$. They are real quantities and given by (Andersen, 1988)

$$<T(J)_{\Lambda 0}> = \frac{\pi_{\Lambda,0}(J,J)}{V^{(\Lambda)}(J)}, \tag{2.6a}$$

for $\mu > 0$,

$$<T(J)_{\Lambda\mu-}> = \frac{1}{2\mathrm{i}}\frac{\pi_{\Lambda\mu}(J,J)^* + (-)^{\mu}\pi_{\Lambda-\mu}(J,J)^*}{V^{(\Lambda)}(J)}, \tag{2.6b}$$

and

$$<T(J)_{\Lambda\mu+}> = \frac{1}{2}\frac{\pi_{\Lambda\mu}(J,J)^* - (-)^{\mu}\pi_{\Lambda-\mu}(J,J)^*}{V^{(\Lambda)}(J)}, \tag{2.6c}$$

with

$$V^{(\Lambda)}(J) = \frac{2^{\Lambda}(2\Lambda+1)^{1/2}}{\Lambda!}\left[\frac{(2J-\Lambda)!}{(2J+\Lambda+1)!}\right]^{\frac{1}{2}} \tag{2.6d}$$

$$= \begin{cases} \dfrac{1}{\sqrt{2J+1}} & \text{if } \Lambda = 0 \\ \dfrac{\sqrt{3}}{\sqrt{(2J+1)(J+1)J}} & \text{if } \Lambda = 1 \\ \dfrac{\sqrt{5}}{\sqrt{(2J+3)(2J+1)(2J-1)(J+1)J}} & \text{if } \Lambda = 2\ . \end{cases} \tag{2.6e}$$

For instance, the state multipole $<T(J)_{1,0}>$ represents the magnetic dipole moment of the excited atomic system, and $<T(J)_{2,0}>$ represents the electronic quadrupole moment. If we take J as the angular momentum operator and we take J_x, J_y and J_z as its x, y and z components, i. e., $\boldsymbol{J} = (J_x,J_y,J_z)$, we have a set of relations for the cases of $\Lambda \leq 2$ that

$$<T(J)_{00}> = 1, \tag{2.7a}$$

$$<T(J)_{10}> = <J_z>, \tag{2.7b}$$

$$<T(J)_{11-}> = <J_y>, \tag{2.7c}$$

$$<T(J)_{20}> = <3J_z^2-\boldsymbol{J}^2>, \tag{2.7d}$$

$$<T(J)_{21+}> = <\sqrt{3}(J_xJ_z+J_zJ_x)>, \tag{2.7e}$$

$$<T(J)_{22+}> = <\sqrt{3}(J_x^2-J_y^2)> \tag{2.7f}$$

and

$$<T(J)_{22-}> = <\sqrt{3}(J_xJ_z+J_yJ_z)>, \tag{2.7g}$$

where the set of braces $<$ and $>$ in the right hand side denotes the statistical average over the incoherent parameters of the collision system such as the impact parameter or the kinetic energy of the colliding particles.

Another example of the set of real polarization parameters is the Fano-Macek parameter (Fano, 1973). It consists of the orientation parameter O_{1-} and alignment parameters A_0, A_{1+}, and A_{2+}. It should be noted that the Fano-Macek parameters usually refer to the standard collision frame, and, in contrast to those, the definitions

of the multipole moments are independent of the choice of the coordinate system. By choosing a common quantization axis for both sets of the moments and parameters, say, by using the standard collision frame, we find the following relations.

$$O_{1-} = \frac{<J_y>}{J(J+1)} = \frac{<T(J)_{11-}>}{J(J+1)}, \tag{2.8a}$$

$$A_0 = \frac{<3J_z^2-J^2>}{J(J+1)} = \frac{<T(J)_{20}>}{J(J+1)}, \tag{2.8b}$$

$$A_{1+} = \frac{<J_xJ_z+J_zJ_x>}{J(J+1)} = \frac{<T(J)_{21+}>}{\sqrt{3}J(J+1)} \tag{2.8c}$$

and

$$A_{2+} = \frac{<J_x^2-J_y^2>}{J(J+1)} = \frac{<T(J)_{22+}>}{\sqrt{3}J(J+1)}. \tag{2.8d}$$

Furthermore, Berezhko and Kabachnik (Berezhko, 1980) have used the longitudinal alignment parameter $A_{2,0}$ defined by (Ferguson, 1965)

$$A_{2,0} = \frac{\pi_{2,0}(J,J)}{\pi_{0,0}(J,J)} \tag{2.9a}$$

$$= -\frac{\sqrt{5}\sum_M [J(J+1)-3M^2]<JM|\rho|JM>}{\sqrt{J(J+1)(2J+3)(2J-1)}} \tag{2.9b}$$

$$= -\frac{\sqrt{5J(J+1)}}{\sqrt{(2J+3)(2J-1)}} \frac{\sum_M (1-\frac{3M^2}{J(J+1)})\sigma_M}{\sum_M \sigma_M}. \tag{2.9c}$$

The relation to the Fano-Macek alignment parameter A_0 is given by

$$A_0 = -\frac{\sqrt{(2J+3)(2J-1)}}{\sqrt{5J(J+1)}} A_{2,0}. \tag{2.10}$$

The explicit expression of the Fano-Macek alignment parameter A_0 is then given by

$$A_0 = \frac{\sum_M (1-\frac{3M^2}{J(J+1)})\sigma_M}{\sum_M \sigma_M}. \tag{2.11}$$

As found in eqs. (2.9), (2.10) and (2.11), the geometrical factor $\frac{\sqrt{5J(J+1)}}{\sqrt{(2J+3)(2J-1)}}$ that appears in $A_{2,0}$, is absent in the Fano-Macek alignment parameter A_0 . Because of the simplicity of its expression, the parameter A_0 can be used conveniently for the analysis of experimental data. On the other hand, the parameter $A_{2,0}$ has a direct relation to the relevant elements of the polarization tensor, and, therefore, the use of $A_{2,0}$ is preferable when we study the anisotropic excitation in close relation to the theory.

The moments of the state multipoles $<T(J)_{\Lambda\mu\pm}>$ with $\Lambda\leq 2$ and so the corresponding alignment and orientation parameters can be determined by the polarization measurements of the optical radiation of the excited atomic states. The polarization of the optical radiation is characterized by a set of three parameters η_1, η_2, and η_3, which are called the Stokes parameters. We take I_{45} and I_{135} as the intensities of the linearly polarized emission of the optical radiation respectively at 45° and 135° with respect to the direction of the polarization vector e_1 , which is set arbitrarily on the plane perpendicular to the direction of the photon propagation. We have

$$\eta_1 = \frac{I_{45} - I_{135}}{I_{45} + I_{135}}. \tag{2.12a}$$

We take I_{RHC} and I_{LHC} as the intensities of the right handed and left handed polarized emission of the optical radiation with respect to the direction of the photon propagation, and we have

$$\eta_2 = \frac{I_{\mathrm{RHC}} - I_{\mathrm{LHC}}}{I_{\mathrm{RHC}} + I_{\mathrm{LHC}}}. \tag{2.12b}$$

And, further, we take I_0 and I_{90} as the intensity of the linearly polarized emission of the optical radiation parallel and perpendicular to the polarization vector e_1 , respectively. We have

$$\eta_3 = \frac{I_0 - I_{90}}{I_0 + I_{90}}. \tag{2.12c}$$

We have, of course, a relation that

$$I \equiv I_{45} + I_{135} = I_{\mathrm{RHC}} + I_{\mathrm{LHC}} = I_0 + I_{90}, \tag{2.12d}$$

where I is the intensity for the optical measurement with no polarizer in front of the photon detector. And I is also a Stokes parameter. According to Blum (Blum, 1981), the Stokes parameters for the optical radiation emitted into the direction with the polar angle θ and its azimuth angle ϕ are given by

$$I = \frac{2}{3}G_0 V^{(0)}(J)<T(J)_{0,0}> + G_1 V^{(2)}(J)[<T(J)_{2,2+}>\sin^2\theta\cos 2\phi$$

$$- <T(J)_{2,1+}>\sin 2\theta\cos\phi + \frac{1}{\sqrt{6}}<T(J)_{2,0}>(3\cos^2\theta - 1)], \tag{2.13a}$$

$$I\eta_1 = G_1 V^{(2)}(J)[<T(J)_{2,2+}>2\cos\theta\sin 2\phi - <T(J)_{2,1+}>2\sin\theta\sin\phi], \tag{2.13b}$$

$$I\eta_2 = 2G_2 V^{(1)}(J)<T(J)_{1,1-}>\sin\theta\cos\phi \tag{2.13c}$$

and

$$I\eta_3 = G_1 V^{(2)}(J)[<T(J)_{2,2+}>(1+\cos^2\theta)\cos 2\phi$$

$$- <T(J)_{2,1+}>\sin 2\theta\cos\phi + \frac{\sqrt{3}}{\sqrt{2}}<T(J)_{2,0}>\sin^2\theta], \tag{2.13d}$$

with

$$G_0 = \sigma_J \frac{1}{\gamma}\frac{e^2 w^4 d\Omega}{2\pi c^3 \hbar}|<J_f||r||J>|^2, \tag{2.13e}$$

where γ is the decay constant, $d\Omega$ denotes the element of solid angle into which the photons are emitted, and $<J_f||r||J>$ is the contracted matrix elements for the dipole transition, and with

$$G_1 = G_0(-)^{J_f - J} W(J,J,1,1;2,J_f)$$

$$= -G_0 \frac{[3(J(J+1) - J_f(J_f+1)]^2 + J(J+1) - 9J_f(J_f+1) + 6)}{2\sqrt{30J(J+1)(2J+1)(2J+3)(2J-1)}} \tag{2.13f}$$

and

$$G_2 = G_0(-)^{J_f - J} W(J,J,1,1;1,J_f)$$

$$= G_0 \frac{J(J+1) - J_f(J_f+1) + 2}{2\sqrt{6J(J+1)(2J+1)}}, \tag{2.13g}$$

where $W(abcd;ef)$ is the Racah coefficient (Rose, 1957).

In the case that $J = 1$ and $J_f = 0$ and the effect of the electronic as well as nuclear spins can be neglected, i.e., in the cases of the optical radiation due to the ${}^1P \rightarrow {}^1S$ or ${}^3P \rightarrow {}^3S$ transitions of the atoms with no hyperfine splittings, the situation becomes simple. The optical radiation field is completely determined by a measurement of three parameters σ_1 , I and η_2 . This set of parameters is related to a conventionally used set of parameters (Kleinpoppen, 1980) σ_1 ,

$$\lambda = |<1,1|\rho|1,0>|^2 = \frac{\sigma_{1,1}}{\sigma_1}, \tag{2.14a}$$

and

$$\chi = \arg\left[\frac{<1,1|\rho|1,0>}{<1,0|\rho|1,0>}\right], \tag{2.14b}$$

where arg indicates to take the argument of the given complex value. We have

$$I = G_0\frac{1}{3}[\frac{1-\lambda}{2}(1-\sin^2\theta\cos 2\phi+\cos^2\theta)+\lambda\sin^2\theta$$

$$+\sqrt{\lambda(1-\lambda)}\cos\chi\sin^2\theta\cos\phi], \tag{2.15a}$$

$$I\eta_2 = G_2\frac{2}{3}\sqrt{\lambda(1-\lambda)}\sin\chi\sin\theta\sin\phi. \tag{2.15b}$$

The number of the independent moments of the state multipoles is two in this case, and they are given by the parameters λ and χ as in the following way.

$$<T(1)_{1,1-}> = -\sqrt{2}\sqrt{\lambda(1-\lambda)}\sin\chi, \tag{2.16a}$$

$$<T(1)_{2,2+}> = \frac{\sqrt{3}}{\sqrt{2}}(\lambda-1), \tag{2.16b}$$

$$<T(1)_{2,1+}> = -\sqrt{6}\sqrt{\lambda(1-\lambda)}\cos\chi \tag{2.16c}$$

and

$$<T(1)_{2,0}> = (1-3\lambda). \tag{2.16d}$$

2.4. Longitudinal alignment parameter

In view of the current status of the plasma diagnostics, it should be natural that we expect the presence of an axial symmetry within an enough small volume in the plasma. Consider the slight break down of the isotropy of any plasma. It will start along a direction determined by the external condition around the plasma, and this direction gives the symmetry axis. Therefore, it is worthwhile to study the axially symmetric plasma at high priority. From now on, we consider only this case and we always take the axial-symmetry axis as the axis of quantization of the system.

The axial symmetry can be classified according to the invariance property with respect to the inversion of the symmetry axis. When the system is invariant under inversion of the $z-$axis , we have a relation that (Blum, 1981)

$$<J',M'|\rho|J,M> = (-)^{M'+M}<J',-M'|\rho|J,-M> \tag{2.17}$$

for the elements of the density matrix. Consequently, we have a relation that

$$\pi_{\Lambda,\mu}(J',J) = (-)^{J'+J+\Lambda}(-)^{\mu}\pi_{\Lambda,-\mu}(J',J) \tag{2.18}$$

for the elements of the polarization tensor.

In this case, all the Fano-Macek parameters in eq.(2.8) vanish except the longitudinal alignment parameter A_0. And also, all the moments of the state multipoles in eq.(2.13) vanish except $<T(J)_{0,0}>$ and $<T(J)_{2,0}>$. From eq.(2.13), we can obtain the intensity of the optical radiation into the direction θ ; that is

$$I(\theta) = \frac{2}{3}G_0V^{(0)}(J)<T(J)_{0,0}>+\frac{1}{\sqrt{6}}G_1V^{(2)}(J)<T(J)_{2,0}>(3\cos^2\theta-1). \tag{2.19a}$$

With the aid of eqs.(2.7), (2.9), (2.10), and (2.11), we further obtain

$$I(\theta) = \frac{2}{3}G_0V^{(0)}(J)\left[1+\alpha_2\frac{V^{(2)}(J)<T(J)_{2,0}>}{V^{(0)}(J)<T(J)_{0,0}>}\mathrm{P}_2(\cos\theta)\right] \tag{2.19b}$$

with

$$\alpha_2 = (-)^{J_f-J}\frac{\sqrt{3(2J+1)}}{\sqrt{2}}W(J,J,1,1;2,J_f)$$

$$= -\frac{3[J(J+1)-J_f(J_f+1)]^2+J(J+1)-9J_f(J_f+1)+6}{4\sqrt{5J(J+1)(2J+3)(2J-1)}}, \tag{2.19c}$$

where $\mathrm{P}_2(\cos\theta)$ is the 2'nd order Legendre polynomial. We recall eqs.(2.6a) and (2.9a). Then, we have $A_{2,0} = \dfrac{V^{(2)}(J)<T(J)_{2,0}>}{V^{(0)}(J)<T(J)_{0,0}>}$. And, we define the relative intensity of the optical radiation to the direction θ by

$$I_{\mathrm{rel}}(\theta) = \frac{I(\theta)}{4\pi\frac{2}{3}G_0V^{(0)}(J)}, \tag{2.20}$$

we obtain

$$I_{\mathrm{rel}}(\theta) = \frac{1}{4\pi}[1+\alpha_2A_{2,0}\mathrm{P}_2(\cos\theta)] \tag{2.21}$$

For the intensity of the linear polarization degree, $I\eta_3$, at angle θ , we similarly obtain

$$I(\theta)\eta_3(\theta) = \frac{2}{3}G_0V^{(0)}(J)\alpha_2A_{2,0}[1-\mathrm{P}_2(\cos\theta)]. \tag{2.22}$$

And, further, with the aid of eq.(2.19), we obtain

$$\eta_3(\theta) = \frac{\alpha_2 A_{2,0}[1 - \mathrm{P}_2(\cos\theta)]}{1 + \alpha_2 A_{2,0}\mathrm{P}_2(\cos\theta)}. \tag{2.23}$$

For example, at an angle perpendicular to the symmetry axis, we have

$$\eta_3(\frac{\pi}{2}) = \frac{3\alpha_2 A_{2,0}}{\alpha_2 A_{2,0} - 2}. \tag{2.24}$$

And the light emitted parallel to the symmetry axis is always unpolarized.

As seen in eqs.(2.21) and (2.23), we can determine the longitudinal alignment parameter $A_{2,0}$, or, equivalently the parameters A_0 or $<T(J)_{2,0}>$ by measuring either the relative angular-distribution of the optical radiation, $I_{\mathrm{rel}}(\theta)$, or the degree of polarization along the polarization axis included in the plane determined by the symmetry axis of the plasma and the position of the photon detector, $\eta_3(\theta)$. And, inversely, if we know the longitudinal alignment parameter $A_{2,0}$, we can predict both $I_{\mathrm{rel}}(\theta)$ and $\eta_3(\theta)$. The actual values of the longitudinal alignment parameter and other elements of the polarization tensor are determined by the dynamics of the atomic excitation processes. The polarization phenomena in electron scattering and heavy particle collisions will be discussed separately in the following two chapters.

References

Andersen,.

Andersen, N., Gallagher, J. W., and Hertel, I. V., "Collisional alignment and orientation of atomic outer shells I. Direct excitation by electron and atom impact," *Phys. Rep.*, vol. 165, pp. 1-188, 1988.

Berezhko,.

Berezhko, E. G. and Kabachnik, N. M., *J. Phys. B*, vol. 10, p. 2467, 1977.

Berezhko,.

Berezhko, E. G. and Kabachnik, N. M., "Alignment of hydrogenlike atoms produced by electron capture in collisions of heavy charged particles with target atoms," *Sov. Phys. JETP*, vol. 52, pp. 205-211, AIP, 1980.

Blum,.

Blum, K., *Density matrix theory and applications,* Plenum Press, New York, 1981.

Fano,.

Fano, U., "Description of states in quantum mechanics by density matrix and operator techniques," *Rev. Mod. Phys.*, vol. 29, pp. 74-93, 1957.

Fano,.

Fano, U. and Macek, J. H., "Impact excitation and polarization of the emitted

light," *Rev. Mod. Phys.*, vol. 45, pp. 553-573, 1973.

Ferguson,.

Ferguson, A., *Angular correlation methods in gamma ray spectroscopy,* North Holland, Amsterdam, 1965.

Heddle,.

Heddle, D. W. O. and Gallagher, J. W., "Measurements of electron impact optical excitation functions," *Rev. mod. Phys.*, vol. 61, p. 221, 1989.

Janev,.

Janev, R. K. and Winter, Hanspeter, "State-selective electron capture in atom-highly charged ion collisions," *Phys. Rep.*, vol. 117, pp. 265-387, 1985.

Kleinpoppen,.

Kleinpoppen, H. and McGregor, I., "New aspects in electron-photon coincidence experiments," *Coherence and correlation in atomic collisions*, vol. H. Kleinpoppen and J. F. Williams Ed., p. 102, Plenum Press, New York, and London, 1980.

Rose,.

Rose, M. E., *Elementary theory of angular momentum,* John Wiley & Sons, Inc., New York, 1957.

Sellin,.

Sellin, I. A., Liljeby, L., Mannervik, S., and Hultberg, S., "Observation of mixed-parity electric-dipole oscillations in charge transfer to the n=2 hydrogen levels by fast protons in gases," *Phys. Rev. Lett.*, vol. 42, pp. 570-573, 1979.

III. ELECTRON SCATTERING

3.1. Introduction

Electron scattering plays an important role in the production of excited states of atoms (or ions) in plasmas. Measurements of the intensity of a spectral line emitted from excited atoms are a useful tool in plasma diagnostics. If the velocity distribution of electrons is spatially anisotropic, the electron scattering can cause unequal populations in the magnetic sublevels within the excited atomic state. The spectral line emitted from this atomic ensemble is in general polarized. Information on the anisotropic velocity distribution of the electrons may be obtained from the polarization properties of the spectral lines. Anisotropy of the velocity distribution is sometimes caused by an electric or magnetic field in the plasma. In these cases, the observation of the line polarization can provide us with information on the electric or magnetic field.

There is a large body of reports concerning the collisional alignment and orientation of atomic states. Most of the recent experimental studies are based on the coincidence measurements of the scattered electrons and the photons emitted from the excited atoms. The aim of this class of measurements is to obtain the basic collision parameters such as the scattering amplitudes. These investigations have made an important contribution to modern atomic physics. However, the results obtained in these experiments are not directly relevant to plasma diagnostics. This is because only the quantities averaged over all electron scattering angles are necessary for the latter purposes. Therefore, we skip the details of the electron-photon coincidence studies. For readers who are interested in this topic, see the review articles written by Kleinpoppen and Scharmann (1978), Blum and Kleinpoppen (1979), Slevin (1984), Crowe (1987), Andersen *et al.* (1988), Bartschat and Burke (1988), and Slevin and Chwirot (1990).

Experimental studies of the polarization properties averaged over all electron scattering angles were first made in 1920's. Since then, many measurements have been done, and the topic is becoming rather classical. In most studies, the polarization properties are obtained by measuring the intensities of emitted photons that are polarized parallel and perpendicular to the direction of the incident electron beam or by measuring the photon angular distribution. The review articles which include this field are: Moiseiwitsch and Smith (1968), Heddle and Keesing (1968), Kleinpoppen (1969), Fano and Macek (1973), Kleinpoppen and Scharmann (1978), Heddle (1979), and Heddle and Gallagher (1989).

In this chapter, we summarize the studies of the photon polarization in the electron beam scattering. Only the direction of the incident electron beam is specified; hence, the cylindrical symmetry is assumed with reference to the electron beam. The present review is not intended to be complete. Rather, for the sake of simplicity, we assume that the ground state of the atom has no orbital angular momentum. In the last part of this chapter, we present a comprehensive list of references in this field. Short comments are added for reader's convenience.

3.2. Polarization and excitation cross sections

We choose the z axis along the electron beam, and consider the emission due to the electric dipole moment. We denote the intensity of the emission in the direction perpendicular to the z axis, polarized parallel and perpendicular to the z axis by $I_{\parallel}(\frac{\pi}{2})$ and $I_{\perp}(\frac{\pi}{2})$, respectively. The degree of polarization is defined by

$$P = \frac{I_{\parallel}(\frac{\pi}{2}) - I_{\perp}(\frac{\pi}{2})}{I_{\parallel}(\frac{\pi}{2}) + I_{\perp}(\frac{\pi}{2})}. \tag{3.1}$$

This quantity can take a value between -1 and 1. (Sometimes it is given in units of %.) The emission intensity in a direction making an angle θ with the z axis is closely related to the degree of polarization in the form

$$I(\theta) = \bar{I}\,\frac{3(1 - P\cos^2\theta)}{3 - P}, \tag{3.2}$$

where $4\pi\bar{I}$ is the total intensity resulting from integrating $I(\theta)$ over all directions. The angular dependence of the degree of polarization (*i.e.*, the Stokes parameter η_3) is given by

$$\eta_3(\theta) = \frac{P\sin^2\theta}{1 - P\cos^2\theta}. \tag{3.3}$$

The longitudinal alignment is also an important parameter in discussing the unequal population in the atomic sublevels. This quantity is defined by (Fano and Macek 1973)

$$A_0^{\rm col} = \frac{I_{\parallel}(\frac{\pi}{2}) - I_{\perp}(\frac{\pi}{2})}{I_{\parallel}(\frac{\pi}{2}) + 2I_{\perp}(\frac{\pi}{2})}.$$

If we know the population in the magnetic sublevels of the excited state, the intensities $I_{\parallel}$ and $I_{\perp}$ can be obtained straightforwardly. In the collision experiment with absence of secondary collisions or external fields, the population is proportional to the excitation cross section. Hence we have, as an example, for excitation to 2^1P from the ground state (1^1S) of helium

$$I_{\parallel}(\tfrac{\pi}{2}) \propto A_0^{\pi} Q_0, \qquad I_{\perp}(\tfrac{\pi}{2}) \propto \frac{1}{2}\,(A_{-1}^{\sigma} Q_{-1} + A_1^{\sigma} Q_1) = A_1^{\sigma} Q_1, \tag{3.4}$$

where A_m^{π} and A_m^{σ} are the photon emission probability from the magnetic sublevel m of the 2^1P state for the π and σ transitions, respectively, and Q_m is the cross section for excitation to the magnetic sublevel m of the 2^1P state. (Because of the cylindrical symmetry, we have $Q_m = Q_{-m}$.) Thus, the degree of polarization can be expressed in terms of the excitation cross section, *i.e.*,

$$P = \frac{Q_0 - Q_1}{Q_0 + Q_1}. \tag{3.5}$$

Generally, we must take the fine structure (fs) and the hyperfine structure (hfs) into account. The theory including these effects was first developed by Penney (1932).

However, this theory is not accurate when the fs or hfs separations are comparable to a line width due to a finite lifetime of the excited state for emitting a photon (natural line width). Later, Percival and Seaton (1958) refined the theory by allowing for a finite natural line width to the excited state.

3.2.1. Case: natural line widths are much smaller than fs or hfs separations.

When there is no overlapping between the fs or hfs levels owing to a small natural line width, the Penney's theory can be applied. The details are summarized in the paper of Percival and Seaton (1958). First, we examine the case that there is no nuclear spin. When the spin-orbit interaction is weak, we can assume the LS coupling scheme to express the atomic state. (Breakdown of the LS coupling scheme is examined in section 3.6.) we denote the collisionally excited state by "SLJ" (the spin, orbital, and total angular momentum, respectively) and the final state reached by emission of a photon by "J''" (the total angular momentum). Then, we have for the degree of polarization

$$P = \frac{3K_z - K}{K_z + K}, \tag{3.6}$$

with

$$K_z(SLJ \rightarrow J'') = \frac{1}{2S+1} \sum_{M_S M_L M_J} \left[C(SLJ; M_S M_L M_J) C(J''1J; M_J 0 M_J)\right]^2 Q_{M_L}, \tag{3.7}$$

$$K(SLJ \rightarrow J'') = \frac{2J+1}{(2S+1)(2L+1)} \sum_{M_L} Q_{M_L}, \tag{3.8}$$

where $C(abc;def)$ is the Clebsch-Gordan coefficient, and Q_{M_L} is the cross section for excitation to the SLM_L state (summed over the spin magnetic quantum number M_S). Since there is no preferred spin direction, we have

$$Q(SLM_S M_L) = \frac{1}{2S+1} Q_{M_L}.$$

If the energy resolution of the observed photon is not sufficient to resolve the fs levels, the degree of polarization should be expressed in terms of the multiplet $SL \rightarrow SL''$. The quantities K_z and K in eq.(3.6) are then given by, respectively

$$K_z(SL \rightarrow SL'') = \frac{2L+1}{2S+1}$$

$$\times \sum_{JJ'' M_S M_L M_J} (2J''+1)\left[C(SLJ; M_S M_L M_J) C(J''1J; M_J 0 M_J) W(LJL''J''; S1)\right]^2 Q_{M_L}, \tag{3.9}$$

$$K(SL \rightarrow SL'') = \sum_{M_L} Q_{M_L}, \tag{3.10}$$

where $W(abcd;ef)$ is the Racah coefficient.

Table 3.1. Values of G, h_0, h_1, and h_2 in eqs.(3.11) and (3.12) for $SLJ \rightarrow J''$ without hfs (Percival and Seaton 1958)

SLJ	J''	G	h_0	h_1	h_2
011	0	1	1	1	—
	1	–1	1	3	—
	2	1	7	13	—
022	1	3	5	9	6
	2	–3	3	7	10
	3	3	15	29	26
110	1	0	—	—	—
111	0	–1	1	3	—
	1	1	3	5	—
	2	–1	13	27	—
112	1	21	47	73	—
	2	–7	11	29	—
	3	1	7	13	—
121	0	3	5	9	6
	1	–3	7	15	18
	2	3	41	81	78
122	1	3	9	17	14
	2	–3	7	15	18
	3	3	29	57	54
123	2	18	41	76	58
	3	–9	11	25	34
	4	3	15	29	26

Table 3.2. Values of G, h_0, h_1, and h_2 in eqs.(3.11) and (3.12) for $SL \rightarrow SL''$ without hfs (Percival and Seaton, 1958)

SL	L''	G	h_0	h_1	h_2
01	0	1	1	1	—
	2	1	7	13	—
02	1	3	5	9	6
	3	3	15	29	26
11	0	15	41	67	—
	2	3	73	143	—
12	1	213	671	1271	1058
	3	213	2171	4271	4058

In a particular case of S to be 0 or 1 (corresponding to a helium atom for example), the degree of polarization takes the form for the P states (L=1)

$$P = \frac{G(Q_0 - Q_1)}{h_0 Q_0 + h_1 Q_1}, \tag{3.11}$$

while for the D states (L=2)

$$P = \frac{G(Q_0 + Q_1 - 2Q_2)}{h_0 Q_0 + h_1 Q_1 + h_2 Q_2}. \tag{3.12}$$

The degree of polarization is always zero if the upper level is in the S states (L=0). Percival and Seaton (1958) calculated the coefficients G, h_0, h_1, and h_2. These values are tabulated in tables 3.1 and 3.2.

Also for the $^2P_J \rightarrow {}^2S$, $^2P \rightarrow {}^2S$ transitions including hfs, the degree of polarization is given in the same form (3.11). The coefficients G, h_0, and h_1 are presented in tables 3.3 and 3.4 for each nuclear spin I. For all cases, the degree of polarization of the $^2P_{\frac{1}{2}} \rightarrow {}^2S$ transition is zero.

Table 3.3. Values of G, h_0, h_1, and h_2 in eq.(3.11) for $^2P_{\frac{3}{2}} \rightarrow {}^2S$ with hfs (Percival and Seaton 1958)

I	G	h_0	h_1
0	3	5	7
$\frac{1}{2}$	15	37	59
1	33	161	289
$\frac{3}{2}$	81	427	773

Table 3.4. Values of G, h_0, h_1, and h_2 in eq.(3.11) for $^2P \rightarrow {}^2S$ with hfs (Percival and Seaton, 1958)

I	G	h_0	h_1
0	3	7	11
$\frac{1}{2}$	15	53	91
1	33	236	439
$\frac{3}{2}$	27	209	391

3.2.2. Case: natural line widths are comparable to fs or hfs separations.

When the natural line width is comparable to or larger than the fs or hfs separations, the expressions (3.7)-(3.10) given in section 3.2.1 are not applicable. Percival and Seaton (1958) discussed the general case that the natural line width is not negligible. They derived the expression of the degree of polarization of the $^2P \rightarrow {}^2S$ transition with the zero nuclear spin. The degree of polarization P and the quantity K are still given by eqs.(3.6) and (3.10), respectively. However, K_z should be replaced by

$$K_z^{\epsilon} = \frac{K_z^{(0)} + \epsilon^2 K_z^{(\infty)}}{1 + \epsilon^2}, \tag{3.13}$$

with

$$K_z^{(0)} = Q_{M_L=0}, \tag{3.14}$$

$$K_z^{(\infty)} = \frac{1}{2} \sum_{M_S M_L J M_J} \left[C(\tfrac{1}{2}1J; M_S M_L M_J) C(\tfrac{1}{2}1J; M_J 0 M_J)\right]^2 Q_{M_L}. \tag{3.15}$$

The degree of polarization depends on the ratio

$$\epsilon = \frac{2\pi\Delta\nu}{A}, \tag{3.16}$$

where $h\Delta\nu = E(^2P_{\frac{3}{2}}) - E(^2P_{\frac{1}{2}})$ is the fs energy separation of the excited states, and A is the radiative transition probability. For $\epsilon^2 \ll 1$ the two lines overlap completely and we can neglect the fs effect. In this case, the degree of polarization reduces to eq.(3.5) as we expect. (The electron spin plays no role.) The case of $\epsilon^2 \gg 1$ is just discussed in the previous section. We can easily show that eq.(3.13) tends to the one obtained from eq.(3.9) in the limit of $\epsilon^2 \to \infty$.

The degree of polarization of the $^2P \to {}^2S$ transition with non-zero nuclear spin was studied by Flower and Seaton (1967). We assume that the fs energy separation is much larger than the line width. Then, the degree of polarization is given by

$$P = \frac{3(9\alpha - 2)(Q_0 - Q_1)}{12Q_0 + 24Q_1 + (9\alpha - 2)(Q_0 - Q_1)}, \tag{3.17}$$

where

$$\alpha = \sum_{F,F'} \frac{\zeta(I,F,F')}{1 + \epsilon_{F,F'}^2}, \tag{3.18}$$

with $\epsilon_{F,F'} = 2\pi\Delta\nu_{F,F'}/A$ ($h\Delta\nu_{F,F'}$ being the hfs energy separation), and

$$\zeta(I,F,F') = \frac{8}{2I+1} \sum_{M}$$

$$\times \left[\sum_{T} (2T+1) C(T1F; M0M) C(T1F'; M0M) W(\tfrac{1}{2}, 1, I, F; \tfrac{3}{2}, T) W(\tfrac{1}{2}, 1, I, F'; \tfrac{3}{2}, T)\right]^2. \tag{3.19}$$

The values of $\zeta(I,F,F')$ calculated by Flower and Seaton (1967) are presented in Table 3.5.

3.2.3. Case: natural line widths are much larger than fs or hfs separations.

When the natural line width is much larger than the fs (or hfs) separations, the degree of polarization is just equal to the one obtained by neglecting the electron (or nuclear) spin.

3.2.4. Examples

Figure 3.1 shows the degree of the polarization for the resonance line ($4^1P \to 4^1S$) of calcium measured by Ehlers and Gallagher (1973). Also shown are the excitation cross

Table 3.5. The factor $\zeta(I,F,F') = p(I,F,F')/q(I)$ in eq.(3.18) for $^2\mathrm{P} \rightarrow {}^2\mathrm{S}$ (Flower and Seaton 1967)

I	$q(I)$	F	F'	$p(I,F,F')$
0	9	$\frac{3}{2}$	$\frac{3}{2}$	4
$\frac{1}{2}$	72	1	1	9
		1	2	3
		2	2	17
1	675	$\frac{1}{2}$	$\frac{1}{2}$	25
		$\frac{1}{2}$	$\frac{3}{2}$	20
		$\frac{3}{2}$	$\frac{3}{2}$	5
		$\frac{3}{2}$	$\frac{5}{2}$	52
		$\frac{5}{2}$	$\frac{5}{2}$	28
		$\frac{5}{2}$	$\frac{7}{2}$	117
$\frac{3}{2}$	1800	0	0	25
		0	1	0
		0	2	25
		0	3	0
		1	1	99
		1	2	30
		1	3	21
		2	2	125
		2	3	70
		3	3	259
2	7875	$\frac{1}{2}$	$\frac{1}{2}$	175
		$\frac{1}{2}$	$\frac{3}{2}$	28
		$\frac{3}{2}$	$\frac{3}{2}$	147
		$\frac{3}{2}$	$\frac{5}{2}$	0
		$\frac{5}{2}$	$\frac{5}{2}$	476
		$\frac{5}{2}$	$\frac{7}{2}$	84
		$\frac{7}{2}$	$\frac{7}{2}$	112
		$\frac{7}{2}$	$\frac{9}{2}$	531
		$\frac{9}{2}$	$\frac{9}{2}$	288
		$\frac{9}{2}$	$\frac{11}{2}$	1000
$\frac{5}{2}$	75600	1	1	2142
		1	2	490
		1	3	1568
		1	4	0
		2	2	4750
		2	3	560
		2	4	1200
		3	3	5047
		3	4	2625
		4	4	8775

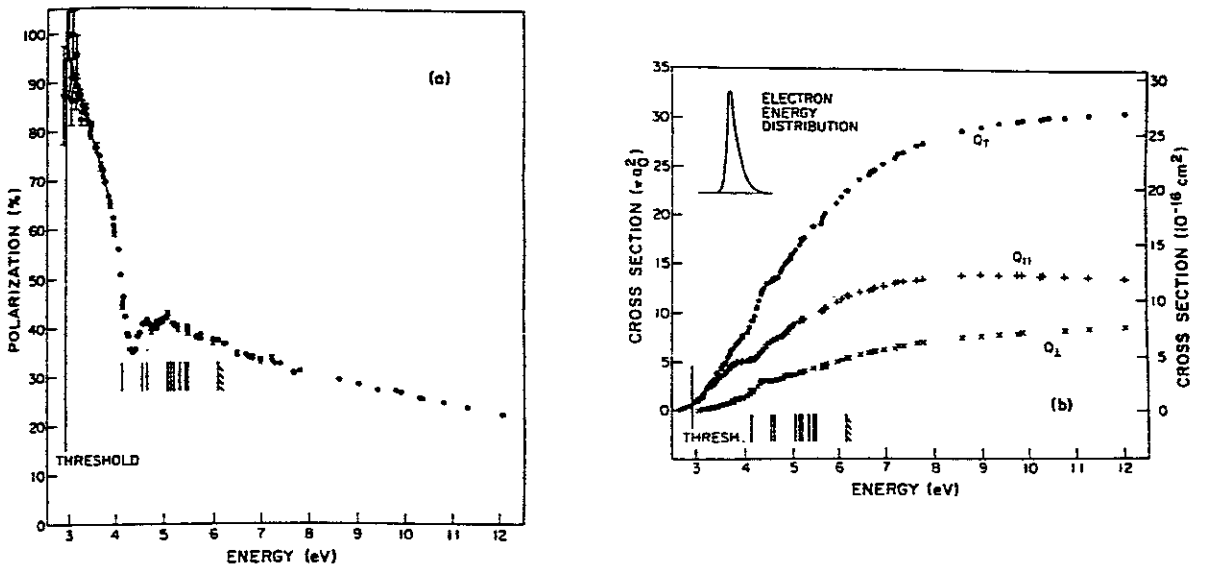

Fig.3.1. (a) Polarization of the $4^1P \rightarrow 4^1S$ transition of calcium; (b) Electron-impact excitation cross sections (Ehlers and Gallagher 1973).

Table 3.6. Values of α in eq.(3.17)

	I	α
H	1/2	0.440
^{6}Li	1	0.413
^{7}Li	3/2	0.326
^{23}Na	3/2	0.288

sections. The polarization for this transition is given by eq.(3.5). Near the threshold with a decrease in energy, the cross section $Q_\perp$ $(=Q_1)$ vanishes much faster than $Q_\parallel$ $(=Q_0)$, and the polarization tends to 100% at the threshold. (See also section 3.3.) The polarization drops rapidly from the threshold energy and reveals some resonance effects in the energy range of 4-6 eV.

Several values of α necessary in the calculation of eq.(3.17) are shown in table 3.6. By using this table, we have for the $^2P \rightarrow {}^2S$ transition of atomic hydrogen

$$P = \frac{Q_0 - Q_1}{2.375Q_0 + 3.749Q_1}, \tag{3.20}$$

which is very close to the expression

$$P = \frac{Q_0 - Q_1}{2.333Q_0 + 3.667Q_1}, \tag{3.21}$$

derived from eq.(3.11) using table 3.4 with I=0. This is because the hfs separations are very small for a hydrogen atom. If we set $\epsilon_{F,F'} = 0$ in eq.(3.18), we have $\alpha = \frac{4}{9} = 0.444\cdots$. This case corresponds to the one discussed in section 3.2.3. For other

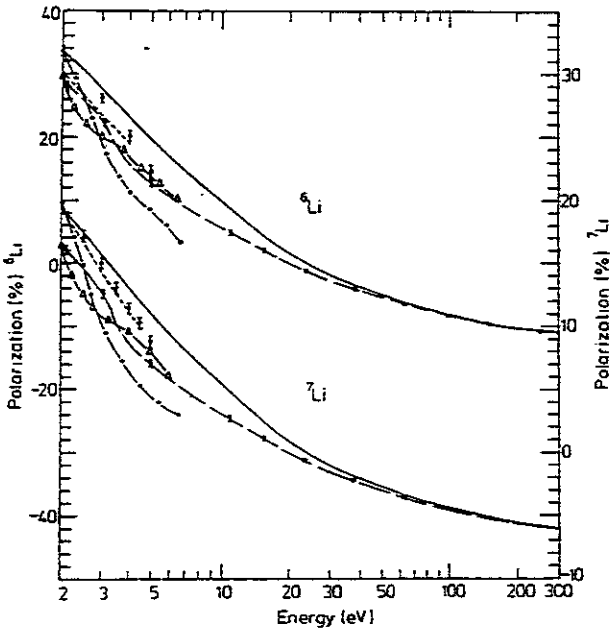

Fig.3.2. Polarization of the 2p → 2s transition of ^{6,7}Li (Kleinpoppen and Scharmann 1978). (—) Kumar and Shrivastava (1976); (−Φ−) experimental results of Leep and Gallagher (1974); (−△−) close-coupling calculations of Burke and Taylor (1969); (− − −) modified close-coupling calculations of Feautrier (1970); (− ● −) variational calculations of McCavert and Rudge (1970); (Φ) experimental data of Hafner and Kleinpoppen (1967).

atoms with finite nuclear spin, the theory including hfs must be used. Figure 3.2 shows various experimental and theoretical results for the polarization of the resonance lines of isotopes ^{6}Li and ^{7}Li. It is evident that the polarization is different for different isotopes.

3.3. Threshold polarization

We consider the electron scattering from a neutral atom. At the threshold energy, the scattered electron has no kinetic energy and hence no orbital angular momentum. Since we assume that the initial state has no orbital angular momentum, only states with M_L=0 can be excited at the threshold. (See Fig.3.1(b) as an example.) This fact enables us to obtain the threshold polarization without any detailed calculations of the cross sections. The threshold polarization is thus obtained by setting $Q_{M_L}/Q_0 = \delta_{M_L 0}$ in the expressions of the degree of polarization given in section 3.2.

For the electron scattering from an ion, however, the above discussion is not valid. Because of the long-range Coulomb force, the partial waves with a finite orbital angular momentum can contribute to the scattering at the zero collision energy. Therefore, we cannot obtain a simple rule for the threshold polarization of the electron-ion scattering. The argument of this section is valid only for a neutral target.

By using eq.(3.17), Flower and Seaton (1967) calculated the threshold polarization for the resonance line of alkaline atoms, and compared with the measurements of Hafner *et al.* (1965). They obtained a good agreement with the experimental result. (See table 3.7.)

Table 3.7. Threshold polarization in %
for resonance lines of lithium and sodium

	Calculated[a]	Measured[b]
^{6}Li	37.5	39.7 ± 3.8
^{7}Li	21.6	20.6 ± 3.0
^{23}Na	14.1	14.8 ± 1.8

[a] Flower and Seaton (1967).
[b] Hafner *et al.* (1965).

In some cases, the polarization shows an abrupt change just above the threshold as shown in Figs.3.1 and 3.3. For this reason, a narrow width of the electron beam energies is required to obtain an accurate degree of polarization near the threshold. For an interpretation of the abrupt change in the polarization, Baranger and Gerjuoy (1958) proposed a theory in which electron-atom compound states are assumed in the energy range just above the threshold. The rapid fall just above the threshold seen in Fig.3.3 is considered to be associated with a $1s4d^2\,^2S$ resonance (Heddle *et al.* 1974). A drastic change in the polarization near the threshold due to resonances was observed for mercury by Ottley and Kleinpoppen (1975).

We cannot always obtain good agreements between theoretical and measured degrees of polarization. Figure 3.4 shows a recent example, the $3^3P \rightarrow 2^3S$ transition of helium, measured by Humphrey *et al.* (1987). From eq.(3.11) and table 3.2, the theoretical threshold polarization is 36.6%. However, the experiment indicates that with a decrease in energy toward the threshold the polarization decreases rather than approaching the theoretical value. In this experiment, very fine energy resolution is

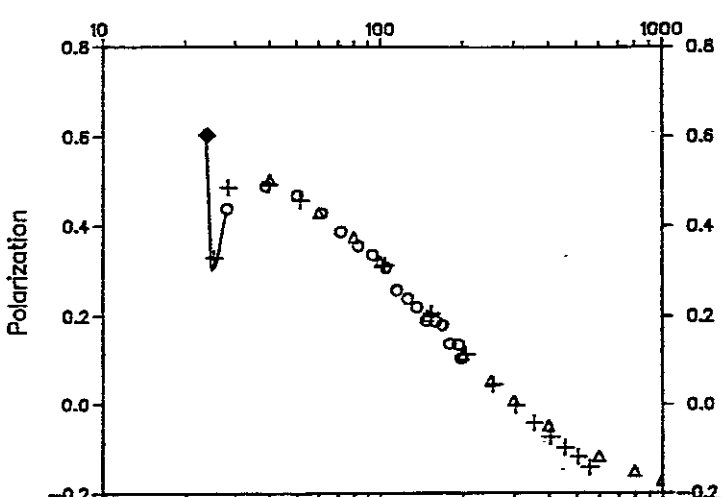

Fig.3.3. Polarization of the $4^1D \rightarrow 2^1P$ transition of helium (Heddle and Gallagher 1989). (+) McFarland (1967); (◯) Clout *et al.* (1971); (△) van Raan *et al.* (1971); (—) Heddle *et al.* (1974); (◆) theoretical threshold value (0.6).

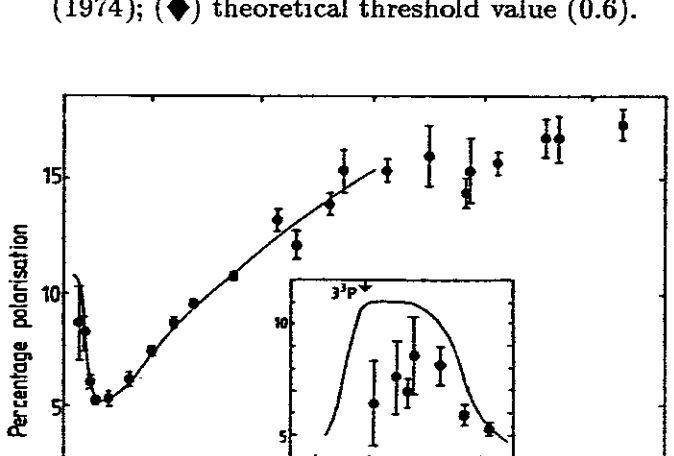

Fig.3.4. Polarization of the $3^3P \rightarrow 2^3S$ transition of helium (Humphrey *et al.* 1987). (◆) Humphrey *et al.* (1987); (—) Whitteker and Dalby (1968).

achieved for electron beams. The unexpected threshold behavior of the measured polarization remains unresolved.

3.4. High energy scattering

By using the Born approximation, we can predict the degree of polarization at high energy collisions. In the limit of infinite energy, the cross section for the excitation 1s $\rightarrow$ nlm of hydrogen is expressed as (Percival and Seaton 1957)

$$\frac{Q(nlm)}{Q(nl)} \longrightarrow \frac{2}{2l+1}|P_l^m(0)|^2, \tag{3.22}$$

where $P_l^m(x)$ is the associated Legendre polynomial. As is discussed in section 3.2, we can neglect the nuclear spin to describe the polarization of hydrogen. Hence eqs.(3.7)-(3.10) togther with eq.(3.22) provide the high energy limit of the polarization for hydrogen. For example, the resonance-series lines have P = -27.3% for ^{2}P $\rightarrow$ ^{2}S and P = -42.9% for $^2P_{3/2} \rightarrow {}^2$S.

In most studies of electron-atom scattering, published results are the cross sections averaged over the magnetic sublevels. From these quantities, we cannot calculate the polarization property directly. Hence, it would be useful if we have an approximation method such that we can deduce the polarization property from the quantities averaged over the magnetic sublevels. Such a method was proposed by Kazantsev *et al.* (1988). When we choose the z axis along the direction of the momentum change vector, the Born approximation indicates that the differential cross section vanishes for excitation to the states with $M_L \neq 0$ (Moiseiwitsch and Smith 1968). Using this fact, Kazantsev *et al.* (1988) showed that the alignment parameters can be calculated from the magnetic-sublevels-averaged differential cross section.

Finally in this section, it should be mentioned that at high energies radiative cascade from higher states contributes to the excitation process and hence influences the observed polarization. This fact should be remembered when we analyze the polarization data.

3.5. Principal quantum number dependence

Vriens and Carriére (1970) calculated the degree of polarization for excitation to n^1P (n=2, 3, 4) of helium by using the Born approximation. Their results show an essential n independence of the polarization. The approximate n independence of alignment and orientation parameters were explained by Csanak and Cartwright (1986) using a quantum defect theory. When perturbation theory is accurate in calculating the excitation cross section, we have approximate n independence of the polarization. Recently, Csanak and Cartwright (1989), using the first-order many-body theory, have studied the n dependence of the polarization for the transitions ^{1}P $\rightarrow$ ^{1}D, ^{1}D $\rightarrow$ ^{1}P, ^{1}D $\rightarrow$ ^{1}F of helium. The results are shown in Fig.3.5. Furthermore, they have confirmed that their results agree well with that of the Born approximation (Vriens and Carrieŕe 1970) for all energies ($E \geq 80$ eV) studied in the latter work. Equation (3.22) shows that the n independence is exactly justified in the high energy limit.

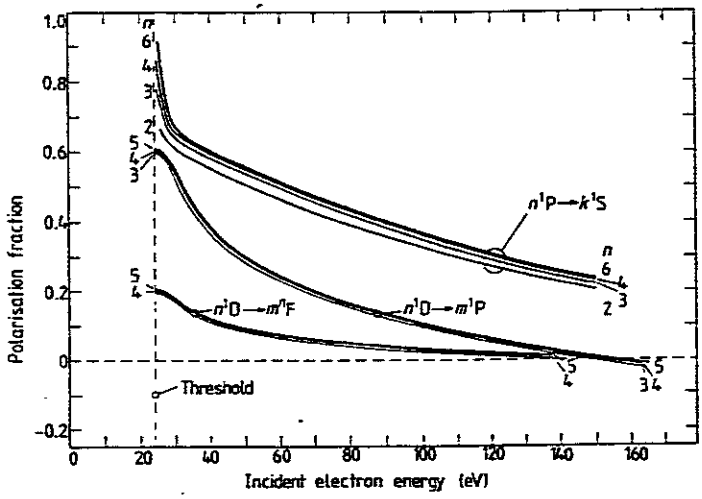

Fig.3.5. Polarization for the n^1P (n=2, 3, ...,6) and n^1D (n=3, 4, 5) states of helium (Csanak and Cartwright 1989).

3.6. Polarization for highly charged ions

For highly charged ions, relativistic effects become important, and we cannot assume the LS coupling scheme. Only the total angular momentum is a good quantum number. In this case, the degree of polarization cannot be expressed in terms of the cross section Q_{M_L} calculated using the LS coupling scheme as in section 3.2.

We denote J_iM_i to be the total angular momentum of the excited state produced by the electron impact. Inal and Dubau (1987) derived the Stokes parameter (3.3) of photons emitted in the transition $J_i \rightarrow J_f$ (with no nuclear spin) in the form †

$$\eta_3(\theta) = \sum_{M_i J=\text{even}\geq 2} N(J_iM_i)\,(-1)^{1-M_i-J_f} \begin{pmatrix} 1 & 1 & J \\ 1 & 1 & -2 \end{pmatrix} \begin{pmatrix} J & J_i & J_i \\ 0 & -M_i & M_i \end{pmatrix} \times \begin{Bmatrix} J & J_i & J_i \\ J_f & 1 & 1 \end{Bmatrix} (2J+1)^{1/2} Y_{J2}(\theta,0) \times \left[\sum_{M_i J=\text{even}} N(J_iM_i)\,(-1)^{-M_i-J_f} \begin{pmatrix} 1 & 1 & J \\ 1 & -1 & 0 \end{pmatrix} \begin{pmatrix} J & J_i & J_i \\ 0 & -M_i & M_i \end{pmatrix} \times \begin{Bmatrix} J & J_i & J_i \\ J_f & 1 & 1 \end{Bmatrix} (2J+1)^{1/2} Y_{J0}(\theta,0) \right]^{-1}. \quad (3.23)$$

Here, $Y_{JM}(\theta,\phi)$ is the spherical harmonic function, and $N(J_iM_i)$ is given by

$$N(J_iM_i) = \sum_{M_0} Q(J_0M_0 \rightarrow J_iM_i) A(J_iM_i), \quad (3.24)$$

† The original expression of η_3 derived by Inal and Dubau (1987) contains the azimuthal angular dependence, which is inconsistent with the assumption of the cylindrical symmetry. In this report, with the consent of the authors we replace $Y_{JM}(\theta,\phi)$ in their expression by $Y_{JM}(\theta,0)$. This replacement has been affirmed by Dubau (private communication).

where $Q(J_0M_0 \rightarrow J_iM_i)$ is the excitation cross section (J_0M_0 being the total angular momentum of the ground state), and $A(J_iM_i)$ is a total decay probability of the excited state. Although the Stokes parameter has been presented here only for the electric dipole transition, Inal and Dubau (1987) provided it for electric or magnetic multipole transitions. Figure 3.6 shows the calculated degree of polarization of some lines of Fe^{24+}.

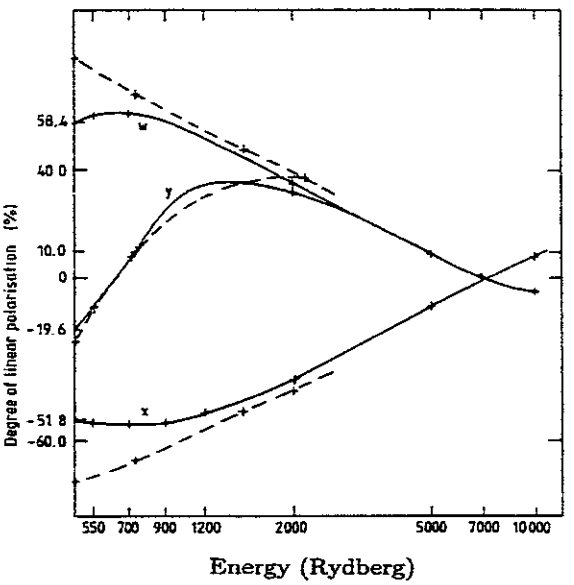

Fig.3.6. Polarization of the Fe^{24+} $1s2p \rightarrow 1s^2$ resonance lines (Inal and Dubau 1987). w, y, and x label the emission lines from the $2^{1,3}P_1$ and $^3P_2$ excited states to the ground state, respectively. The full and broken curves are the distorted wave and the Coulomb wave calculations, respectively.

For the transitions $2^{1,3}P_1 \rightarrow 1^1S_0$ of He-like ions, we have

$$P = \eta_3(\tfrac{\pi}{2}) = \frac{Q_0 - Q_1}{Q_0 + Q_1}. \tag{3.25}$$

This result is the same as eq.(3.5) except that the subscript of Q in eq.(3.25) is M_{J_i} but not M_L. If the relativistic effect is negligible, eq.(3.25) is exactly the same as eq.(3.5) for the $2^1P_1 \rightarrow 1^1S_0$ transition because $J = L$ in that case. For Fe^{24+}, the relativistic effect is expected not to be so strong. Hence, for the $2^1P_1 \rightarrow 1^1S_0$ transition of Fe^{24+}, eq.(3.5) should be a good approximation. From Fig.3.6, however, the threshold polarization differs significantly from 100% for the $2^1P \rightarrow 1^1S$ transition. This is due to the Coulomb force present in the collision system as is discussed in section 3.3.

Using the results of Fig.3.6, Inal and Dubau (1987) estimated the degree of polarization that should be observed owing to energetic nonthermal electrons in the solar flares or tokamaks. They have assumed that the suprathermal electrons have a power-law energy distribution and have a pitch-angle (α) distribution about magnetic field lines that is proportional to the powers of $\cos\alpha$. The result is shown in Fig.3.7.

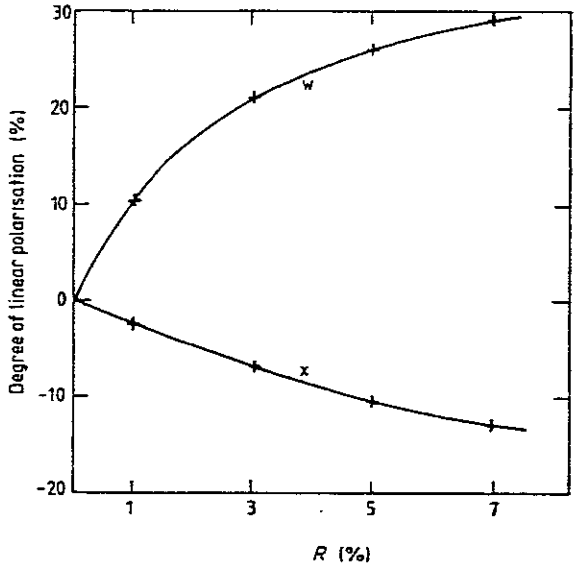

Fig.3.7. Polarization of the Fe^{24+} lines $w(2^1P_1)$ and x $(^3P_2)$ as a function of the ratio R corresponding to the relative density of suprathermal electrons (Inal and Dubau 1987). The electron temperature is 2×10^7K.

Recently, Henderson *et al.* (1990) succeeded in observing the polarization of x-ray emission lines from Sc^{19+} by using the electron-beam-ion-trap technique (Fig.3.8). The measured degree of polarization is in good agreement with a theoretical calculation with consideration of the nuclear spin of Sc ($I = \frac{7}{2}$). (See table 3.8.)

Table 3.8. Degree of polarization of Sc^{19+} at the electron energy of 4.36 keV (Henderson *et al.* 1990)

Line	Calculated		Measured
	No hyperfine	With hyperfine	
w	0.60	0.60	0.70±0.06
x	-0.52	-0.068	-0.05±0.09
y	-0.37	-0.054	0.00±0.09
z	0.00	0.00	-0.02±0.10

Finally, we mention the nuclear charge (Z) dependence along an isoelectronic sequence. Here, we assume that the non-relativistic treatment is valid, and the effect of non-zero nuclear spin is negligible. Under this assumption, Itikawa *et al.* (1991) calculated the alignment parameters for hydrogenic and helium-like ions by a distorted wave method. They showed that when the alignment parameters are plotted against the energy (E) in the threshold unit (ΔE), they are nearly independent of the nuclear charge Z along an isoelectronic sequence. In Fig.3.9, we show the polarization of the $2^1P \rightarrow 1^1S$ transition for helium-like ions as a function of $X = \Delta E/E$. We can see the polarization is nearly independent of Z. Although the results for Fe^{24+} was obtained by making a relativistic calculation (Inal and Dubau 1987), the relativistic effect is not

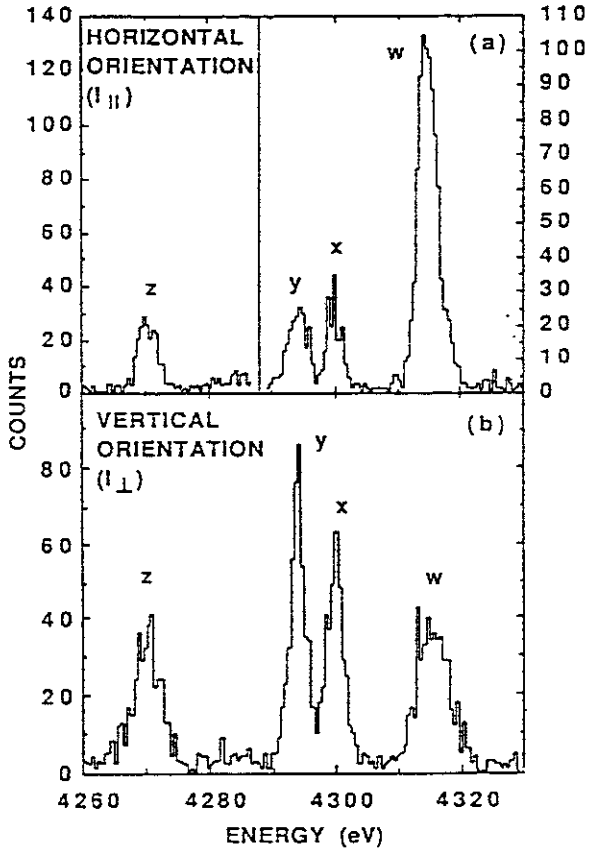

Fig.3.8. Spectra of the Sc^{19+} lines $w(2^1P_1)$, $x(^3P_2)$, y $(^3P_1)$, and $z(^3S_1)$ (Henderson *et al.* 1990) at the electron energy of 4.36 keV.

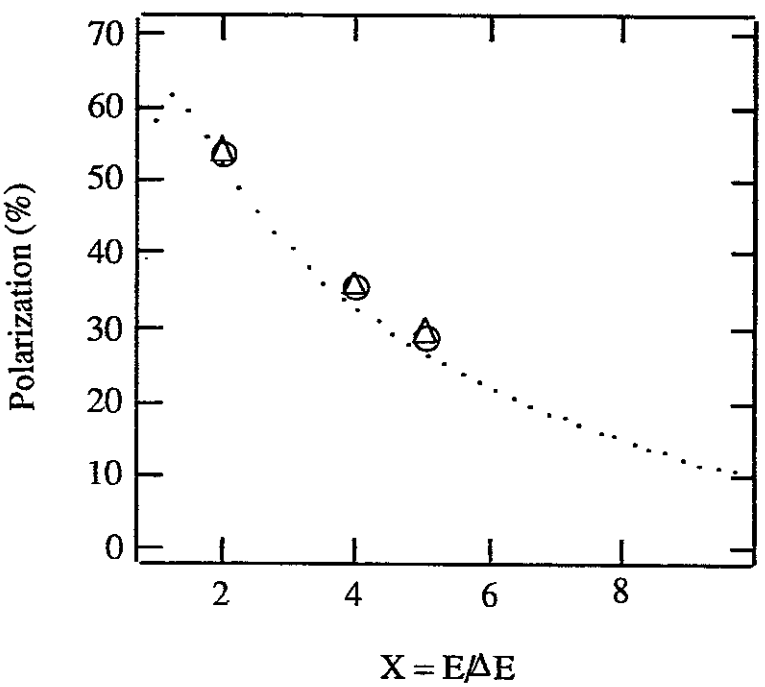

Fig.3.9. Polarization of the $2^1P \rightarrow 1^1S$ transition of helium-like ions as a function of $X = E/\Delta E$. $(\cdots)$ Fe^{24+} (Inal and Dubau 1987). $(\bigcirc)$ O^{6+}; $(\triangle)$ Li^+ (Itikawa *et al.* 1991).

so significant in this case.

Bibliography

Andersen N., Gallagher J.W., and Hertel I.V., 1988, Phys. Rep., **165**, 1.
Collisional alignment and orientation of atomic outer shells
I. Direct excitation by electron and atomic impact
[Review.]

Baranger E. and Gerjuoy E., 1858, Proc. Phys. Soc. London **72**, 326.
Some consequences of the compound ion model
[Theory. Near threshold. Compound model.]

Bartschat K. and Burke P.G., 1988, in "Coherence in Atomic Collision Physics", ed. by H.J. Beyer, K. Blum, and R. Hippler (Plenum Press, New York), p.1.
Electron scattering from heavy atoms
[Review.]

Blum K. and Kleinpoppen H., 1979, Phys. Rep. **52**, 203.
Electron-photon angular correlation in atomic physics
[Review.]

Burke P.G., Schey H.M., and Smith K., 1963, Phys. Rev. **129**, 1258.
Collisions of slow electrons and positrons with atomic hydrogen
[Theory. H. 1s-2s-2p close-coupling. k^2 = 0.81-4.0 au.]

Burke P.G. and Taylor A.J., 1969, J. Phys. **2**, 869.
The scattering of electrons by lithium atoms
[Theory. ^{6,7}Li. 2s-2p close coupling. E = threshold-7 eV.]

Chen S.T. and Gallagher A., 1976, Phys. Rev. **A14**, 593.
Excitation of the Ba and Ba^+ resonance lines by electron impact on Ba atoms
[Ba: $6^1P \rightarrow 6^1S$, 5535Å. e+Ba$\rightarrow$Ba$^+$+2e: $6^2P_{3/2} \rightarrow 6^2S_{1/2}$, 4554A. E = threshold-1500 eV.]

Chen S.T. and Gallagher A., 1977, Phys. Rev. **A15**, 888.
Electron excitation of thallium $7^2S_{1/2}$ and $6^2D_{3/2,5/2}$ lines
[Tl. $6^2D_{3/2} \rightarrow 6^2P_{1/2}$, 2768Å. E = threshold-1500 eV.]

Chen S.T. and Gallagher A., 1978, Phys. Rev. **A17**, 551.
Electron excitation of the resonance lines of the alkali-metal atoms
[$^2P \rightarrow ^2S$. H, Li, Na, K, Rb, Cs: systematic behavior. E = threshold-1500 eV.]

Crandall D.H., Taylor P.O., and Dunn G.H., 1974, Phys. Rev. **A10**, 141
Electron-impact excitation of the Ba^+ ion
[Ba^+. $6^2P_{3/2} \rightarrow 6^2S_{1/2}$, 455.4nm. $6^2P_{1/2} \rightarrow 6^2S_{1/2}$, 493.4nm. $6^2D_{5/2} \rightarrow 6^2P_{3/2}$, 413.1 nm + $6^2D_{3/2} \rightarrow 6^2P_{3/2}$, 416.6nm. E = threshold-750 eV.]

Crowe A., 1987, Adv. At. Mol. Phys. **24**, 269.

Correlations in electron-atom scattering
[Review.]

Csanak G. and Cartwright D.C., 1989, J. Phys. B**22**, 2769.
Principal quantum number dependence of polarization fractions for electron impact excitation of the n^1P and n^1D states of helium
[Theory. He. First-order many-body theory. n^1P, n^1D ($n \leq 6$). E = threshold-500 eV.]

Damburg R. and Gailitis M., 1963, Proc. Phys. Soc. London **82**, 1068.
Calculations in the vicinity of the 2s, 2p threshold of the cross sections for the excitation of hydrogen atoms by electron
[Theory. H. 1s-2s-2p close-coupling. k_{2p}^2 = 0.01-0.05 au.]

Ehlers V.J. and Gallagher A.C., 1973, Phys. Rev. A**7**, 1573.
Electron excitation of the calcium 4227-A resonance line
[Ca. $4s^2\ ^1S_0$-$4s4p\ ^1P_1$, 4227Å. E = threshold-12 eV.]

Enemark E.A. and Gallagher A., 1972, Phys. Rev. A**6**, 192.
Electron excitation of the sodium D lines
[Na. 3s-3p D line, 5890-5896Å. E = threshold-1000 eV.]

Fano U. and Macek J.H., 1973, Rev. Mod. Phys. **45**, 553.
Impact excitation and polarization of the emitted light
[Review.]

Feautrier N., 1970, J. Phys. B**3**, L152.
Polarization of lithium atom resonance lines excited by electron impact
[Theory. Li. 2s-2p close-coupling with polarization.]

Flower D.R. and Seaton M.J., 1967, Proc. Phys. Soc. London **91**, 59.
On the polarization of alkali atom resonance lines excited by electron impact
[Theory. ^{6}Li, ^{7}Li, ^{23}Na. Resonance line.]

Hafner H., Kleinpoppen H., and Kruger H., 1965, Phys. Letters **18**, 270.
Polarization of alkali line radiation excited by electron impact
[^{6,7}Li, Na. Resonance line.]

Hafner H. and Kleinpoppen H., 1967, Z. Physik **198**, 315.
Polarization of atomic line radiation I. Excitation of electron impact
[^{6,7}Li, Na. Rresonance line.]

Hammond P., Karras W., McConkey A.G., and McConkey J.W., 1989, Phys. Rev. A**40**, 1804.
Polarization of rare-gas radiation in the vacuum-ultrviolet region excited by electron impact: Helium and neon
[He: n^1P$\rightarrow 1^1$S. Ne. E = threshold-500 eV.]

Heddle D.W., 1979a, Adv. At. Mol. Phys. **15** 381.

Excitation of atoms by electron impact
[Review.]

Heddle D.W., 1979b, J. Phys. **B12**, 489.
The Bethe approximation: where to draw the line
[Modifications of the Bethe expression.]

Heddle D.W., 1983, J. Phys. **B16**, 275.
On the polarization of atomic line radiation excited by electron impact
[Theory. Bethe approximation. Parametrization of the polarization.]

Heddle D.W.O. and Gallagher J.W., 1989, Rev. Mod. Phys. **61**, 221.
Measurements of electron impact optical excitation functions
[Review.]

Heddle D.W.O. and Keesing R.G., 1967a, Proc. R. Soc. London A**299**, 212.
Threshold behavior of electron excitation and polarization functions in helium
[He. 4^1D-2^1P, 4922Å. 3^1P-2^1S, 5016Å. 3^3P-2^3S, 3899Å. 4^3S-2^3P, 4713Å. E = threshold-30 eV.]

Heddle D.W.O. and Keesing R.G., 1967b, Adv. At. Mol. Phys. **4**, 267.
Measurements of electron excitation functions
[Review.]

Heddle D.W.O., Keesing R.G.W., and Watkins R.D., 1974, Proc. R. Soc. London A**337**, 443.
High resolution studies of electron excitation
III. Polarization near threshold of light from the 4D states of helium
[He. 4^1D-2^1P, 492.2nm. 4^3D-2^3P, 447.2nm. Energy range of 0.8eV above threshold.]

Henderson J.R., Beiersdorfer P., Bennett C.L., Chantrenne S., Knapp D.A., Marrs R.E., Doshek G.A., Seely J.F., Brown C.M., LaVilla R.E., Dubau J., and Levine M.A., 1990, Phys. Rev. Letters **65**, 705.
Polarization of x-ray emission lines from heliumlike scandium as a probe of the hyperfine interaction
[Sc^{19+}. $1s2p^{1,3}P_{1,2}$, $1s2s^3S_1$, ~2.9Å. E = 4.36 and 5.62 keV.]

Huang, 1981, Solar Phys. **71**, 77.
Electron impact polarization of X-ray lines from hydrogen-like ions during solar flares
[Theory. H-like ions. Lα doublet. E ~ keV. Coulomb-Born approximation.]

Humphrey I., Williams J.F., and Heck E.L., 1987, J. Phys. B**20**, 367.
A feasibility study of the measurement of the Stokes parameters of 3^3P, 3^1D and 3^3D states of helium
[He. 3^3P-2^3S, 388.9nm. E = threshold-75 eV.]

Inal M.K. and Dubau J., 1987, J. Phys. B**20**, 4221.

Theory of excitation of He-like and Li-like atomic sublevels by direct electrons: application to X-ray line polarization
[Theory. Fe^{24+} resonance line. Innershell excitation of Fe^{23+}. Distorted-wave calculation. See Inal M.K. and Dubau J., 1989, J. Phys. **B22**, 3329 for erratum.]

Itikawa Y, Srivastava R, and Sakimoto K, 1991, Phys. Rev. **A44**, 7195.
Alignment and orientation in the electron-impact excitation of H- and He-like ions
[Theory. H- and He-like ions. Resonance line. Distorted-wave and Coulomb-Born calculations.]

Kazantsev S.A., Polynovskaya N.Y., Pyatnitskii L.N., and Edel'man S.A., 1988, Sov. Phys. Usp. **31**, 785.
Polarization of atomic ensembles in ionizaed gases
[Review.]

King G.C.M., Adams A., and Read F.H., 1972, J. Phys. **B5**, 254.
Polarization studies using the electron photon coincidence technique
[He. 3^1P-2^1S, 5016Å(E = 75-150 eV). 4^1S-2^1P, 5048Å(threshold polarization).]

Kleinpoppen H., 1969, in "Physics of the One- and Two-Electron Atoms", ed. by F. Bopp and H. Kleinpoppen (North-Holland, Amsterdam) p.612.
Polarization of atomic line radiation
[Review.]

Kleinpoppen H. and Scharmann A., 1978, in "Progress in Atomic Spectroscopy Part A", ed. by W. Hanle and H. Kleinpoppen (Plenum Press, New York) p.329.
Excitation of atoms by impact processes
[Review.]

Kumar S. and Shrivastava M.K., 1976, Proc. Phys. Soc. London **91**, 59.
Glauber calculation of the polarization of the 2p→2s resonance line of lithium
[^{6,7}Li. 2p→2s. E = 2-250 eV.]

Leep D. and Gallagher A., 1974, Phys. Rev. **A10**, 1082.
Electron excitation of the lithium 6708Åresonance line
[Li. 2s-2p, 6708Å. E = threshold-1400 eV.]

Leep D. and Gallagher A., 1976, Phys. Rev. **13**, 148.
Excitation of the Mg and Mg^+ resonance lines by electron impact on Mg atoms
[Mg: 3^1P-3^1S, 2852Å. e+Mg→Mg^++2e: 3^2P-3^2S, 2796 + 2803Å(unresolved). E = threshold-1400 eV.]

McCavert P. and Rudge R.H., 1970, J. Phys. **B3**, 1286.
On the approximation in scattering theory
[Theory. Modified Born approximation. H: 1s-2p, 2s-2p, 2p-3d. Li: 2s-2p, 2p-3d. Na: 3s-3p,3p-3d. K: 4s-4p,4p-3d.]

McConkey J.W., 1988, J. Phys. **B21**, L317.

Use of the optical polarization data to obtain sublevel cross sections following electron impact excitation
[H. Balmer-α, n=3→2.]

McFarland R.H., 1967, Phys. Rev. **156**, 55.
Crossed-beam measurement of the electron-impact polarization of helium 4922A optical radiation
[He. 4^1D_2-2^1P_1, 4922Å. E = threshold-600 eV.]

Moisseiwitsch B.L. and Smith S.J., Rev. Mod. Phys. **40**, 238
Electron impact excitation of atoms
[Review.]

Moores D.L. and Nocross D.W., 1972, J. Phys. B**5**, 1482.
The scattering of electrons by sodium atoms
[Theory. Na. D_1 D_2 lines. 3s-3p-4s-3d close-coupling. E<5 eV.]

Mumma M.J., Misakian M., Jackson W.M., and Faris J.L., 1974, Phys. Rev. A**9**, 203.
Angular distributions and polarization functions of lithium resonance radiation (n^1P-1^1S) in the extreme ultraviolet and $2n^1P \rightarrow 1^1S$.
[He. $n^1P \rightarrow 1^1S$ (unresolved). E = threshold-150 eV.]

Oppenheimer, J.R., 1927, Proc. Nat. Acad. Sci. **13**, 800.
On the quantum theory of the polarization of impact radiation
[Theory.]

Ott W.R., Kauppila W.E., and Fite W.L., 1963, Phys. Rev. Letters **19**, 1361.
Polarization of Lyman-alpha radiation produced in collisions of electrons and hydrogen atoms

Ottley T.W. and Kleinpoppen H., 1975, J. Phys. B**8**, 621.
Resonances near threshold in the electron impact excitation and polarization of the 6^1S_0-6^3P_1 line of mercury
[Hg. $6^1S_0 \rightarrow 6^3P_1$, 2537Å.]

Penney W.G., 1932, Proc. Nat. Acad. Sci., **18**, 231.
Effect of nuclear spin on the radiation excited by electron impact
[Theory.]

Percival I.C. and Seaton M.J., 1958, Phil. Trans. R. Soc. London, Ser.A**251** 113.
The polarization of atomic line radiation excited by electron impact
[Theory. General expressions of the polarization.]

Phelps J.O. and Lin C.C., 1981, Phys. Rev. A**24**, 1299.
Electron-impact excitation of the sodium atom
[Na. $^3P_{3/2}$-$^3S_{1/2}$. $^3D_{5/2}$-$^3P_{3/2}$ + $^3D_{3/2}$-$^3P_{3/2}$. $^3D_{3/2}$-$^3P_{1/2}$. $^4D_{5/2}$-$^3P_{3/2}$ + $^4D_{3/2}$-$^3P_{3/2}$. $^4D_{3/2}$-$^3P_{1/2}$. $^5D_{5/2}$-$^3P_{3/2}$ + $^5D_{3/2}$-$^3P_{3/2}$. $^5D_{3/2}$-$^3P_{1/2}$. 3p-3s. E = threshold-150 eV.]

Phelps J.O., Phillips M.H., Anderson L.W., and Lin C.C., 1983, J. Phys. B**16**, 3825.

The measurement of the electron excitation cross sections of the Zeeman states of the neon 1s levels by laser-induced fluorescence
[Ne. $1s_{2-5}$. E = 18.2 eV.]

Phelps J.O., Solomon J.E., Korff D.E., Lin C.C., and Lee E.T.P., 1979, Phys. Rev. **A20**, 1418.
Electron-impact excitation of the potassium atom
[K. $^4P_{3/2}$-$^4S_{1/2}$. $^4P_{1/2}$-$^4S_{1/2}$. $^3D_{5/2}$-$^4P_{3/2}$ + $^3D_{3/2}$-$^4P_{3/2}$. $^3D_{3/2}$-$^4P_{1/2}$. E = threshold-50 eV.]

Rogers W.T., Dunn G.H., Ostgarrd O.J., Reading M., and Stefani G., 1982, Phys. Rev. **A25**, 681.
Absolute emission cross sections for electron-impact excitation of Zn^+(4p ^{2}P) and (5s ^{2}S) terms. I
[Zn^+. 4p $^2P_{1/2,3/2}$, 202.5, 206.2 nm. E = threshold-790 eV.]

Slevin J.A., 1984, Rep. Prog. Phys. **47**, 461.
Coherence in inelastic low-energy electron scattering
[Review.]

Slevin J.A. and Chwirot S., 1990, J. Phys. **B23**: At. Mol. Opt. Phys. 165.
Coherence and correlation in electron-atom collisions
[Review.]

Steph N.C. and Golden D.E., 1982, Phys. Rev. **A26**, 148.
Polarization fraction of ^{1}P line radiation in helium
[He. 2^1P, 3^1P-1^1S. E = 30-500 eV.]

Taylor P.O. and Dunn G.H., 1973, Phys. Rev. **A8**, 2304.
Absolute cross sections and polarization for electron-impact excitation of the *K* and *H* resonance lines of the Ca^+ ion
[Ca^+. *K*3934, *H*3968Å. E = threshold-700 eV.]

Taylor P.O., Phaneuf R.A., and Dunn G.H., 1980, Phys. Rev. **A22**, 435.
Absolute cross sections and polarization for electron-impact excitation of the resonance multiplet of the Be^+ ion
[Be^+. 2p-2s, 313.1nm. E = threshold-740 eV.]

Tripathi A.N., Mathur K.C., and Joshi S.K., 1973, J. Phys. **B6**, 1431.
On the polarization of the resonance line of lithium and sodium atoms by electron impact
[Theory. Glauber approximation. ^{6,7}Li, Na. E = 2-5 eV.]

Vriens L. and Carriere J.D., 1970, Physica **49**, 517.
Analytical representations of generalized oscillator strengths excitation cross sections and polarization fractions
[Theory. Born approximation. He. $2,3^1P \rightarrow 1^1S$, $3,4^1D \rightarrow 2^1P$. Expression of polarization using GOS.]

Webb C.J., MacGillivray W.R., and Standage M.C., 1987, J. Phys. B18, L259.
A stepwise electron and laser excitation study of the 6^3P_2 metastable state of atomic mercury
[^{200}Hg. 6^3P_2. E = 5.50-6.75 eV.]

Whitteker J.H. and Dalby F.W. 1968, Can. J. Phys. **46**, 193.
Polarization of electron-impact light from helium
[He. 2^3P-2^3S, 10829A. 3^3P-2^3S, 3889Å.]

IV. HEAVY PARTICLE COLLISIONS

4.1. Introduction

The anisotropy of the population of atomic excited states can be created by heavy particle impacts on atoms or ions in plasma. When the collision system under consideration has an axial symmetry and the invariance property under the inversion of the symmetry axis, the anisotropy or the polarization of the optical radiation due to the spontaneous decay of the excited atomic states can be described completely by only the longitudinal alignment parameter $A_{2,0}$ defined by eq.(2.9). If the collision system has no such symmetries, other elements of the polarization tensor play an important role for realization of the anisotropy and the polarization of the emitted radiation of light from atoms or ions. During the last two decades, an extensive study has been carried out on this direction in the field of the atomic collision research. And a comprehensive review has been given for example by Andersen et al (Andersen, 1988). However, in the present chapter, we will concentrate ourselves to the cases that only the longitudinal alignment parameter $A_{2,0}$ plays the decisive role for the formation of the character of the optical radiation. As noted already in chapter 2, the study of the longitudinal alignment of the plasma should be performed on top priority to develop the polarization plasma spectroscopy or diagnostics.

The longitudinal alignment parameter $A_{2,0}$ is determined by the dynamics of the electron capture or the direct excitation process. We shall consider these dynamics in the following two subsections. The subsection 4.2 is devoted to the electron capture processes, and the subsection 4.3 to the direct excitation processes. In these two subsections we restrict ourselves to the cases with no effect from the electronic or nuclear spins. We consider the effect of the spin in the subsection 4.4. The subsection 4.5 is devoted to the description of the polarizations observed in He^+ – He collisions.

4.2. Longitudinal alignment in the electron capture processes in collisions of ions with atoms or ions

a. High energy collisions

Under the conditions that we have a closed shell core in the projectile product ion and we have only the direct capture population of the final states with the orbital angular momentum $l = 1$, i.e., the p -states, the alignment parameter $A_{2,0}$ can be expressed in terms of the cross sections $\sigma^n_{p_0}$ and $\sigma^n_{p_1}(= \sigma^n_{p_{-1}})$, where n is the principal quantum number of the final atomic state, and p_0, p_1, and p_{-1} in the subscripts indicate the components with the magnetic quantum numbers $m = 0$, 1, and -1, respectively. We have

$$A_{2,0} = \sqrt{2}\frac{(\sigma^n_{p_1}-\sigma^n_{p_0})}{(2\sigma^n_{p_1}+\sigma^n_{p_0})}. \tag{4.1}$$

When we change the collision energy, the cross sections $\sigma^n_{p_0}$ and $\sigma^n_{p_1}$ probably change in different ways. The alignment parameter $A_{2,0}$ varies in the range from $-\sqrt{2}$ to $1/\sqrt{2}$. For np - $n's$ transitions, the degree of linear polarization can be written as

$$P_L(np{-}n's) = \frac{(\sigma^n_{p_0}-\sigma^n_{p_1})}{(\sigma^n_{p_1}+\sigma^n_{p_0})} \tag{4.2}$$

and can in principle be varied from -1 to $+1$. Also for other nl states, we can easily obtain the expression of $A_{2,0}$ under the same assumptions.

The alignment parameters $A_{2,0}$, for example, for $2p$ and $3p$ and $3d$ states of a hydrogen-like ion (Z,e), populated in the $(Z_0,e)_{n_0s}+Z\rightarrow Z_0+(Z,e)_{nl}$ reaction have the following forms in the OBK (Ochkur-Brinkmann-Kramers) approximation for (Berezhko, 1980) σ^n_{lm}:

$$A_{2,0}(2p) = -\frac{1}{\sqrt{2}}\frac{11s^2-4}{7s^2+4}\left[1+\frac{30\beta s(s^2+4)+6\beta^2(s^2+4)^2}{5(11s^2-4)}\right], \tag{4.3a}$$

$$A_{2,0}(3p) = -\frac{1}{\sqrt{2}}\frac{33s^6-216s^4+38s^2-64}{21s^6-108s^4+144s^2+64}, \tag{4.3b}$$

$$A_{2,0}(3d) = -\frac{1}{16}\frac{\sqrt{10}}{\sqrt{7}}\frac{117s^4+12s^2-32}{9s^4+9s^2+4}, \tag{4.3c}$$

with

$$\beta = \frac{1}{4Mu}, \quad u = \frac{2v}{Z}, \quad s = \frac{(\frac{n}{\zeta})^2-1}{u}+u, \quad \zeta = \frac{Z}{(\frac{Z_0}{n_0})}, \tag{4.3d}$$

where $n = 2$ or 3, M is the reduced mass of the collision system, and v is the collision velocity. The behavior of the alignment parameters $A_{2,0}(2p)$, $A_{2,0}(3p)$ and $A_{2,0}(3d)$ as a function of the reduced velocity u is shown in Fig. 4.1 for different values of the charge ratio ζ. The above expressions for $A_{2,0}$ show that, in the limit of high collision velocity, i.e., at $u\rightarrow\infty$, the alignment parameters tend to the values

$$A_{2,0}(2p) = A_{2,0}(3p) = -1.11, \quad A_{2,0}(3d) = -0.971. \tag{4.4}$$

When the resonance condition for the $n_0\rightarrow n$ transition is fulfilled ($\zeta = n$), the above alignment parameters take their maxima of possible values $A_{2,0}(2p) = A_{2,0}(3p) = 1/\sqrt{2}$ and $A_{2,0}(3d) = \sqrt{10/28}$. Figure 4.1 shows that for small values of ζ, the alignment parameters are slowly varying negative valued functions of the reduced velocity u. With increasing ζ, $A_{2,0}$-parameters begin to vary rapidly with u and reverse their sign. For $A_{2,0}(2p)$, for instance, this happens for $\zeta > \sqrt{11/3}$.

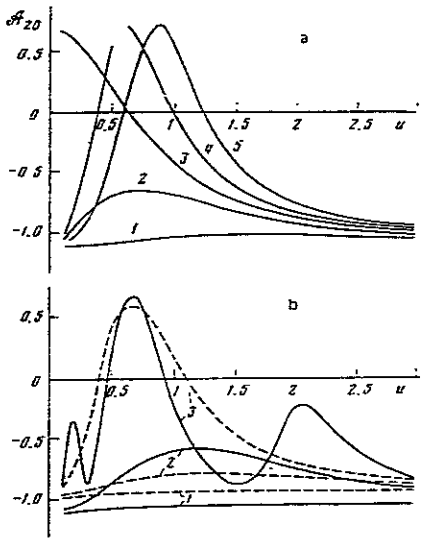

Figure 4.1 Degrees of alignment of the $2p$ (a), $3p$ (b, solid lines), and $3d$ (b, dashed lines) states versus the reduced velocity of the incident particle for different values of ζ (see eq.(4.3d)): a) 1-1.0; 2-1.667; 3-2.0; 4-2.5; 5-4.0; b) 1-1.0; 2-2.0; 3-4.0.

The above considerations are only qualitative concerning the alignment of hydrogen-like excited states produced in high energy charge-exchange collisions. Nevertheless, they show some of the major features of $A_{2,0}$ and, hence, the degree of linear polarization P_L as a function of the reduced parameters u and ζ. Similar investigations of the anisotropy parameters for the $2p$ hydrogen-like state have been performed using the OBK- and Coulomb-BK (CBK) approximations (Burgdoerfer, 1981). The latter includes the internuclear interaction in the electron capture amplitudes.

At extremely high velocity collisions, there is an extensive experimental study by Salah et al (Salah, 1987). They have bombarded the Ne, Ar, and Kr target atoms with 3 GeV bare Kr^{36+} ions (33MeV/amu), resulting into the charge transferred $Kr^{35+}(2p)$ state. They have measured the angular distribution of the Lyman α emission of radiation. They have obtained -0.8 for the value of the alignment parameter $A_{2,0}$ irrespective to the species of the target atoms. This suggests that the alignment of the charge transferred final states is insensitive to the details of the target neutral atoms. In this sense, we can compare their experimental results with the theoretical value given in eq.(4.4), which has been evaluated on the basis of the hydrogenic orbitals. We see that the theoretical value -1.11 of $A_{2,0}(2p)$ in eq.(4.4) is not inconsistent with the Salah et al's result. Furthermore, they have pointed out (Salah, 1987) that their result is in good agreement with the result of the CDW (Continuum Distorted Wave) calculation.

For somewhat lower collision energies, We can compare the theory of Berezhko and Kabachnik (Berezhko, 1980) with earlier experimental resalts of the alignment and polarization of the radiation for the $2p \rightarrow 1s$ transitions. In Fig. 4.2a we show the parameters $-A_{2,0}$ and P_L for the $2p-$ electron capture of hydrogen atomic ions in collisions with the Ne target. Experimental results by Gaily et al (Gaily, 1968) and by Needham et al (Needham, 1970) are illustrated by symbols, whereas the theoretical values by solid curves. In Fig. 4.2b we show the parameters $-A_{2,0}$ and P_L for the Ar target. Experimental results by Gaily et al (Gaily, 1968) and by Needham et al (Needham, 1970) are illustrated by symbols, whereas the theoretical values by solid curves. In these two figures the theoretical calculation, which is based on the OBK approximation, can claim the validity only when the proton velocity exceeds the orbital velocity of the captured electron, i. e., when the proton impact energy exceeds 20 keV in these cases. We have also shown in figures 4.2a and 4.2b the values of the parameters with cascade correction.

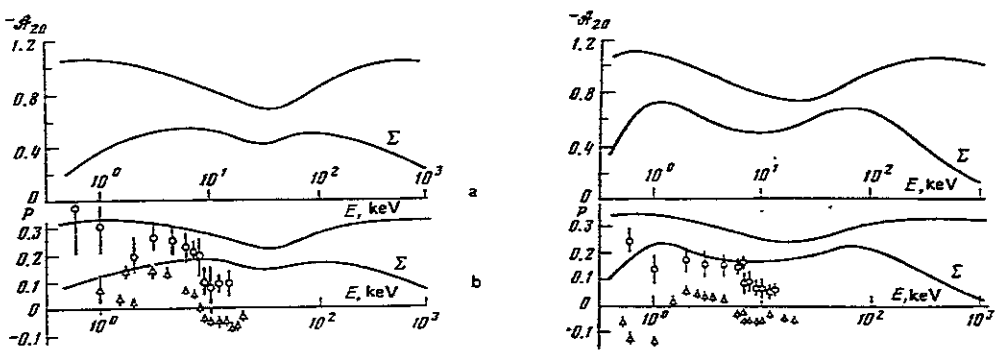

Figure 4.2a (left) Degree of alignment of the $2p$ state of the hydrogen atom (a) and degree of polarization of the L_α line (b) in p+Ne collisions, as a function of the incident proton energy. The letter Σ marks curves calculated with allowance for cascade population of the $2p$ state via $3s$, $3d$, and $4s$ states. Symbols are of the experiments: open circles - Gaily et al (Gaily, 1968), open triangles - Needham et al (Needham, 1970).
Figure 4.2b (right) The same as in Fig. 4.2a, but for p+Ar collisions.

It is seen from these figures that allowance for the cascade correction changes significantly the degree of alignment. We further illustrate the comparison between the theory and experiment (Pedersen, 1975) in Fig. 4.3 for the $F^{+9}(2p)$ state formed by electron capture from He and Ar targets. In this case, the cascade correction does not change very much the degree of alignment at high energy regime. The theory and experiment agree very well with each other.

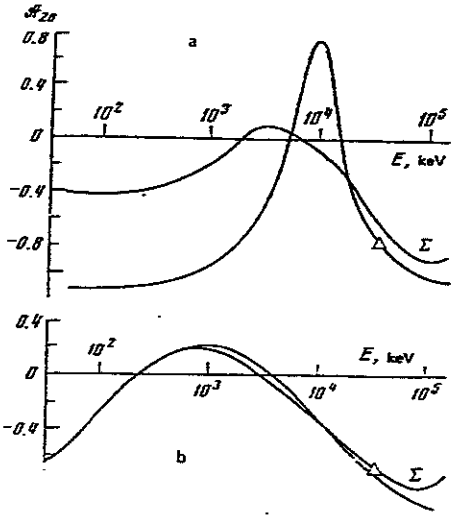

Figure 4.3 Degree of alignment of $2p$ state of F^{+8} ion produced in F^{+9}+He (a) and F^{+9}+Ar (b) collisions. The letter Σ marks the curve calculated with allowance for population via $3s$, $3d$, and $4s$ states. The experimental points (open triangles) are from the data by Pedersen et al (Pedersen, 1975).

b. Intermediate energy collisions

At intermediate collision energies, the theoretical efforts have been made mainly in the framework of the atomic-orbital expansion method. Jain et al (Jain, 1987) have employed 19-states AO+ expansion method, and have calculated the following charge transfer process:

$$H^+ + He \rightarrow H(n=3) + He^+$$

for the H^+ impact energies between 25 and 100 keV. They have tried to obtain the density matrix of the charge transferred $H(n=3)$ states. We show in table 4.1 their results for the normalized density matrix at the collision energy of 60 keV together with the corresponding experimental results by W. B. Westerveld and by M. C. Brower, which are referred by Jain et al (Jain, 1987) as their private communications, and also together with the experimental results by Ashburn et al (Ashburn, 1987), which will be discussed below in somewhat more detail.

Jain et al (Jain, 1987) have analyzed the density matrix in terms of the dipole moments and the Runge-Lenz vector, and they have provided a simple classical orbital picture of the average electron density and current distributions after electron capture.

Experiments on the same collision system have been performed extensively also by Aschburn et al (Ashburn, 1987). They have made the measurement for the H^+ impact energies between 20 and 200 keV. They have determined all the elements of the 9×9 normalized density matrix. In table 4.1 we compare their results with the theoretical results of Jain et al (Jain, 1987). Ashburn et al (Ashburn, 1987) have

Table 4.1 Density matrix (normalized to the 3s cross section) for the $n = 3$ manifold of H atoms formed in H^+ + He collisions at 60 keV. Entries named Westerveld, Brower and Ashburn are the experimental data by W. B. Weserveld, M. C. Brower, and Ashburn et al (Ashburn, 1987).

Element	Present	Westerveld	Brower	Ashburn
s_0	1.0	1.0	1.0	1.0
s_0p_0	0.27-i0.134	0.30-i0.05	...	0.333-i0.046
s_0d_0	0.11+i0.02	0.09-i0.05	...	0.086-i0.050
p_0	0.232	0.22	0.16	0.220
p_1	0.012	+0.014	...	0.014
p_0d_0	0.062+i0.056	0.039+i0.016	...	0.0039+i0.0016
p_1d_1	0.004+i0.004	0.00+i0.002	...	0.000+i0.002
d_0	0.03	0.03	0.011	0.027
d_1	0.0024	-0.005	0.018	-0.005
d_2	0.00014	0.009	-0.001	0.009

measured the intensity and polarization of Balmer- α radiation emitted by H(n=3) atoms.

c. Low energy collisions

Theoretical calculation for low energy ion atom collisions normally employs the molecular-state expansion method (Janev, 1985,Delos, 1981). When the collision velocity is low compared with the characteristic orbital velocity of the electrons of the collision system, the colliding atomic system forms the quasimolecular states. The electronic states are conveniently described by the molecular-fixed wavefunctions. A main drawback of this choice of the coordinate system is from the fact that the molecular-fixed frame of coordinate rotates during the collisions with respect to the space-fixed frame of coordinate. Furthermore, we must introduce a proper electron-translation factor (ETF) (Delos, 1981) in the calculation to recover a correct scattering boundary condition. The distribution of the electron capture cross sections with respect to the azimuth component m of the orbital angular momentum of the charge transferred atomic state is sensitive to the accuracy of the electron-translation factors in practical numerical calculations (Salin, 1984). Although many molecular state calculations have been performed by many authors, we are still in lack of the theoretical values for the m-distribution of the electron capture cross sections.

We, here, introduce an experiment by Vernhet et al (Vernhet, 1985). They have measured relative intensities and polarization rates of $n^1P \rightarrow 1^1S$ x rays emitted in collisions of 4 keV/amu Ne^{9+} ions with H_2. They have discussed their experimental results in connection with the molecular calculations for F^{9+}+H, which can be

considered as similar to the $Ne^{9+}+H_2$. They have experimentally observed a large relative population of $m = 0$ in the $6P$ and $5P$ states of Ne^{8+}; the ratios of the $m = 1$ intensity to the $m = 0$ intensity are less than 0.21 for the $6P$ state and about 0.26 for the $5P$ state, respectively, where the z-axis is taken to be parallel to the incident ion-beam direction. Although this result is at variance with the statistical distribution between the m-substates, they (Vernhet, 1985) have pointed out that the experimental result is consistent with the molecular calculation by themselves. The predominance of the $m = 0$ substates may be interpreted as to be due to the fact that the electronic velocity vector relative to the electron capturing ions sits almost in the scattering plane in such the high energy collisions. This suggests the presence of a strong rotational coupling between the neighboring m-sublevels in the molecular-fixed frame of coordinate. This is verified by the theoretical calculations (Salin, 1984).

Furthermore, Tsurubuchi et al (Tsurubuchi, 1988, Tsurubuchi, 1987, Tsurubuchi, 1983, Tsurubuchi, 1981) have studied extensively the collisions of Li^+-ions with rare gas atoms for the ion-impact energies between a few hundreds of eV and a few keV. They have observed the polarization of radiation from $2p-2s$ transitions of $Li(2p)$ state which is created by the electron capture process. They have resolved the absolute magnitude of the electron capture cross sections for different magnetic sublevels. They have found, for instance, that, in Li^++Ar collisions, the $2p_1$ (or $2p_{-1}$) magnetic sublevels are predominantly excited except for the lowermost collision energy regime. The predominance of the $2p_1$ (or $2p_{-1}$) cross section has been explained toward the predominance of the rotational couplings between the initial $2p\sigma$- and the final $2p\pi$- molecular orbitals in the process of the electron capture into the $Li(2p)$ states.

4.3. Longitudinal alignment in the direct excitation processes in collisions of ions with atoms or ions

As for the alignment and orientation in inelastic excitation of outer shell electrons of atoms, we could list a comprehensive review by Andersen et al (Andersen, 1988). Since they have investigated only the cases which have a well-defined planner symmetry, i. e., the cases in which the initial and final relative momentum of the interacting particles are well defined by differential scattering techniques, this review is not fully relevant to the present subject of our interest. However, the review is helpful for us to gain a current status of the alignment and orientation study in atomic collision research. As for the information of the experiments or theories in which the collision parameters are averaged over the scattering angles, we can introduce several extensive studies as in the followings.

At rather high collision energies, Wigger et al (Wigger, 1984) have measured the M_3, M_4 and M_5 alignment of thorium in ionizing collisions with protons of the impact

energy ranging from 0.15 to 4.0MeV. They have observed the polarization of the emitted M x-rays and obtained the longitudinal alignment parameter $A_{2,0}$ for various inner shell vacancies. In Fig. 4.4, we show their results for the M_3 subshell alignment parameter $A_{2,0}$ as a function of the reduced velocity V which is defined by $V = v_i/v_0$, where v_i is the incoming particle velocity and v_0 is the inner-shell atomic electron velocity. The values of other experiments and theories are also plotted in the figure for comparison.

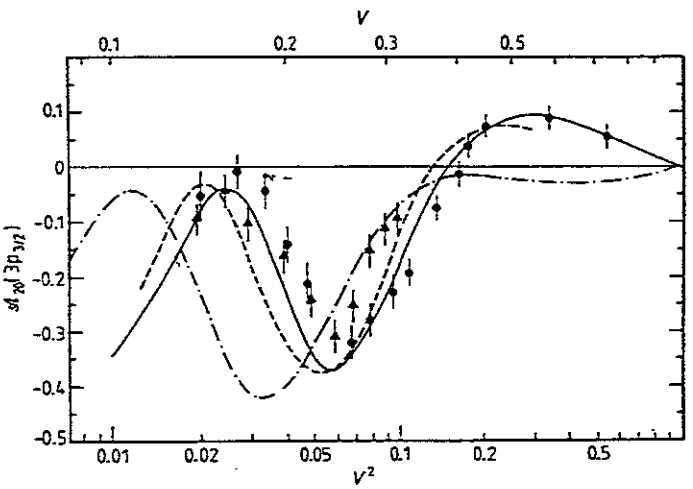

Figure 4.4 M_3 subshell alignment $A_{2,0}$ due to proton impact ionization plotted against the reduced velocity V and V^2 respectively. Experiment: closed circle, p→Th (Wigger, 1984); closed triangle, p→Au (Borisov, 1983). Theory: solid line, Th (Kabachnik 1981, private communication by Wigger et al (Wigger, 1984) ; dashed line, Au (Borisov, 1983); dot-dashed line, Kr (Sizov, 1980)

It has been pointed out that the general dependence of $A_{2,0}$ on the reduced velocity V is well described by the PWBA (plane wave Born approximation) calculations based on the Hartree-Fock-Slater wavefunctions (Borisov, 1983, Sizov, 1980) in the range of $V > 0.3$. And the discrepancies between the theory and experiment at slower collisions are interpreted as to be of the Coulomb deflection of the ionizing projectiles.

As for the low and intermediate energy collisions, there is an extensive series of close-coupling calculations for collisions of singly charged light ions with sodium atoms. Fritsch (Fritsch, 1987) have made a semiclassical close-coupling calculation based on the atomic-orbital (AO) expansion method. He has investigated H^++Na collisions at H^+ impact energies from 0.7 to 50keV, and obtained the Fano-Macek alignment parameter A_0 (see eq.(2.10)) for Na($3p$)-excited state. He has obtained

an excellent agreement with the experimental data by Jitschin et al (Jitschin, 1986). In Fig. 4.5, we show his theoretical result for the Na $3p$ alignment (note here that $A_0 = A_{2,0}/\sqrt{2}$ is plotted against the proton impact energy) together with the experimental data by Jitschin et al (Jitschin, 1986).

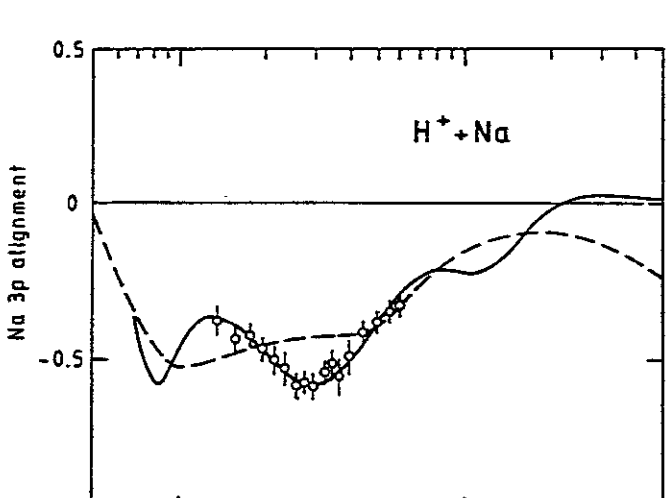

Figure 4.5 Na($3p$) alignment $A_0 = A_{2,0}/\sqrt{2}$ in collisionally induced Na($3s \rightarrow 3p$) excitation. The solid line indicates results of Fritsch (Fritsch, 1987), and the dashed line, the results of the MO calculation shown in Jitschin et al's paper (Jitschin, 1986). Experimental data are also by Jitschin et al (Jitschin, 1986).

Furthermore, Fritsch et al (Fritsch, 1989) have made close coupling calculations based on the molecular-orbital as well as the atomic orbital expansion method for the collisions of He^+ with Na($3s$) atoms. They have calculated the electron capture and excitation cross sections for the He^+ impact energies between 0.05 and 20keV/amu. They have obtained the Fano-Macek alignment parameter A_0 for Na($3p$)-excited state and pointed out that their results are consistent with other properties of this system.

4.4. The effect of the depolarization of the excited states due to the electron spin or the nuclear spin dependent interactions

The population of the magnetic substates, which is represented by $<JM|\rho|JM>$, or the coherences between the magnetic substates, which is represented by $<JM'|\rho|JM>$, can significantly be perturbed by the spin-orbit and hyperfine interactions in the excited product ions. These interactions decrease the anisotropy of the population of the magnetic sub-levels (or the polarization) of the excited product ions. The magnetic (spin-dependent) interactions, leaving the total population

unchanged, introduce characteristic modulations in the anisotropy of the intensities in the exponential radiative decay of the excited states (Fano, 1973, Blum, 1981). The influence of the spin-dependent interactions on the anisotropy of the populations in the magnetic sublevels of the excited states can be most easily described using the polarization-tensor formalism (Berezhko, 1980, Macek, 1971). Following the work of Berezhko and Kabachnik (Berezhko, 1980), we shall present below some of the results for hydrogen-like excited states. We shall confine our consideration to the alignment parameter $A_{2,0}$ only.

Inclusion of the spin-orbit interaction in the treatment of the anisotropy of the populations of the magnetic sub-levels in an *nl*-level leads to appearance of a multiplicative factor $D_\lambda(l)$ in the polarization tensors $\pi_{\lambda,\mu}(l,l)$. The expression for $D_\lambda(l)$ is

$$D_\lambda(l) = \frac{1}{2}\sum_{JJ'}(2J+1)(2J'+1)[W(J',J,l,l;\lambda,\frac{1}{2})]^2 \times\left\{1-\exp(-\gamma_l\Delta t)\left[\cos(\omega_{JJ'}\Delta t)-\varepsilon_{JJ'}\sin(\omega_{JJ'}\Delta t)\right]\right\}, \tag{4.5}$$

where J is the total angular momentum of the electronic state, $\omega_{JJ'}$ is the energy difference between the fine structure levels J and J' , γ_l is the total radiative decay width of the *nl*-level, $\varepsilon_{JJ'} = \omega_{JJ'}/\gamma_l$, and Δt is the time of the observation of the emitted radiation measured from the instant of formation of the excited state. From the sum rule for the $6j$-symbols, it follows that $0 \le D_\lambda(l) \le 1$ and, thus, its multiplication of the tensors $\pi_{\lambda,\mu}(l,l)$ leads to the loss of the alignment and orientation of the excited state. $D_\lambda(l)$ are usually called depolarization coefficients. The oscillatory factors in eq.(4.5) suggest that the $D_\lambda(l)$-coefficients introduce time modulations in the anisotropy parameters of excited states, which are observable, in principle, in the polarization and angular distribution of emitted radiation as the quantum beats. When the fine-structure splitting is considerably larger than the decay width γ_l ($\varepsilon_{JJ'} \gg 1$) , the modulations take place with a frequency equal to the precession frequency of the orbital angular momentum l. (Note that since the total angular momentum $\boldsymbol{J} = \boldsymbol{l}+\boldsymbol{s}$ is a constant of motion in our case, the periodic changes of the orientation of the electronic orbit must be accompanied by the corresponding (180 ° out of phase) oscillations of the spin orientation.) The oscillations of the anisotropy parameters can be observed only when the registration time Δt is comparable to the lifetime γ_l^{-1} of the *nl*-level. For $\Delta t \gg \gamma_l^{-1}$, the expression for $D_\lambda(l)$ becomes

$$D_\lambda(l) = \frac{1}{2}\sum_{JJ'}(2J+1)(2J'+1)[W(J',J,l,l;\lambda,\frac{1}{2})]^2\frac{1}{(1+\varepsilon_{JJ'}^2)\gamma_l}. \tag{4.6}$$

If we include also the hyperfine magnetic interaction into the treatment, the depolarization coefficient $D_\lambda^{(m)}(l)$ is obtained in a form similar to eq.(4.5), which, in the limit of $\Delta t \gg \gamma_l^{-1}$, becomes (Blum, 1981):

$$D_\lambda^{(m)}(l) = \sum_{JJ',FF'}\frac{(2J+1)(2J'+1)(2F+1)(2F'+1)}{2(2I+1)}[W(J',J,l,l;\lambda,\frac{1}{2})]^2$$

$$\times[W(F',F,J,J';\lambda,\frac{1}{2})]^2\frac{1}{(1+\varepsilon^2_{JF,J'F'})\gamma_l}, \tag{4.7}$$

where F is the total angular momentum of the ion ($\boldsymbol{F} = \boldsymbol{J}+\boldsymbol{I}$) , I is the spin of the nucleus, $\varepsilon_{JF,J'F'} = \omega_{JF,J'F'}/\gamma_l$, and $\omega_{JF,J'F'}$ is the energy splitting between the fine-structure levels. If $\Delta t \approx \gamma_l^{-1}$, the Δt-dependent term has to be associated with $D^{(m)}_{\lambda}(l)$, and this term has the same form as the corresponding one in eq.(4.5) with the difference that $\omega_{JJ'}$ and $\varepsilon_{JJ'}$ are replaced by $\omega_{JF,J'F'}$ and $\varepsilon_{JF,J'F'}$, respectively. We should note that in the alignment parameter $A_{2,0}$ the depolarization coefficients $D_{\lambda}(l)$ appear both in the numerator and denominator (see eq.(2.9a)). Therefore, despite the strong dependence of the quantities γ_l, $\omega_{JJ'}$, and $\omega_{JF,J'F'}$ on the ionic charge Z ($\gamma_l \approx Z^4$, $\omega_{JJ'} \approx Z^4$, $\omega_{JF,J'F'} \approx Z^4$), the Z-dependence of anisotropy parameters is scarcely affected by the inclusion of the spin-orbit and the hyperfine interactions into the treatment.

4.5. Polarizations observed on helium atoms in He^+–He collisions

General considerations about the polarization of excited atoms produced by heavy particle collisions are given in section 4.2 and follows. In the present section, we review experimental results of the He-atom excitation in He^+–He collisions, as an example of the scattering polarization.

Figure 4.6 shows the excitation functions of He(3^1P) for collisions with electrons and protons, in addition to the collisions with He^+ (Okasaka, preparation.). The cross section of the electron-capture excitation in the electron-transfer process is also shown in the figure. As mentioned in previous sections, the energy regions of heavy particle collisions are classified into three categories, which are the low, intermediate and high energy regions, respectively. In the low-energy region, where the relative velocity of the colliding two nuclei $v_{\rm rel}$ is much lower than the typical orbital velocity of the atomic electrons $v_{\rm orbit}$, quasimolecular states are formed during the collisions. Because we are considering the symmetric collision systems, the electrons are equally bounded to the two nuclei and, hence, the probabilities of finding a valence electron in the target or in the projectile are almost equal after the collisions. Thus, for low energy collisions of the symmetric systems, the cross sections are nearly the same between the direct (target) excitations and the electron-capture (projectile) excitations. We find this characteristic in Fig. 4.6 below 20 keV of the He^+ impact energy. In the high-energy region ($v_{\rm rel} \gg v_{\rm orbit}$) of the He^+–He collisions, only the singlet level excitations of the target atoms are significant (Okasaka, preparation.). Every excitation function for collisions with electrons, protons or He^+ shows similar velocity dependence in Fig. 4.6 at the collision velocities higher than 3×10^6m/s (about 200 keV in He^+–He collisions). This fact suggests that the electron-transfer excitation occurs scarcely and that the structure of the impinging particle gives no essential contributions to the excitation process. The maximum of the 1^1S–3^1P dipole excitation appears at 650 keV (Hasselkamp, 1972) and the maxima of the 1^1S–3^1S and

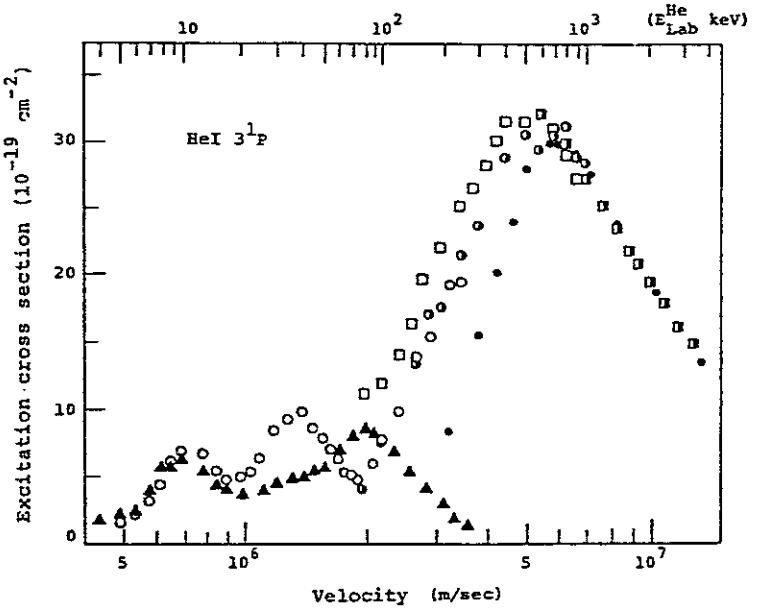

Figure 4.6 The excitation cross sections of HeI3^1P level. He^+–He [target]: ○ Okasaka et al (1991), ◑ Hasselkamp et al (1972). He^+–He [projectile]: ▲ Okasaka et al (1990). He^+–He : □ Okasaka et al (1990), ◨ Hipller et al (1974) e–He : ● Donaldsonet al (1972).

1^1S–3^1D quadrupole excitations appear at 200-250 keV (Okasaka, preparation.), which are similar in the behavior to the electron impacts at the corresponding velocities. Finally, in the intermediate energy region ($v_{rel} \approx v_{orbit}$), which spans between 20 keV and 200 keV in the present case, we find still another cross section maximum at 40 keV of the He^+ ion impact energy in Fig. 4.6 for the target 3^1P excitation. This peak position 40 keV is much different from 80 keV for the projectile excitation; the energy dependences of the cross sections are significantly different between the target and projectile excitations in the intermediate energy region.

In the following subsections, we look into the details of the characteristics of the collisional excitations separately for the three energy regions.

a. Low energy collisions

The polarizations of the total optical emissions in the low-energy region were measured by Clark et al (Clark, 1975) and Okasaka et al (Okasaka, 1989). Figure 4.7 (a) shows the total emission cross section of the $2^3P - 3^3D$ transition and Fig. 4.7 (b) shows the polarization of the emissions (Tani, 1991). The magnitude of the cross section of the direct process, if averaged over the oscillations, agrees with that of the electron-capture process (Fig. 4.7(a)) and we also see similar tendencies in the polarizations (Fig. 4.7(b)). The similarities of the cross sections and of the polarizations between the two processes suggest the quasimolecule formation during

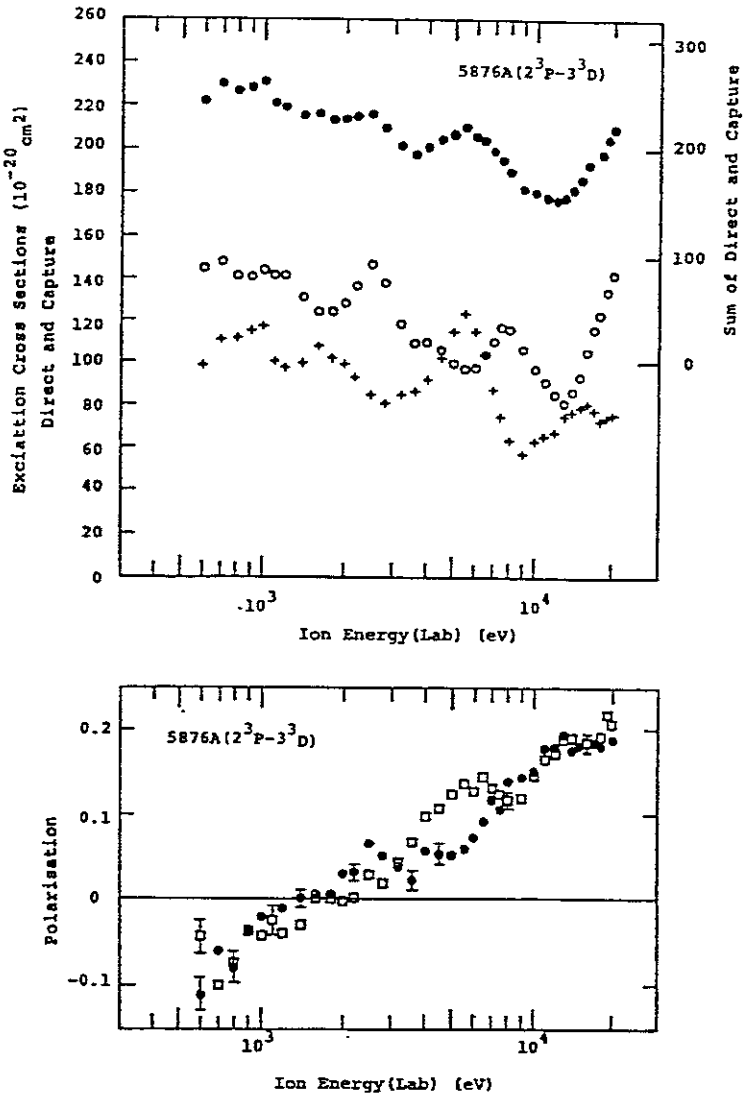

Fig. 4.7 The excitation cross sections (a) and the polarizations of emitted light (b) for HeI 3^3D level. (a) ○ direct excitation. + electron-capture excitation. ● sum of direct and electron-capture excitation. (b) ● direct excitation. □ electron capture excitation.

collisions. The origin of the oscillatory structure on the cross sections was ascribed to the interference between the Π_g and Π_u molecular states in the He^+–He symmetric system (Tani, 1991).

Both the radial coupling and the rotational coupling contribute equally to the excitations in this energy region. The radial coupling of the incident g-state with upper excited states is effective in collisions of 1 keV or less for He^+–He collisions. In collisions of a few keV or more, the rotational couplings between the g-states or between the u-states at small internuclear distances become a principal excitation mechanism (Okasaka, 1987). When we can neglect the effect of the fine and the

hyper-fine structures, the Λ quantum number, which is the projection of the electronic orbital angular momentum onto the quasimolecular axis, is equal to the magnetic quantum number M_L of the atomic state in magnitude at the separated atom limit after the collision, where the quantization axis must be parallel to the interatomic line. For one particle excitation, the Σ -state populates the magnetic sublevel of M_L=0 , the Π -state populates the $|M_L|$=1 level, and so on. The Stark-mixing method used in the studies of hydrogen atoms (see 4.2b) is inappropriate to the studies of the Zeeman coherence among magnetic sublevels of helium atoms. Muller et al (Muller, 1982) and Avci and Neitzke (Avci, 1989) studied the level-crossing signals resulting from the crossings of Zeeman sublevels of the $^1D_2$ levels in electric and magnetic fields E_z and H_z. These level crossings cause changes of the angular distribution and of the polarization of the light emitted by the impact-excited atoms. Measuring the light intensity in a fixed direction, they observed the intensity changes ΔI by sweeping the magnetic field through the position of level crossing. Figure 4.8(a) shows an example of the level-crossing signal of the $1s4d\ ^1D_2$ level and Figure 4.8(b) shows excitation cross sections of Zeeman sublevels obtained from the level crossing signals (Muller, 1982).

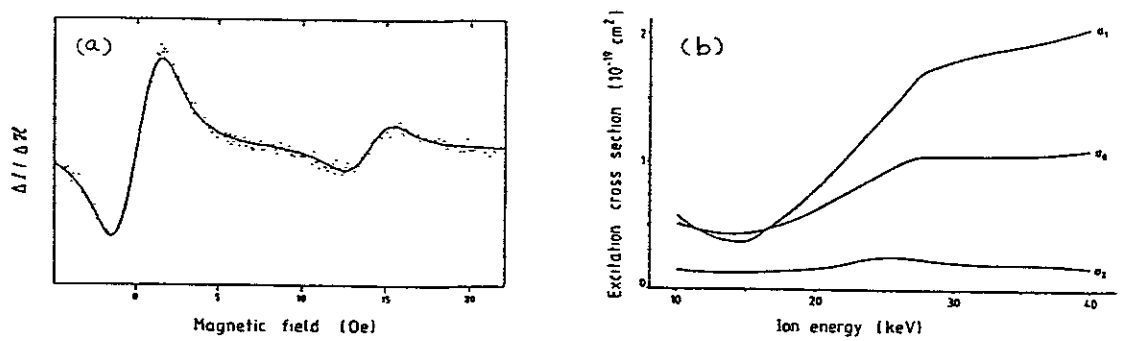

Fig. 4.8 (a) Level-crossing signals of the $1s4d\ ^1D_2$ level excited in 14 keV He^+–He collisions. The magnetic depolarization signal is split by an electric field of 300 V/cm. (b) Excitation cross sections of Zeeman sublevels of the $^1D_2$ level (Muller, 1982).

b. Intermediate-energy collisions

Figure 4.9 shows the cross sections of the target and the projectile (electron-capture) excitations of the $3\ ^3P$ level and Fig. 4.10 shows the cross sections of the target excitation of the n=3 triplet levels of various angular momenta. We see the characteristics of the excitation functions of the intermediate-energy collisions in Figs. 4.6, 4.9 and 4.10.

i) Contrary to the collisions in the low-energy region, where the profiles of the excitation functions are similar for the target and the projectile excitation

processes, the energy point attaining the maximum of the cross section of the target excitation is significantly lower than that of the projectile excitation (Figs. 4.6 and 4.9).

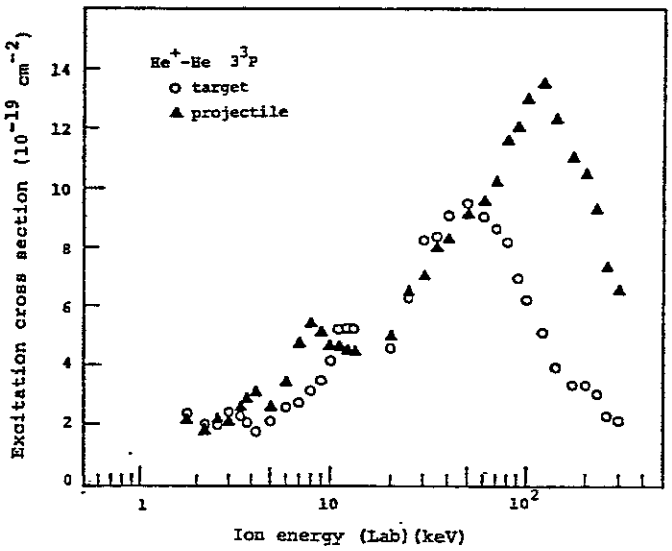

Fig. 4.9 The excitation cross sections of HeI 3 ^3P level

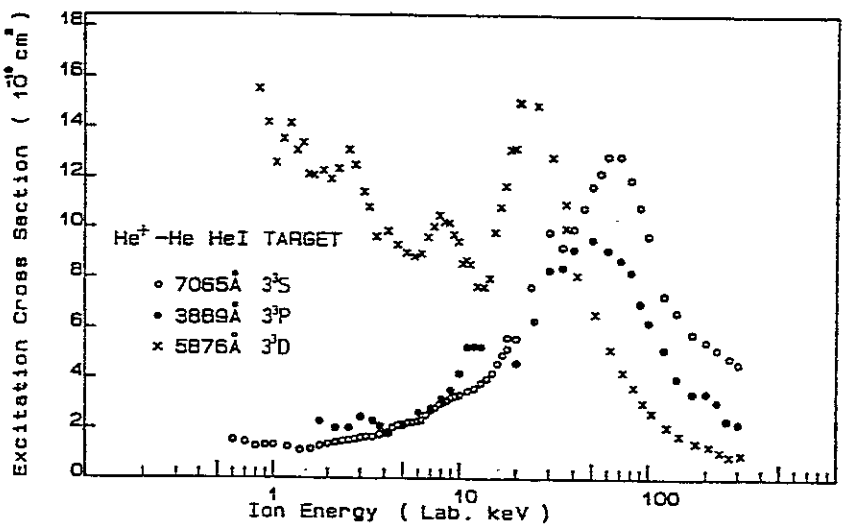

Fig. 4.10 The cross sections of target excitation of the HeI triplet levels

ii) The energy at the maximum of the singlet level cross section is smaller than that of the triplet cross section in each process of the target and the projectile excitations for the same angular momentum levels (Figs.4.6 and 4.9).

iii) For the same spin-state level excitations, the position of the maximum of the cross section shifts toward the lower impact energies with the increase of the angular momentum (Fig. 4.10 and de Heer 1965b).

A systematic relation between the peak positions of the projectile excitation (one- electron transfer) and that of the target excitation (electron exchange) observed in the triplet level cross sections is also found in the cross sections of the direct target-excitation of the singlet levels. An exchange of electrons with the same spin results in apparent no-charge-transfer process. Okasaka and coworkers (Okasaka, preparation.) supposed an intimate correlation of the electron-transfer process to the excitation mechanism in the intermediate-energy collisions.

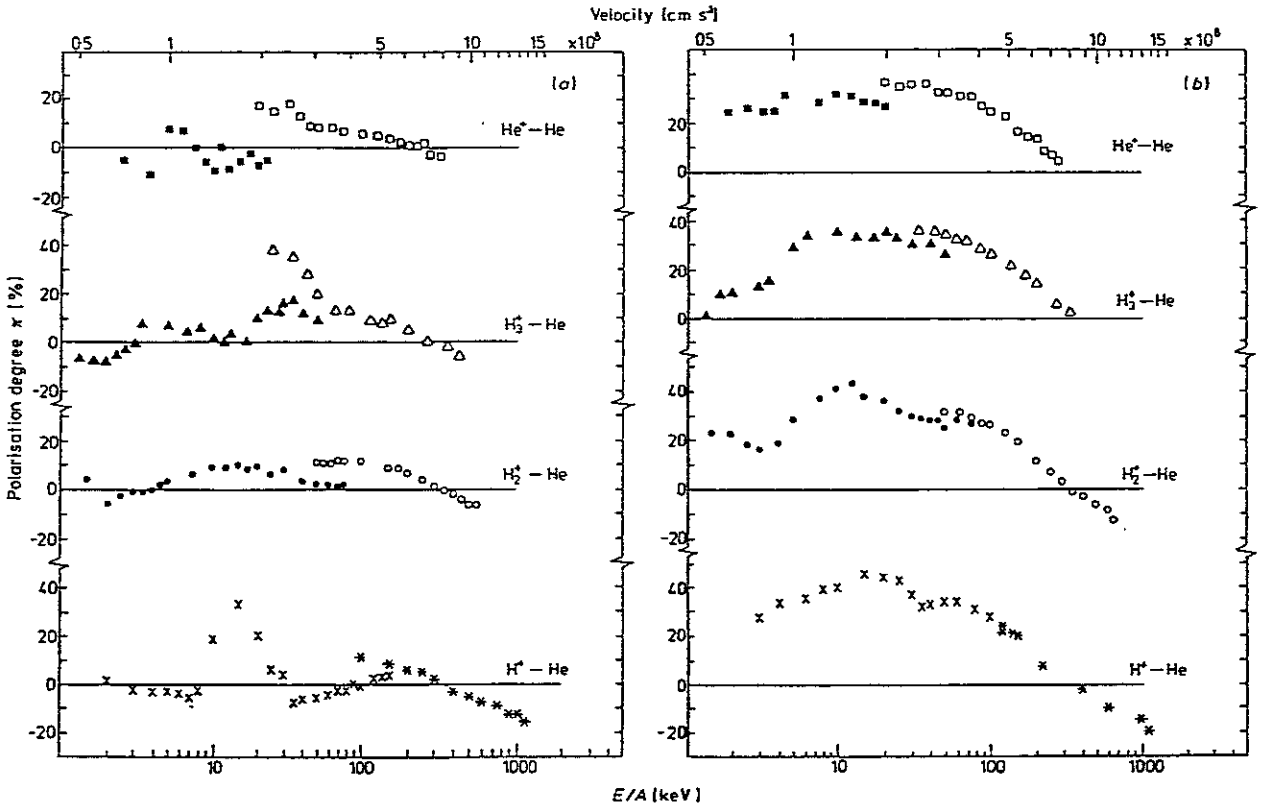

Fig. 4.11 The polarization of the radiation corresponding to the transition (a) $3\ ^1P$–$2\ ^1S$ and (b) $4\ ^1D$–$2\ ^1P$ as a function of the reduced energy E/A covering a large range of the projectile velocities. $*$, ○ , Δ , □ Hasselkamp et al (1990); × , ● , ▲ van den Bos et al (1968,1969); ■ de Heer and van den Bos (1965a).

Very few things have been obtained about characteristic behavior of the polarization of the emitted light in the intermediate-energy collisions. Any remarkable change in the polarization does not occur throughout this energy region. Slight difference of the polarizations between the target- and projectile-excitation was observed in He^+–He collisions (Okasaka, preparation.). The deviation of the electronic charge center from the atomic nucleus observed in the electron- captured proton in H^+–He collisions (Ashburn, 1990) has not yet been found in He^+–He collisions.

c. High-energy collisions

The polarizations of the total optical emissions in the high-energy regions have been measured by de Heer and van den Bos (Heer, 1965) and Hasselkamp et al (Hasselkamp, 1978). Figure 4.11 shows the polarizations of the target helium atoms for the $2\ ^1S$–$3\ ^1P$ and $2\ ^1P$–$4\ ^1D$ transitions with various collision partners (Hasselkamp, 1978). We see again the characteristics of the high-energy collisions that has been recognized on the excitation cross sections, that is, the polarizations in the energy region higher than 50 keV/A are not so sensitive to the structure of the projectiles.

References

Andersen,.

Andersen, N., Gallagher, J. W., and Hertel, I. V., "Collisional alignment and orientation of atomic outer shells I. Direct excitation by electron and atom impact," *Phys. Rep.*, vol. 165, pp. 1-188, 1988.

Ashburn,.

Ashburn, J. R., Cline, R. A., Burgt, P. J. M. van der, Westerveld, W. B., and Risley, J. S., "Precision determination of the density matrix of H(n=3) atoms formed in electron transfer between energetic protons and helium atoms," *Electronic and Atomic Collisions,H. B. Gilbody, A. E. Kingston, C. J. Latimer and H. J. Walters*, p. 490, North Holland, Amsterdam, 1987.

Ashburn,.

Ashburn, J. R., Cline, R. A., Burgt, P. J. M. van der, Westerveld, W. B., and Risley, J. S., *Phys. Rev. A*, vol. 41, p. 2407, 1990.

Avci,.Avci, H. and Neitzke, H. P., "Alignment to orientation conversion for a collisionally excited He 3D state in an external magnetic field," *J. Phys. B: At. Mol. Opt. Phys.*, vol. 22, p. 459, 1989.

Berezhko,.

Berezhko, E. G. and Kabachnik, N. M., "Alignment of hydrogenlike atoms produced by electron capture in collisions of heavy charged particles with target atoms," *Sov. Phys. JETP*, vol. 52, pp. 205-211, AIP, 1980.

Blum,.

Blum, K., *Density matrix theory and applications,* Plenum Press, New York, 1981.

Borisov,.

Borisov, A. M., Kerkow, H., Petukhov, V. P., and Romanovsky, E. A., *J. Phys. B*, vol. 16, pp. L495-L498, 1983.

Bos,.Bos, J. van den, Winter, G. J., and Heer, F. J. de, "Excitation of helium by proton in 1-150 kev region," *Physica*, vol. 40, p. 357, 1968.

Bos,.Bos, J. van den, Winter, G. J., and Heer, F. J. de, "Excitation of helium by H_2^+ and H_3^+ (1-150 keV)," *Physica*, vol. 42, p. 143, 1969.

Burgdoerfer,.

Burgdoerfer, J., "Angular momentum coherences in the differential capture amplitude in hydrogen," *J. Phys. B*, vol. 14, pp. 1019-1034, 1981.

Clark,.

Clark, D. A., Macek, J., and Smith, W. W., *Proc. 9th Int. Conf. on the Physics of Electronic and Atomic Collisions (Seattle) (Seattle, University of Washington Press) Abstract*, p. 731, 1975.

Delos,.

Delos, J. B., "Theory of electronic transitions in slow atomic collisions," *Rev. Mod. Phys.*, vol. 53, pp. 287-357, 1981.

Donaldson,.

Donaldson, F. G., Hender, M. A., and McConkey, J. W., "Vacuum ultraviolet measurements of the electron impact excitation of helium," *J. Phys. B: At. Mol. Phys.*, vol. 5, p. 1192, 1972.

Fano,.

Fano, U. and Macek, J. H., "Impact excitation and polarization of the emitted light," *Rev. Mod. Phys.*, vol. 45, pp. 553-573, 1973.

Fritsch,.

Fritsch, W., "Theoretical study of Na excitation and ionization in H^++Na collisions," *Phys. Rev. A*, vol. 35, pp. 2342-2344, 1987.

Fritsch,.

Fritsch, W., Kimura, M., and Lane, N. F., "A comparative molecular-orbital and atomic orbital study of electron transfer and excitation in He^++Na($3s$) collisions at energies of 0.05− to 20keV/amu," *J. Phys. B*, vol. to be published, 1989.

Gaily,.

Gaily, T. D., Jaecks, D. H., and Geballe, R., *Phys. Rev.*, vol. 167, p. 81, 1968.

Hasselkamp,.

Hasselkamp, D., Scharmann, A. H. R., and Schartner, K. H., "Cross sections for the excitation of the $4\ ^1S-$, $4\ ^1D-$ and $3\ ^1P-$levels of helium excited by fast He^+-ions," *Z. Phys.*, vol. 257, p. 43, 1972.

Hasselkamp,.

Hasselkamp, D., Scharmann, A. H. R., and Schartner, K. H., "The polarization degree of some prominent helium lines after collisional excitation by fast ions," *J. Phys. B: At. Mol. Phys.*, vol. 11, p. 1975, 1978.

Heer,.Heer, F. J. de and Bos, J. van den, "Excitation of helium by He^+ and polarization of the resulting radiation," *Physica*, vol. 31, p. 365, 1965.

Heer,.Heer, F. J. de, Wolterbeek, L. Muller, and Geballe, R., "Electron capture into excited states by helium ions incident on helium," *Physica*, vol. 31, p. 1745, 1965b.

Hippler,.

Hippler, R. and Schartner, K. H., "Absolute cross sections for the excitation of $n\,^1P$-levels of helium by proton impact (150-1000 keV)," *J. Phys. B: At. Mol. Phys. 7*, p. 618, 1974.

Jain,.Jain, A., Lin, C. D., and Fritsch, W., "Density matrix for the H(n=3) atoms formed in electron-capture process of H^+-helium collisions at 25−100keV," *Phys. Rev. A*, vol. 35, p. 3180, 1987.

Janev,.

Janev, R. K. and Winter, Hanspeter, "State-selective electron capture in atom-highly charged ion collisions," *Phys. Rep.*, vol. 117, pp. 265-387, 1985.

Jitschin,.

Jitschin, W., Osimitsch, S., Mueller, D. W., Reihl, H., Allan, R. J., Schoeller, O., and Lutz, H. O., *J. Phys. B*, vol. 19, p. 2299, 1986.

Macek,.

Macek, J. and Jaecks, D. H., "Theory of Atomic Photon-Particle Coincidence Measurements," *Phys. Rev. A*, vol. 4, pp. 2288-2300, 1971.

Muller,.

Muller, R., Open, G. von, Perschmann, W. D., and Schilling, W., "Level-crosssing measurements on the excitation of 1snd ^1D levels of HeI in He^+−He collisions," *J. Phys. B: At.Mol. Phys.*, vol. 15, p. 3179, 1982.

Needham,.

Needham, P. B., Teubner, P. J. O., and Sartwell, B. D., *Phys. Rev. A*, vol. 2, p. 1686, 1970.

Okasaka,.

Okasaka, R., Konishi, Y., Sato, Y., and Fukuda, K., "Excitation cross sections in He^+−He collisions: I. Excitation function and potential curve crossing," *J. Phys. B: At. Mol. Phys.*, vol. 20, p. 3771., 1987.

Okasaka,.

Okasaka, R., Sakakibara, H., Okumoto, K., and Tani, M., "Excitation cross sections in He^+−He collisions: II. Polarisation of emission," *J. Phys. B:*, vol. 22, p. 863., 1989.

Okasaka,.

Okasaka, R., Kawabe, K., Kawamoto, S., Kuma, H., Iwai, T., and Tani, M., Excitation cross sections in He^+−He collisions: III. Charge-transfer excitation and non-charge-transfer excitation, 1991 in preparation..

Pedersen,.

Pedersen, E. H., Czuchlewski, S. J., Brown, M. D., Ellsworth, L. D., and Macdonald, J. R., *Phys. Rev. A*, vol. 11, p. 1267, 1975.

Salah,.

Salah, F. B., Wohrer, K., Chetioui, A., Bouisset, P., Rozet, J. P., Touati, A., Vernhet, D., Stephan, C., and Gayet, R., "Alignment of Kr^{35+} capture states in

high velocity collisions," *Electronic and Atomic Collisions,*, p. 493, North Holland, Amsterdam, 1987.

Salin,.

Salin, A., *J. Phys. (Paris)*, vol. 45, p. 671, 1984.

Sizov,.

Sizov, V. V. and Kabachnik, N. M., *J. Phys. B*, vol. 13, pp. 1601-1610, 1980.

Tani,.Tani, M., Hishikawa, A., and Okasaka, R., "The g-u interference oscillations observed in the emission cross sections and the optical polarizations in He^+–He collisions," *J. Phys. B: At. Mol. Opt. Phys.*, vol. 24, p. 1359, 1991.

Tsurubuchi,.

Tsurubuchi, S. and Iwai, T., *J. Phys. B*, vol. 14, p. 243, 1981.

Tsurubuchi,.

Tsurubuchi, S. and Arikawa, T., *Chem. Phys. Lett.*, vol. 98, p. 515, 1983.

Tsurubuchi,.

Tsurubuchi, S. and Arikawa, T., *J. Phys. Soc. Jpn.*, vol. 56, p. 1996, 1987.

Tsurubuchi,.

Tsurubuchi, S. and Arikawa, T., "Excitation of Li($2p$) in collisions of Li^+ with Ar and Kr Atoms," *J. Phys. Soc. Jpn.*, vol. 57, pp. 1220-1225, 1988.

Vernhet,.

Vernhet, D., Chetioui, A., Wohrer, K., Rozet, J. P., Piquemal, P., Hits, D., Dousson, S., Salin, A., and Stephan, C., "Alignment of Ne^{8+} n^1P states produced by collisions of Ne^{9+} with H_2 at 4keV/amu," *Phys. Rev. A*, vol. 32, pp. 1256-1259, 1985.

Wigger,.

Wigger, J., Altevogt, H., Bruessermann, M., Richter, G., and Cleff, B., "M_3, M_4 and M_5 alignment of thorium by proton impact ionisation," *J. Phys. B*, vol. 17, pp. 4721-4741, 1984.

V. ANISOTROPIC EXCITATION BY RADIATION

5.1. Introduction

Until recently, excitation of atoms by photo-absorption has been rather insignificant in plasma spectroscopy, except in the optical pumping experiment or the Hanle effect experiment. In recent years, however, the laser-induced-fluorescence spectroscopy (LIFS or LIF) method is being used for plasma diagnostics purposes, and knowledge of the ralationship between the photo-excitation and the subsequent fluorescence is essential now.

A remarkable feature of this mode of excitation-observation is that whole the processes is described in a closed form (except for relaxation). It therefore serves as a heuristic example of the polarization phenomena.

As one example, we first look at the following experiment (Fujimoto et al. 1985); in a mild glow discharge plasma of neon we have neutral metastable $1s_3$ atoms (Paschen notation, $2p^53s$ configuration). We excite these atoms by pulsed laser light to the $2p_2$ ($2p^53p$ configuration) level. Subsequent fluorescence light emitted by these atoms is observed. Suppose the atoms are located near the origin in Fig. 5.1, and the laser light is linearly polarized in the z-direction (the quantization axis). The fluorescence is observed from the direction with the polar angle θ. Figure 5.2 shows the result of the observed intensities following excitation with a 5ns laser pulse. The "6164 A" is the direct fluorescence for transition $1s_3$ (J = 0) – $2p_2$ (J = 1) and the "6599 A" is another fluorescence for transition $1s_2$ (J = 1) – $2p_2$ (J = 1), where J denotes the total angular momentum quantum number of the level. It is obvious that, for the same 'population' in the upper level, the observed fluorescence intensities depends on the direction of observation.

The direction dependence of the direct fluorescence intensity may be understood in terms of the classical-atom model in which an electron makes harmonic oscillation around the ion; the electron whose oscillation has been excited in the z-direction by the polarized laser light emits the dipole radiation which is strong in the directions in the x-y plane ($\theta = 90°$) and absent in the z-direction ($\theta = 0°$).

If the above interpretation is correct, the emitted fluorescence should be linearly polarized in the plane containing the quantization axis. Figure 5.3a shows the result of the measurement in which the direct fluorescence ($1s_3 - 2p_2$) is observed in the x-y plane ($\theta = 90°$) with its polarized components resolved. The π light is the linearly polarized component in the direction of the quantization axis and the σ light is that perpendicular to that. It is seen that the above prediction is supported.

For the second fluorescence, "6599A" in Fig. 5.2, however, the above classical interpretation fails.

The quantum interpretation of the above phenomena is given in terms of the Kastler diagram shown in Fig. 5.4. An atomic level is resolved into its magnetic sublevels, and the sublevels belonging to the upper and lower levels are connected by the electric dipole transitions. In our case, the laser light is the π light that does not have an angular momentum in the direction of the quantization axis. This light excites the atoms from the lower $1s_3$ ($J = 0$, $m_J = 0$) level to the ($J = 1$, $m_J = 0$) sublevel of $2p_2$, and no population is created in the ($J = 1$, $m_J = \pm 1$) sublevels of $2p_2$. These atoms emit only the π light for the direct fluorescence (Fig. 5.3a), and its consequence is the same as the classical interpretation. The second fluorescence corresponds to the diagram in Fig. 5.4b. The atoms in the $m_J = 0$ sublevel of $2p_2$ emit only the σ light ($m_J = 0 \longleftrightarrow m_J = 0$ transition is forbidden), and the direction dependence of its intensity is different from that of the π light; its intensity ratio in the direction of the z-axis ($\theta = 0°$) and in the direction of the x – y plane ($\theta = 90°$) is 2 : 1, in accordance with Fig. 5.2. (The observed intensity ratio is slightly different from this ratio owing mainly to the different sensitivities of our detector to the light having different polarization directions. See later for more detail.)

The above example demonstrates that the observed intensity depends not only on the upper-level population but also on the angular momentum pair of the upper and lower levels together with the experimental geometry. In the following the general formalism is introduced and the above experiment is interpreted in its terms.

5.2. Density matrix and radiation

The relationship between the characteristics of the atomic ensemble, i.e., the population and the anisotoropy, and those of the emission line, i.e., the intensity and polarization, is conveniently expressed in terms of the irreducible tensor components of the density matrix of the excited atoms (Omont 1977). Let $\rho^k_q (J_u J_u')$ be the q component of the rank k irredicible representation of the density matrix spanning the space of the upper states J_u and J_u'.

$$\rho (J_u J_u') = \sum_{k\,q} \rho^k_q (J_u J_u') \, T^{(k)}_q (J_u J_u') \qquad (5.1)$$

where $T^{(k)}_q (J_u J_u')$ is the standard irreducible tensorial component. We assume that the density matrix is unnormalized. It is noted that $\rho^k_q (J_u J_u')$ corresponds to $\pi_{kq} (J_u J_u')$ introduced in Chap. 2. Suppose we measure the intensity of the emission radiation, I(e), specified by the polarization vector e, accompanying the spontaneous transition $(u, u') \longrightarrow f$. Then the ovserved intensity per unit solid angle is given by

$$I (e) = C_D \sum_{kq J_u J_u' J_f} \phi^k_q (e) \; B_k (J_u J_u' , \; J_f) \; \rho^k_q (J_u J_u')^* \qquad (5.2)$$

with

$$C_D = \omega^4 / 2\pi c^3 r^2 \qquad (5.3)$$

where ω is the transition frequency, c the speed of light and r the distance from the atom to the detector. $\phi_q^k(\mathbf{e})$ is the irreducible component of the normalized photon density matrix (Baylis 1979)

$$\phi_q^k(\mathbf{e}) = (2k+1)^{1/2} \sum_{ts} \mathbf{e}\cdot\mathbf{t}\,(\mathbf{e}\cdot\mathbf{s})^*\ (-1)^{1-s} \begin{pmatrix} 1 & k & 1 \\ t & q & -s \end{pmatrix} \qquad (5.4)$$

(**t** and **s** span the unit spherical tensors of rank 1, namely, $\pm\mathbf{1} = +(\mathbf{x} \pm i\mathbf{y})/\sqrt{2}$ and $\mathbf{0} = \mathbf{z}$), ( ) is the 3–j symbol and the dynamics are determined by

$$B_k(J_u J_u', J_f) = (-1)^{J_u+J_f+k+1} \begin{Bmatrix} J_u & J_u' & k \\ 1 & 1 & J_f \end{Bmatrix} d_{J_u J_f}\, d_{J_u' J_f}^* \qquad (5.5)$$

Here $d_{J_u J_f}$ is the reduced matrix element of the electric dipole and { } is the 6–j symbol.

The components of the density matrix inside a particular subspace $\{J_u\}$ have a clear physical meaning; ρ_0^0 is called the population (See later for its relationship to the conventional definition of the population.), ρ_q^1 the orientation and ρ_q^2 the alignment. Table 5.1 gives examples of the explicit expressions of the irreducible components of the density matrix.

A common situation in plasma spectroscopy, including the laser-induced fluorescence spectroscopy (LIFS, or LIF), would be a simple case in which there is no coherence between the different upper states J_u and J_u', and we treat the isolated transition u —> f. (The case of atoms and ions having the fine structure or the hyperfine structure is treated in §5.5.) From the experimental view point, it would be sufficient to take the summation in eq.(5.2) only to k = 2;

$$I(\mathbf{e}) = \frac{1}{8\pi r^2}\, n(u)\ A(u,f)\, h\omega \left[1 + 3(-1)^{J_u+J_f} \begin{Bmatrix} J_u & J_u & 1 \\ 1 & 1 & J_f \end{Bmatrix} \sqrt{2J_u+1} \sum_q \phi_q^1(\mathbf{e}) \frac{\rho_q^1(J_u J_u)^*}{\rho_0^0(J_u J_u)}\right.$$

$$\left. + 3(-1)^{J_u+J_f+1} \begin{Bmatrix} J_u & J_u & 2 \\ 1 & 1 & J_f \end{Bmatrix} \sqrt{2J_u+1} \sum_q \phi_q^2(\mathbf{e}) \frac{\rho_q^2(J_u J_u)^*}{\rho_0^0(J_u J_u)}\right] \qquad (5.6)$$

where $(\mathbf{e}) = 3^{-1/2}$ and $B_0(J_u J_u) = [3(2J_u+1)]^{-1/2}\ d_{J_u J_f} d_{J_u J_f}^*$ have been used. We have also introduced the spontaneous transition probability A (u, f) and the population density of the upper level n (u);

$$A(u, f) = \frac{4\omega^3}{3\hbar c^3 (2J_u + 1)} d_{J_u J_f} d_{J_u J_f}^{*} \qquad (5.7)$$

$$n(u) = (2J_u + 1)^{1/2} \rho_0^0 (J_u J_u) \qquad (5.8)$$

The photon density matrix is expressed in terms of the component of the polarization vector $\mathbf{e} = \alpha \mathbf{e}_x + \beta \mathbf{e}_y + \gamma \mathbf{e}_z$, where $\mathbf{e}_x$, $\mathbf{e}_y$ and $\mathbf{e}_z$ are the unit vectors along the x-, y- and z-axis.

$$\begin{aligned}
&\phi_0^0(\mathbf{e}) = 1/\sqrt{3} \\
&\phi_0^1(\mathbf{e}) = (i/\sqrt{2})(\alpha\beta^* - \alpha^*\beta) \\
&\phi_{\pm 1}^1(\mathbf{e}) = (1/2)(\alpha\gamma^* - \alpha^*\gamma) \mp (i/2)(\beta\gamma^* - \beta^*\gamma) \\
&\phi_0^2(\mathbf{e}) = (1/\sqrt{6})(1 - 3|\gamma|^2) \\
&\phi_{\pm 1}^2(\mathbf{e}) = \pm(1/2)(\alpha\gamma^* + \alpha^*\gamma) - (i/2)(\beta\gamma^* + \beta^*\gamma) \\
&\phi_{\pm 2}^2(\mathbf{e}) = (1/2)(|\beta|^2 - |\alpha|^2) \pm (i/2)(\alpha\beta^* + \alpha^*\beta)
\end{aligned} \qquad (5.9)$$

The first term in the square brackets in the right-hand side of eq. (5.6) corresponds to the population or the isotropic part of the emission line intensity. The second term represents the degree of circular polarization and the third term the linear polarization.

Of particular importance is the case in which only ρ_0^2 is present besides ρ_0^0. That is, the excitation is symmetric about the quantization axis. We define the longitudinal alignment for the emitted radiation in the direction perpendicular to the quantization axis.

$$A_L = [I(\mathbf{e}_{//}) - I(\mathbf{e}_{\perp})] / [I(\mathbf{e}_{//}) + 2I(\mathbf{e}_{\perp})] \qquad (5.10)$$

Where $\mathbf{e}_{//}$ and $\mathbf{e}_{\perp}$ are the polarization vectors in the direction parallel and perpendicular to the quantization axis, respectively. Equation (5.10) reduces to

$$A_L = (-1)^{J_u + J_f} \sqrt{3(2J_u + 1)/2} \begin{Bmatrix} J_u & J_u & 2 \\ 1 & 1 & J_f \end{Bmatrix} \rho_0^2 / \rho_0^0 \qquad (5.11)$$

Thus the longitudinal alignment is proportional to the longitudinal alignment parameter $\rho_0^2 / \rho_0^0 = A_{2,0}$ (eq. (2.9a)).

The intensity of radiation propagating in the direction $\mathbf{k}$ making angle θ to the quantization axis (Fig. 5.1) and observed by a detector having no polarization selectivity is given by

$$I(\mathbf{k}) = \frac{n(u)\, A(u,f)\hbar\omega}{4\pi r^2} [\, 1 + (-1)^{J_u+J_f+1} \sqrt{3(2J_u+1)/2} \begin{Bmatrix} J_u & J_u & 2 \\ 1 & 1 & J_f \end{Bmatrix} \frac{\rho_0^2(J_uJ_u)}{\rho_0^0(J_uJ_u)} P_2(\cos\theta)\,] \qquad (5.12)$$

where the second-order Legendre polynomial is

$$P_2(\cos\theta) = \frac{1}{2}(3\cos^2\theta - 1) \qquad (5.13)$$

It is noted that eq. (5.12) is identical to eq. (2.19a,b). The factor α_2 (eq. (2.19c)) is equal to the corresponding factors in the right-hand-side of eq. (5.11).

If we choose in eq. (5.12) the magic angle $\theta = 54.7°$ with which the Legendre polynomial is zero, $P_2(\cos\theta) = 0$, the observed intensity is independent of the alignment. In this case, however, the emission radiation is polarized and if our detector has a polarization selectivity the magic angle excitation does not eliminate the effect of alignment.

In the following sections we review the photo-excitation resulting in production of the multipole moments of the density matrix in the upper level, i.e., the population, the orientation, and in particular, the alignment. Throughout the discussion the initial lower level atoms are assumed to be isotropic or unpolarized.

5.3. Weak light excitation

Suppose we illuminate the atoms in state l with the light having the polarization vector $\mathbf{e}_0$ to excite them into state u. The polarization characteristics of the observed emission radiation u $\longrightarrow$ f are determined by the two quantities $\rho_q^1(J_u\,J_u)^* / \rho_0^0(J_u\,J_u)$ and $\rho_q^2(J_u\,J_u)^* / \rho_0^0(J_u\,J_u)$ through eq. (5.6). In the case of weak light excitation, these quantities are expressed in terms of the photon density matrix and B_k which is defined by eq. (5.5).

$$\rho(J_uJ_u) \propto \sum_{kq} \phi_q^k(\mathbf{e}_0)\; B_k(J_uJ_u, J_l)\; T_q^{(k)}(J_uJ_u) \qquad (5.14)$$

Therefore, eq. (5.2) or (5.6) is rewritten as

$$I(\mathbf{e}) \propto \sum_{kq} \frac{B_k(J_uJ_u, J_f)}{B_0(J_uJ_u, J_f)} \frac{B_k(J_uJ_u, J_l)}{B_0(J_uJ_u, J_l)} \phi_q^k(\mathbf{e})\, \phi_q^k(\mathbf{e}_0)^* \qquad (5.15)$$

The proportionality factor is called the depolarization coefficient

$$W_k(J_l\,J_u\,J_f) = [B_k / B_0]\,[B_k / B_0]$$

$$= (-1)^{J_l - J_f}\ 3\ (2J_u + 1) \begin{Bmatrix} J_u & J_u & k \\ 1 & 1 & J_f \end{Bmatrix} \begin{Bmatrix} J_u & J_u & k \\ 1 & 1 & J_l \end{Bmatrix} \qquad (5.16)$$

It is always smaller than unity except that

$$W_0\ (J_l\ J_u\ J_f) = W_k\ (0\ 1\ 0) = 1 \qquad (5.17)$$

The explicit expressions of W_1 and W_2 are given by Omont (1977), and W_2 is reproduced in Table 5.2. It is readily shown that W_2 given by eq. (5.16) is identical to the longitudinal alignment A_L given by eq. (5.11).

In the following we assume a simple geometry; The atoms are located near the origin, and we illuminate these atoms with polarized light. (Fig. 5.1) In the case of linear polarization the polarization vector is taken along the z-axis and in the case of circularly polarized light the beam direction is taken along the z-axis. We observe the fluorescence light in the direction z' which makes angle θ to the z-axis. As an example, we show below the case of the linearly polarized light excitation. In this case, in eq. (5.15), the k = 1 term is absent and ϕ_q^2 terms are null except for ϕ_0^2 . (See eq. (5.9).) In eq. (5.6) we have only ρ_0^0 and ρ_0^2 . The two polarized components, the polarization vectors of which are expressed as $\mathbf{e}_r$ and $\mathbf{e}_l$, are observed. (Fig. 5.1) Then, we have the simple relationship

$$I(\mathbf{e}) = \frac{1}{8\pi r^2}\, n(u)\ A(u, f)\ \hbar\omega\ [1 - f_0^2(\mathbf{e})\ W_2\ (J_l\ J_u\ J_f)] \qquad (5.18)$$

where

$$f_0^2\ (\mathbf{e}_r) = 1$$
$$f_0^2\ (\mathbf{e}_l) = 1 - 3\ \sin^2\theta \qquad (5.19)$$

When our light beam is unpolarized, this beam may be regarded as incoherent superposition of the right-circularly polarized light and the left-circularly polarized light. It is straightforward to show that, when we take the z-axis in the direction of the beam propagation, eq. (5.18) becomes valid with W_2 replaced by $-W_2 / 2$. Thus, the effect of the anisotropic excitation is smaller by a factor of 2, but still remains (Fujimoto et al. 1985).

Now we look at the example of Fig. 5.3. This is for the $J_l = 0 \longrightarrow J_u = 1 \longrightarrow J_f = 0$ excitation-observation scheme, and $W_2 = 1$ (eq. (5.17)). For $\theta = 90°$ the polarized component $\mathbf{e}_l$ corresponds to the π-light and $\mathbf{e}_r$ to the σ-light. In the right-hand side of eq. (5.18) the number in the square brackets is 3 for the π-light and 0 for the σ-light, in consistent with experiment. (The finite intensity of the σ-light is the result of the alignment relaxation. See Chapter 7.) Figure 5.2 is interpreted from eq. (5.18) by summing the intensities for the two orthogonal polarized components. The resulting intensity is given by equation with the square brackets of $[2 - (3\ \cos^2\theta - 1)\ W_2]$. For the case of $J_f = 0$ ('6164 A') the number in the brackets is 0 for $\theta = 0°$ and 3 for $\theta = 90°$, in accordance with experiment. Whereas, for the case of $J_f = 1$ ('6599A') $W_2 = -1/2$ and the number is 3 for $\theta = 0°$ and 3/2 for $\theta = 90°$. Here again, the small inconsistency of the experiment with this calculation is due to the alignment relaxation and the different sensitivities of our detection system for the different polarization components. (Of course, the A coefficient is different for the two transitions and our detector has different sensitivities for different wavelengths.)

5.4. Strong light excitation

Consider as an example the Kastler diagram of Fig. 5.5 for $J_l = J_u = 2$ and suppose we excite the lower level atoms to the upper level by the π-light. If the light intensity is low the relative populations in the upper magnetic sublevels are proportional to the corresponding transition probabilities indicated in the figure: the distribution is (4 : 1 : 0 : 1 : 4) for $m_J = (-2, -1, 0, 1, 2)$. This is the situation assumed in the preceding section. When the incident radiation is intense, various new factors should be taken into account. For instance, a phase correlation develops between the upper and lower states (optical coherence) as well as, in the case of σ-excitation, between the magnetic sublevels in the upper level (Zeeman coherence), and a treatment becomes extremely complicated. However, if the incident light is such that at most one optical process, i.e., absorption or induced emission, occurs during the correlation time of the radiation, an extension of the treatment in §5.3. is rather straightforward. We call this mode of excitation the broad line excitation, and we assume this condition in this section. In this case, the only difference is the atomic density matrix which becomes different from the weak excitation case. In the above example, the population density distribution becomes (1, 1, 0, 1, 1) for the π-light excitation.

The density matrix of the atomic ensemble in level u is not given by eq. (5.14) any more, and the orientation parameter ρ_0^1 / ρ_0^0 and the alignment parameter ρ_0^2 / ρ_0^0 are different from the weak excitation case. Thus the depolarization coefficient is not given by eq. (5.16). Hirabayashi et al. (1986) investigated the alignment under this condition. They give the values of the depolarization coefficient $W_2 = A_L$ as defined

by eq. (5.10) or (5.11) in the limit of intense excitation. The result is reproduced in Table 5.2. They also give the saturated population of the upper level in this limit. Table 5.3 gives the result. It is noted that the population ratio between the upper and lower levels are not given by their statistical weights, as conventionally assumed.

The depolarization coefficient for unpolarized light excitation is not related to that for polarized light excitation as has been the case in §5.3. These authors give W_2 for this case. The result is reproduced in Table 5.4.

When the incident light intensity is intermediate between the limits of weak and strong, the polarization characteristics as well as the total intensity are not expressed by the simple formulas. Instead, the temporal development of the density matrix of the upper and lower levels should be considered, and the coupled equations should be solved. An example is given in Hirabayashi et al.(1986). Figure 5.6 compares the result of calculation with the experiment for the π-light excitation (a), and the unpolarized-light excitation (b). The experimental depolarization factor, or the lognitudinal alignment, tends to take values that are calculated for higher intensity. This is probably due to the partial breakdown of the assumption of the broad-line excitation made in the calculation: the laser light having a coarse mode pattern may saturate the alignment of atoms having absorption frequancies that coincide with the laser mode frequancies. However, population is saturated only with the help of power broadening, and this needs a higher apparent intensity.

5.5. Fine or hyperfine structure

Luypaert and van Craen (1977) treat the case in which the upper level has a hyperfine structure. They give the formula for weak light excitation. Let l, u and f denote the initial, upper and final levels, respectively, and the nuclear angular momentum I results in the hyperfine levels denoted by F_u and so on. We give here the extention of eq. (5.18).

$$I(\mathbf{e}) = \frac{1}{8\pi r^2} n(u)\, A(u,f)\, \hbar\omega \left[1 - \left(\frac{1}{2I+1}\right) f_0^2(\mathbf{e})\, W_2(J_l\, J_u\, J_f)\right.$$

$$\left. \times \sum_{F_u F_u'} (2F_u+1)(2F_u'+1) \begin{Bmatrix} F_u & F_u' & 2 \\ J_u & J_u & I \end{Bmatrix} \begin{Bmatrix} F_u' & F_u & 2 \\ J_u & J_u & I \end{Bmatrix} \exp\{-i\omega(F_u, F_u')\, t\}\right] \tag{5.20}$$

where $\omega(F_u, F_u')$ is the Bohr angular frequency of the energy separation between the respective sublevels.

For lines with the fine structure, the above formula is modified such that J_u, I and F_u are replaced, respectively, by L, the orbital angular momentum, S, the spin angular momentum and J, the total angular momentum.

5.6. Transfer of anisotropy by the spontaneous transition

Omont (1977) gives the transfer rate of the multipole moment due to the spontaneous transition $u \longrightarrow e$.

$$d\rho^k_q (J_e J_e) / dt = (-1)^{J_u+J_e+k+1} \; A(u, e) (2J_u + 1) \begin{Bmatrix} J_u & J_u & k \\ J_e & J_e & 1 \end{Bmatrix} \rho^k_q (J_u J_u) \qquad (5.21)$$

For a transition between the magnetic sublevels (J, M) $\longleftrightarrow$ (J', M'), the relative transition probability is given by

$$A(JM, J'M') \propto \begin{pmatrix} J & 1 & J' \\ -M & q & M' \end{pmatrix}^2 \qquad (5.22)$$

with $q = 0$ for π-light ($M' = M$) and $q = \pm 1$ for σ-light ($M' = M \pm 1$). Figure 5.7 gives Kastler diagrams with the relative transition probabilities for several combinations of the angular momenta.

References

Baylis W.E.,1979, *Progress in Atomic Spectroscopy*, Part B, eds. W. Hanle and H. Kleinpoppen (Plenum, New York) p.1227.

Collisional depolarization in the excited state

Luypaert R. and van Craen J., 1977, J. Phys. B **10**, 3627.

Hyperfine-structure quantum beats: Application of the graphical methods of angular-momentum theory to the calculation of intensity profiles

Fujimoto T., Goto C., Uetani Y. and Fukuda K., 1985, Jpn. J. Appl. Phys. **24**, 875.

Effects of anisotropic excitation in laser-induced fluorescence spectroscopy (LIFS)

Hirabayashi A., Nambu Y. and Fujimoto T., 1986, Jpn. J. Appl. Phys. **25**, 1563.

Excitation anisotropy in laser-induced-fluorescence spectroscopy ----------

High-intensity, broad-line excitation

Omont A., 1977, Prog. Quantum Electron. **5**, 69.

Irreducible components of the density matrix. Application to optical pumping

Table 5.1 Examples of the irreducible tensor components of the atomic density matrix. (Omont 1977)

J = 1 / 2	$\rho_0^0 = 1/\sqrt{2}\,(\rho_{1/2\,1/2} + \rho_{-1/2-1/2})$
	$\rho_0^1 = 1/\sqrt{2}\,(\rho_{1/2\,1/2} - \rho_{-1/2-1/2})$
	$\rho_1^1 = -\rho_{1/2\,-1/2}$
J = 1	$\rho_0^0 = 1/\sqrt{3}\,(\rho_{11} + \rho_{00} + \rho_{-1-1})$
	$\rho_0^1 = 1/\sqrt{2}\,(\rho_{11} - \rho_{-1-1})$
	$\rho_1^1 = -1/\sqrt{2}\,(\rho_{10} + \rho_{0-1})$
	$\rho_0^2 = 1/\sqrt{6}\,(\rho_{11} - 2\rho_{00} + \rho_{-1-1})$
	$\rho_1^2 = -1/\sqrt{2}\,(\rho_{10} - \rho_{0-1})$
	$\rho_2^2 = \rho_{1-1}$
J = 3 / 2	$\rho_0^0 = 1/2\,(\rho_{3/2\,3/2} + \rho_{1/2\,1/2} + \rho_{-1/2-1/2} + \rho_{-3/2-3/2})$
	$\rho_0^1 = 1/\sqrt{20}\,(3\rho_{3/2\,3/2} + \rho_{1/2\,1/2} - \rho_{-1/2-1/2} - 3\rho_{-3/2-3/2})$
	$\rho_1^1 = -1/\sqrt{10}\,(\sqrt{3}\rho_{3/2\,1/2} + 2\rho_{1/2-1/2} + \sqrt{3}\rho_{-1/2-3/2})$
	$\rho_0^2 = 1/2\,(\rho_{3/2\,3/2} - \rho_{1/2\,1/2} - \rho_{-1/2-1/2} + \rho_{-3/2-3/2})$
	$\rho_1^2 = -1/\sqrt{2}\,(\rho_{3/2\,1/2} - \rho_{-1/2-3/2})$
	$\rho_2^2 = 1/\sqrt{2}\,(\rho_{3/2-1/2} + \rho_{1/2-3/2})$
	$\rho_0^3 = 1/\sqrt{20}\,(\rho_{3/2\,3/2} - 3\rho_{1/2\,1/2} + 3\rho_{-1/2-1/2} - \rho_{-3/2-3/2})$
	$\rho_1^3 = 1/\sqrt{5}\,(-\rho_{3/2\,1/2} + \sqrt{3}\rho_{1/2-1/2} - \rho_{-1/2-3/2})$
	$\rho_2^3 = 1/\sqrt{2}\,(\rho_{3/2-1/2} - \rho_{1/2-3/2})$
	$\rho_3^3 = -\rho_{3/2-3/2}$

Table 5.2 Depolarization coefficients W_2 for linearly polarized light excitation. (Omont 1977, Hirabayashi et al. 1986)

J_l	J_u	J_f	Weak exc.	Intense exc. J=integer	Intense exc. J=half-integer
$J-1$	J	$J-1$	$\frac{(J+1)(2J+3)}{10J(2J-1)}$	$\frac{1}{2J-1}$	$\frac{1}{2J-1}$
		J	$-\frac{2J+3}{10J}$	$-\frac{1}{J+1}$	$-\frac{1}{J+1}$
		$J+1$	$\frac{1}{10}$	$\frac{J}{(2J+3)(J+1)}$	$\frac{J}{(2J+3)(J+1)}$
J	J	$J-1$	$-\frac{2J+3}{10J}$	$-\frac{J+1}{4J(2J-1)}$	0
		J	$\frac{(2J-1)(2J+3)}{10J(J+1)}$	$\frac{1}{4J}$	0
		$J+1$	$-\frac{2J-1}{10(J+1)}$	$-\frac{1}{4(2J+3)}$	0
$J+1$	J	$J-1$	$\frac{1}{10}$	0	0
		J	$-\frac{2J-1}{10(J+1)}$	0	0
		$J+1$	$\frac{J(2J-1)}{10(J+1)(2J+3)}$	0	0

Table 5.3 The upper-level population in the limit of intense excitation. The lower-level population before the laser excitation is 1. (Hirabayashi et al. 1986)

J_l	J_u	linearly-polarized light exc. $J=$ integer	linearly-polarized light exc. $J=$ half-integer	unpolarized light exc. $J=$integer	unpolarized light exc. $J=$ half-integer
$J-1$	J	$\frac{1}{2}$	$\frac{1}{2}$	$\frac{J(4J^2-2)}{(2J-1)^2(2J+1)}$	$\frac{2J+1}{4J}$
J	J	$\frac{J}{2J+1}$	$\frac{1}{2}$	$\frac{2J(J+1)}{(2J+1)^2}$	$\frac{1}{2}$
$J+1$	J	$\frac{2J+1}{2(2J+3)}$	$\frac{2J+1}{2(2J+3)}$	$\frac{(J+1)(4J^2+8J+2)}{(2J+3)^2(2J+1)}$	$\frac{2J+1}{4(J+1)}$

Table 5.4 Depolarization coefficients W_2 for unpolarized light excitation. (Hirabayashi et al. 1986)

J_l	J_u	J_f	Intense exc. J=integer	J=half-integer
$J-1$	J	$J-1$	$-\frac{J+1}{4J(2J-1)(2J^2-1)}$	0
		J	$\frac{1}{4J(2J^2-1)}$	0
		$J+1$	$-\frac{1}{4(2J+3)(2J^2-1)}$	0
J	J	$J-1$	$\frac{1}{4J(2J-1)}$	0
		J	$-\frac{1}{4J(J+1)}$	0
		$J+1$	$\frac{1}{4(J+1)(2J+3)}$	0
$J+1$	J	$J-1$	$\frac{1}{4(2J-1)(2J^2+4J+1)}$	0
		J	$-\frac{1}{4(J+1)(2J^2+4J+1)}$	0
		$J+1$	$\frac{J}{4(J+1)(2J+3)(2J^2+4J+1)}$	0

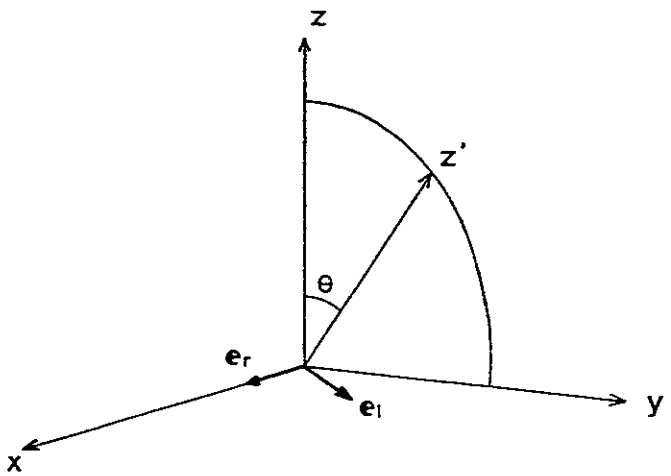

Fig.5.1 Excitation and observation geometry. The quantization axis is the z-axis. The propagation of the fluorescence light is along the z'-axis and the polarization vectors for observation are $\mathbf{e}_r$ and $\mathbf{e}_l$. The z'-axis and the z-axis are related through the rotation angle θ around the x-axis.

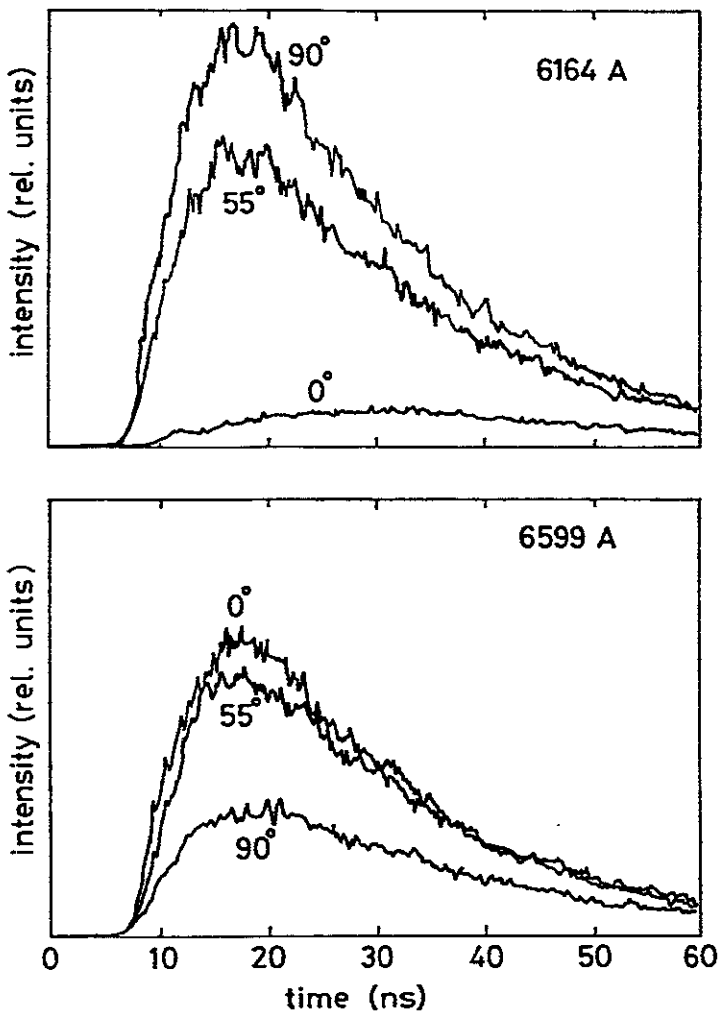

Fig.5.2 Temporal variation of observed fluorescence intensities following pulsed polarized-light excitation. The discharge tube is 5 mm in diameter, the neon pressure is 2 Torr and the discharge current is 0.3 mA. Dye laser light of ~ 5 ns duration excited the 6164 Å line. Fluorescence is observed with a monochromator-photomultiplier system from the direction with the angle θ to the direction of the laser-light polarization vector. (Fujimoto et al. 1985)

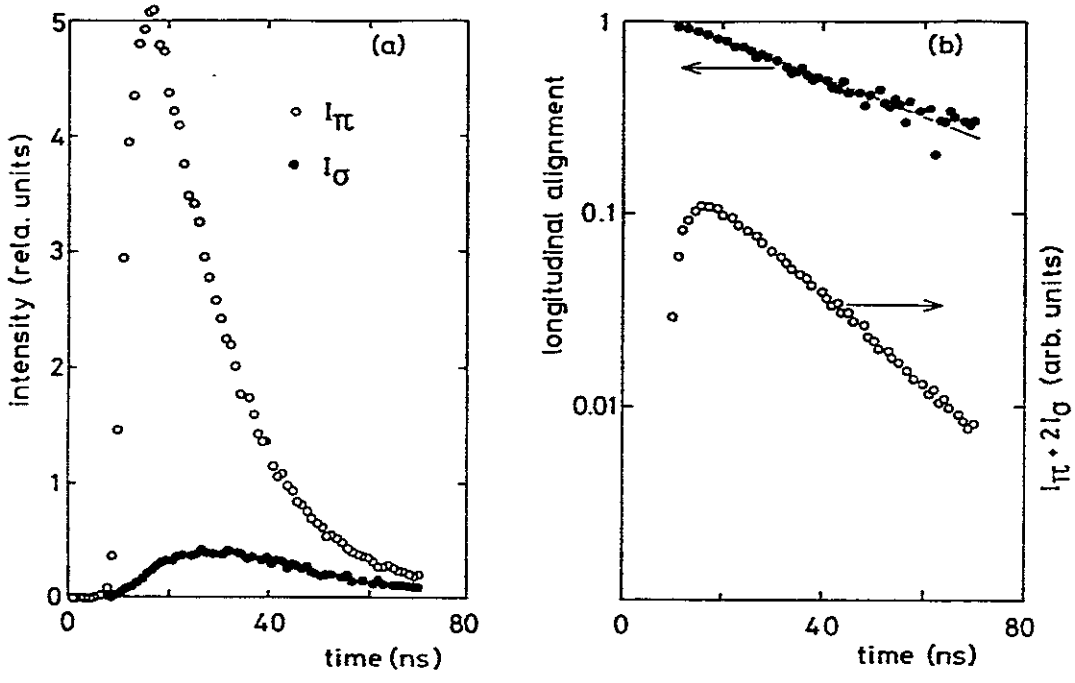

Fig.5.3 (a) Temporal variation of fluorescence intensitites I_π and I_σ of neon 6164 Å line following the π-light excitation.
(b) upper trace : longitudinal alignment. Lower trace : total population.
(Fujimoto et al. 1985)

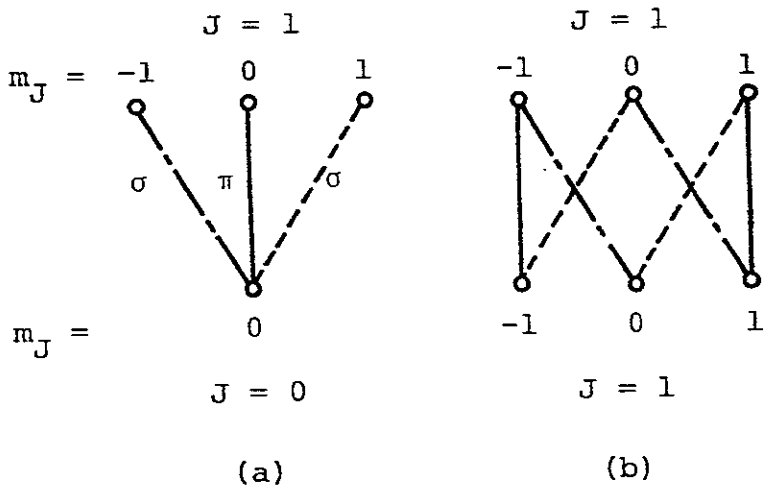

Fig.5.4 Kastler diagrams relevant to the cases of Figs.5.2 and 5.3.

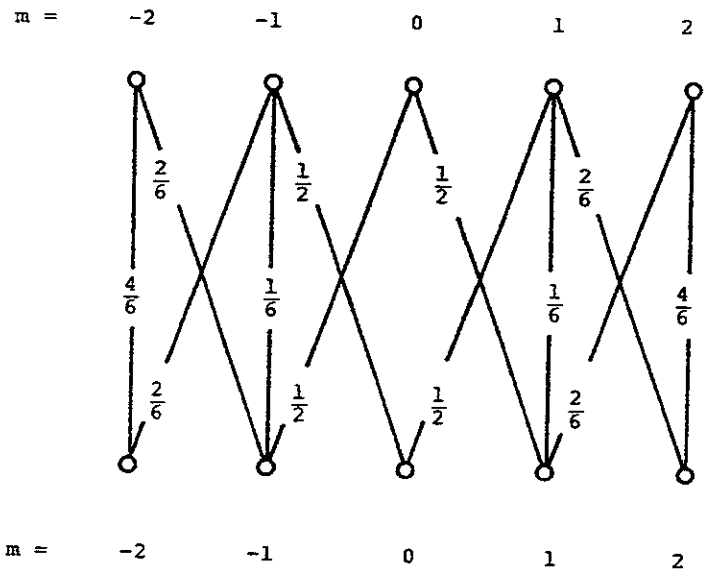

Fig.5.5 Kastler diagram for the $J_l = J_u = 2$ case. The relative transition probability between the upper and lower substrates is given.

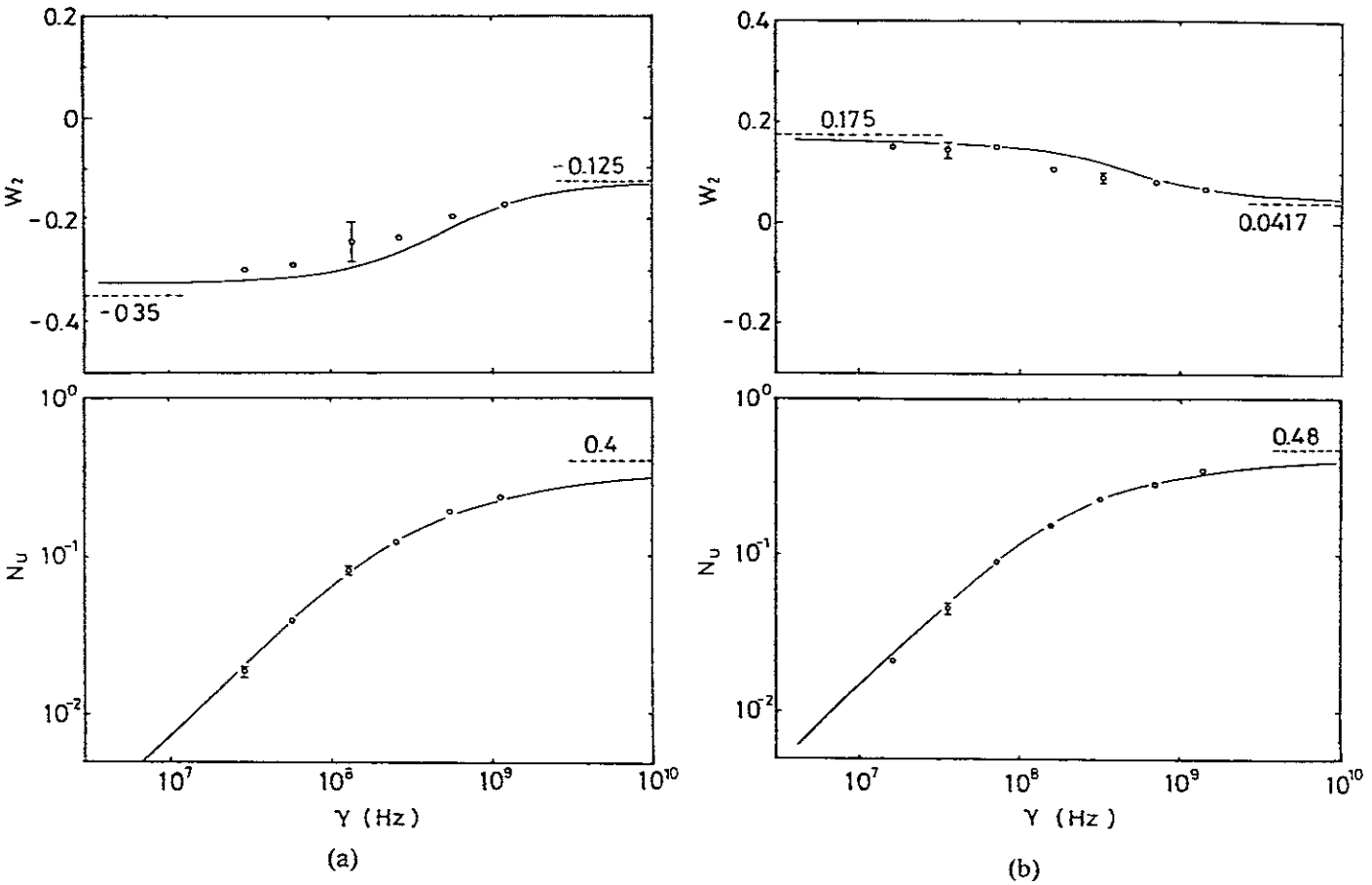

Fig.5.6 Laser-light intensity dependence of W_2 and the population of the upper level. (a) linearly-polarized light excitation and (b) unpolarized-light excitation. The dashed lines in the upper figures indicate the weak- and intense-excitation limits. In the lower figures, the dashed lines indicate the saturation limit of the upper-level population while the lower-level population before excitation is set at 1. (Hirabayashi et al. 1986)

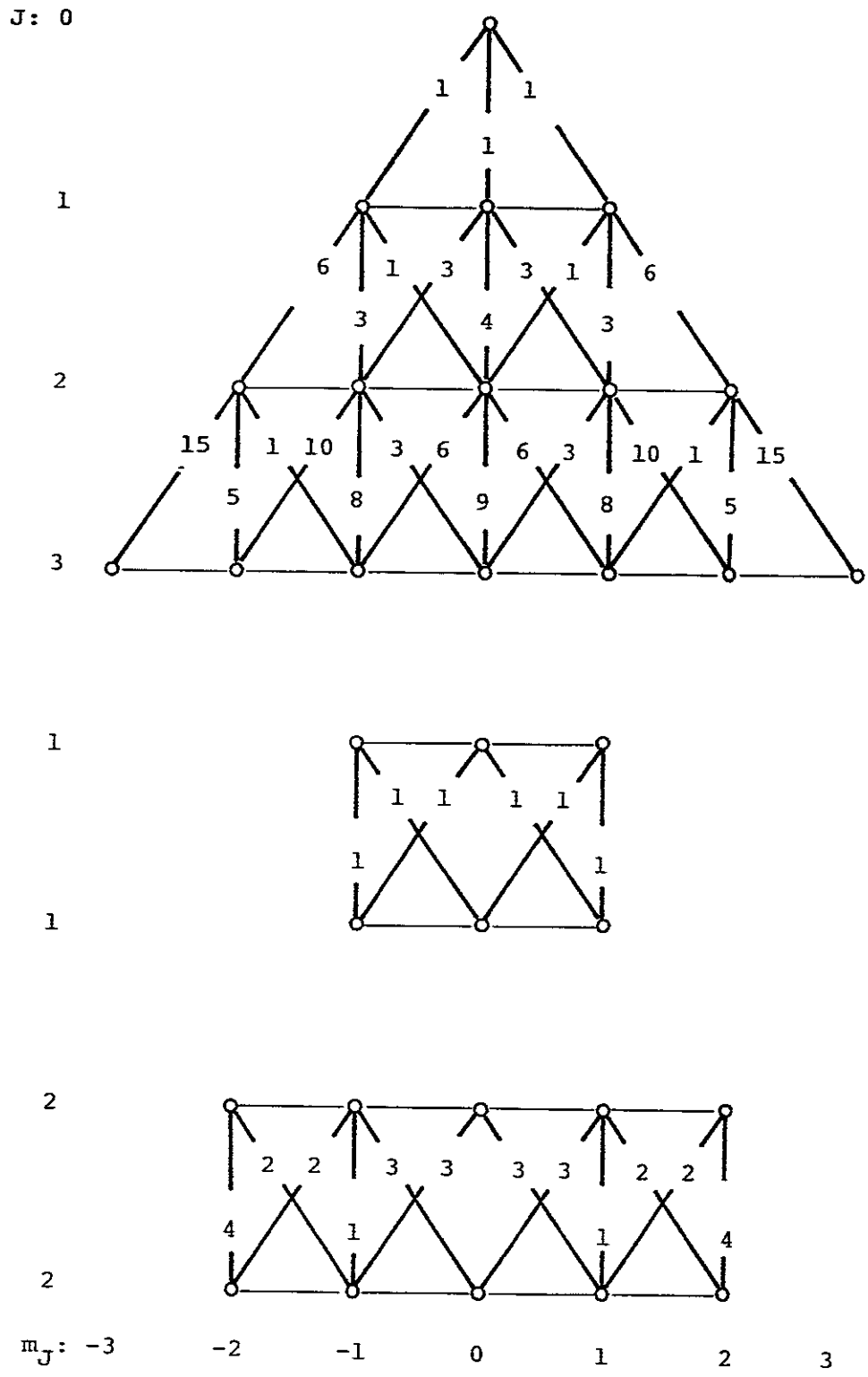

Fig.5.7 Kastler diagrams for several cases of electric dipole transition.

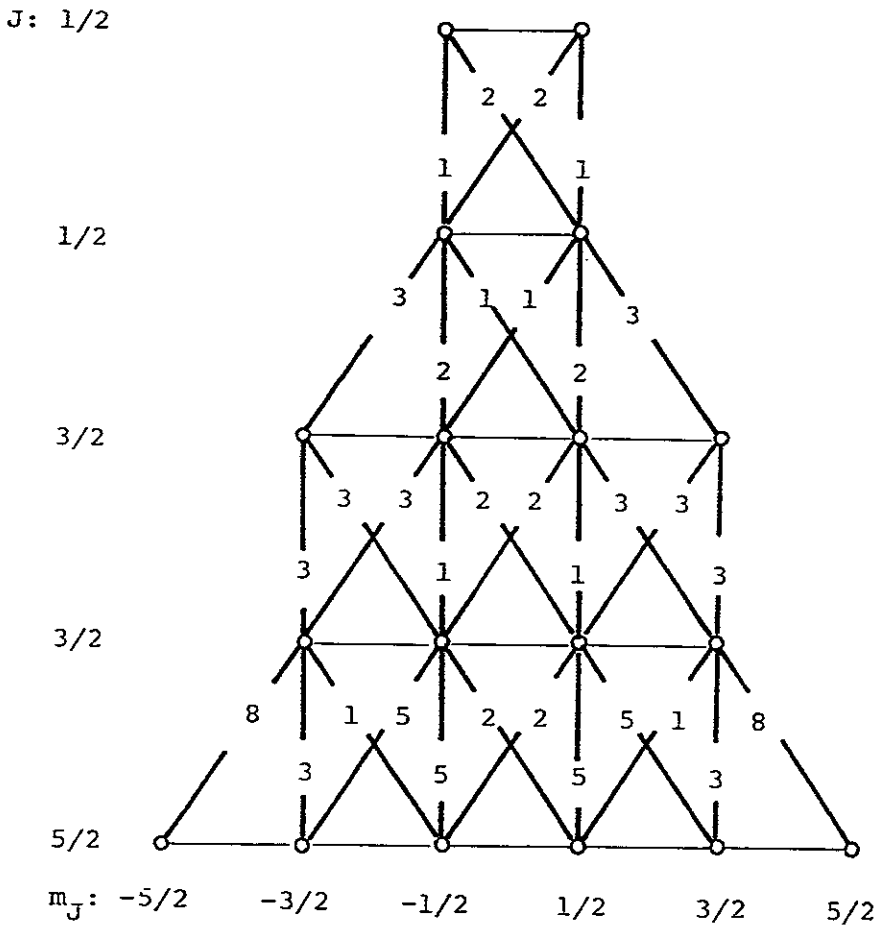

Fig.5.7 (cont.)

VI. RECOMBINATION AND BREMSSTRAHLUNG

6.1. Direct radiative recombination

The cross section is expressed analytically, in the nonrelativistic dipole approximation, for radiative recombination of an electron in a continuum states with a fully stripped ion to form a hydrogenic state which is specified by the quantum number (n, l, m). The differential cross section for recombination of the electron having the initial velocity v emitting a photon having the polarization vector **e** into the solid angle $d\Omega$ is given as (Cooper and Zare 1969)

$$d\,\sigma_{nl}(\mathbf{e}, \mathbf{v}) = \sigma_{nl}(\mathbf{e}, \mathbf{v})\,[1 + \beta_{nl}\,P_2(\mathbf{v}\cdot\mathbf{e}/v)]\,d\Omega / 4\pi \qquad (6.1)$$

where $\sigma_{nl}(\mathbf{e}, \mathbf{v})$ is the total recombination cross section integrated over the solid angle and summed over the degenerate m states, $P_2(x)$ is the second-order Legendre polynomial

$$P_2(x) = (1/2)(3x^2 - 1) \qquad (6.2)$$

and β_{nl} is the asymmetry parameter. The asymmetry parameter depends on the angular momentum l, the radial matrix elements and the Coulomb phase shifts. In general β_{nl} takes values between -1 and 2, and for s ($l = 0$) states $\beta_{ns} = 2$. Thus we have for $n = 1$

$$d\sigma_K(\mathbf{e}, \mathbf{v}) = \sigma_{1s}(\mathbf{e}, \mathbf{v})\,[1 + 2\;P_2(\mathbf{v}\cdot\mathbf{e}/v)]\,d\Omega / 4\pi \qquad (6.3)$$

For $n = 2$ we have

$$\begin{aligned} d\sigma_L(\mathbf{e}, \mathbf{v}) &= \sigma_{2s}(\mathbf{e}, \mathbf{v})\,[1 + 2\,P_2(\mathbf{v}\cdot\mathbf{e}/v)]\,d\Omega / 4\pi \\ &\quad + \sigma_{2p}(\mathbf{e}, \mathbf{v})\,[1 + \beta_{2p}\,P_2(\mathbf{v}\cdot\mathbf{e}/v)]\,d\Omega / 4\pi \\ &= \sigma_L(\mathbf{e}, \mathbf{v})\,[1 + \beta_L\,P_2(\mathbf{v}\cdot\mathbf{e}/v)]\,d\Omega / 4\pi \end{aligned} \qquad (6.4)$$

In Table 6.1 the aymmetry paramters β_{2p} and β_L are given (Milchberg and Weisheit 1982).

Suppose we observe the emission radiation from the direction perpendicular to v with its polarized components separately. Let $\mathbf{e}_{//}$ and $\mathbf{e}_{\perp}$ denote the polarization vectors whose directions are parallel and perpendiculat to **v**. The degree of polarization of the emitted continuum radiation is defined as

$$P = [I(\mathbf{e}_{//}) - I(\mathbf{e}_{\perp})] / [I(\mathbf{e}_{//}) + I(\mathbf{e}_{\perp})] \qquad (6.5)$$

$$= [d\sigma(\mathbf{e}_{//}) - d\sigma(\mathbf{e}_{\perp})] / [d\sigma(\mathbf{e}_{//}) + d\sigma(\mathbf{e}_{\perp})] \qquad (6.5a)$$

Figure 6.1 shows P as a function of β (the curve with $\theta = 0°$, see later for other curves.). (Lamoureux et al. 1989)

Scofield (1989) calculated the cross sections on the basis of the relativistic formulation for heliumlike nickel and neonlike barium. The electrons were treated as moving in a self-consistent Hartree-Fock central potential. Figure 6.2 shows the result of the ratio $d\sigma(\mathbf{e}_\perp) / d\sigma(\mathbf{e}_{//})$ for recombination from neonlike barium.

It may be interesting to note that if we define a quantity corresponding to the longitudinal alignment, eq. (5.10)

$$A_L = [d\sigma(\mathbf{e}_{//}) - d\sigma(\mathbf{e}_\perp)] / [d\sigma(\mathbf{e}_{//}) + 2d\sigma(\mathbf{e}_\perp)] \tag{6.6}$$

this has a very simple expression

$$A_L = \beta / 2 \tag{6.7}$$

We now consider the recombination continuum radiation emitted from a plasma. We assume the plasma to have a cylindrical symmetry (Lamoureux et al. (1989) uses the term the toroidal symmetry.). Figure 6.3 shows the geometry; $\mathbf{k}$ is the direction of photon propagation (different from the definition in Lamoureux et al.), $\mathbf{e}_{//}$ and $\mathbf{e}_\perp$ are the orthogonal directions of the polarization vector and $\mathbf{u}$ is the axis of symmetry of the plasma lying in the plane of ($\mathbf{k}$, $\mathbf{e}_{//}$). The direction of the electron velocity is defined by the vector $\mathbf{v}$ making the pitch angle θ from this axis, and the velocity distribution is assumed to be symmetrical around the axis.

The degree of polarization for this angular distribution of electron velocities is

$$P = \frac{1.5\,\beta_n(v)\sin^2\psi\,(3\cos^2\theta - 1)}{2\,\{[2 - \beta_n(v)] + 1.5\,\beta_n(v)\,(1 - \cos^2\theta)\} + 1.5\,\beta_m(v)\sin^2\psi\,(3\cos^2\theta - 1)} \tag{6.8}$$

For observation from the direction of the symmetry axis, $\Psi = 0°$, we have no polarization, as expected. Figure 6.1 shows the result of eq. (6.8) for the case of perpendicular observation, $\Psi = 90°$. When the cone pitch angle is the magic angle, $\theta = 54.7°$, we have no polarization.

We now expand the distribution function of electron velocities in terms of the Legendre polynomials

$$f(v, \theta) = \sum_i f_i(v)\ \ P_i(\cos\theta) \tag{6.9}$$

Then the polarization degree is expressed as

$$P = \frac{3\,[f_2(v)/f_0(v)]\,[\beta_n(v)\sin^2\psi]}{20 + [f_2(v)/f_0(v)]\,[\beta_n(v)(1 - 3\cos^2\psi)]} \tag{6.10}$$

For the perpendicular observation we have

$$P = \frac{3\,(f_2/f_0)\,\beta}{20 + (f_2/f_0)\,\beta} \tag{6.11}$$

or

$$A_L = (\beta/10)\,(f_2/f_0) \tag{6.11a}$$

The direct radiative recombination of beam electrons produces the polarized atoms or ions. Scofield (1991) calculated the longitudinal alignment parameter, defined by eq. (2.9) or ρ_0^2 / ρ_0^0 , for several cases. In his calculation he included the cascading contributions from higher-lying state ions which were also produced by recombination. Figure 6.4 shows an example of the results for the case of hydrogenlike and heliumlike titanium.

6.2. Bremsstrahlung

The incoming electron having velocity **v** in the direction Ω is scattered by the ion with the nuclear charge z into the direction Ω' with its final velocity **v'** with a photon being emitted in the direction **k** with its polarization **e**. The analytical expression for the differential cross section is given in the nonrelativistic Born approximation (Lamoureux et al. 1989)

$$\frac{d\sigma(\mathbf{k}, \mathbf{v}, \mathbf{e}, \Omega, \Omega')}{d(h\nu)} = \frac{z^2 \alpha^3 \hbar^2}{m^2 \pi^2} \frac{v'}{v} \frac{1}{h\nu} \cdot \frac{(\mathbf{v}\cdot\mathbf{e} - \mathbf{v}'\cdot\mathbf{e})^2}{|\mathbf{v} - \mathbf{v}'|^4}\, \varepsilon(v, v') \tag{6.12}$$

with α being the fine-structure constant and the Elwert factor

$$\varepsilon(v, v') = \frac{v}{v'} \frac{1 - \exp[-2\pi z\,(2R/mv^2)^{1/2}]}{1 - \exp[-2\pi z\,(2R/mv'^2)^{1/2}]} \tag{6.13}$$

Figure 6.5 shows the angular distribution of the emitted photon intensities for the example that z = 28 and 95 % of the initial energy is transformed into the photon

energy. The dash-dotted curve shows the result of eq. (6.12). Figure 6.6 shows the degree of polarization. These results are independent of energy. In these figures results of calculations based on other models are compared with the present one. The dashed curves correspond to the parametric expressions which are based on an approximate solution to the full nonrelativistic dipole Sommerfeld theory. This method was adoped by several workers for their calculation. (Kirkpatrick and Wiedmann 1945, Eidmann 1975) The solid curves show the result of the calculation with the relativistic central field model. It is seen that the intensity distribution by the relativistic theory shows asymmetries around the perpendicular direction ("forward scattering") and that the nonrelativistic Born approximation significantly overestimates the polarization degree.

Figure 6.7 shows the degree of polarization of radiation emitted perpendicularly as a function of the photon energy relative to the initial kinetic energy of the electron (the curve $\theta = 0°$. For other curves see later.). (Lamoureux et al. 1989) This calculation is based on the Born approximation, eq. (6.12).

Similar results have been reported on the basis of the Sommerfeld theory (Kirkpatrick and Wiedmann 1945, Eidmann 1975) and of the relativistic calculation (Gluckstern and Hull 1953). Figure 6.8 shows an expmple of the latter calculation for the electron kinetic energy of mc^2 (0.53 MeV). (The sign of the definition of polarization is reversed from eq. (6.5).) In harmony with the relativistic calculation in Fig. 6.6 the higher degree of polarization for the forward scattering is apparent.

We now consider the plasma with the cylindrical symmetry and adopt Fig. 6.3 for the coordinate system. Again we rely on the Born approximation. For the electron velocity with the cone pitch angle θ, we have the degree of polarization.

$$P=\frac{\sin^2\psi\,(1-3\cos^2\theta)\left[-3+\frac{-v^2+3v'^2}{2vv'}\ln\left[\frac{v+v'}{v-v'}\right]\right]}{(1-3\cos^2\theta)(2-3\sin^2\psi)+\frac{2(3v^2-v'^2)+2(-v^2+3v'^2)\cos^2\theta+(-v^2+3v'^2)\sin^2\psi(1-3\cos^2\theta)}{2vv'}\ln\left[\frac{v+v'}{v-v'}\right]} \qquad (6.14)$$

Figure 6.7 shows the polarization degree according to eq. (6.14) for the perpendicular observation, $\Psi = 90°$. It is seen that when the relative photon energy is 12 % of the initial electron energy or when the pitch angle is the magic angle we have no polarization. We note that the expression (6.14) for the tip ($v' = 0$) reduces to eq. (6.8) with $\beta = 2$ for the radiative recombination.

6.3. Dielectronic recombination

When radiative recombination occurs through a resonance in electron scattering, the process is called dielectronic recombination. Essentially this process should not be distinguished from the direct radiative recombination discussed in the previous section. However, since the photon emission during dielectronic recombination is observed as a line (satellite line), the process is sometimes treated as a separate one. Since dielectronic recombination is a resonance process, the observation of the polarization of the satellite line provides information relating to the electrons with a specific discrete (resonance) energy.

We consider the following process:

$$e + A^{z+}(J_0) \rightarrow [A^{(z-1)+}]^{**}(J) \rightarrow [A^{(z-1)+}]^{*}(J') + \gamma, \tag{6.15}$$

where $[A^{(z-1)+}]^{**}$ indicates the ion in a resonance state, J_0, J, and J' are the total angular momentum of the corresponding states, respectively. Inal and Dubau (1989) investigated the polarization of the satellite line. They treated the case that the target ion has no total angular momentum *i.e.*, J_0=0 and the radiative emission occurs through the electric dipole interaction. When there is no overlapping in the resonances (*i.e.*, the satellite lines are well separated each other), the degree of polarization has the following form

$$P = -3\sqrt{15}\,(2J+1) \begin{pmatrix} 2 & J & J \\ 0 & 1/2 & -1/2 \end{pmatrix} \begin{Bmatrix} 2 & J & J \\ J' & 1 & 1 \end{Bmatrix}$$
$$\times \left[2\sqrt{2}\,(-1)^{J'-1/2} - \sqrt{15}\,(2J+1) \begin{pmatrix} 2 & J & J \\ 0 & 1/2 & -1/2 \end{pmatrix} \begin{Bmatrix} 2 & J & J \\ J' & 1 & 1 \end{Bmatrix} \right]^{-1} . \tag{6.16}$$

It should be noted that the polarization does not depend on the collision cross sections and the probabilities of autoionization and radiative emission. (This is not true when the resonances overlap each other.) Table 6.2 shows some values of the polarization calculated from eq.(6.16).

Next, we discuss the satellite line radiation emitted from plasmas. As in the previous section, we assume cylindrical symmetry about the z axis for the spatial distribution of electrons. Consider that the detection direction makes an angle θ from the z axis and the direction of the incident electron is represented by a pitch angle α. Then, the

Stokes parameter η_3 is given by

$$\eta_3(\theta,\alpha) = \frac{P(3\cos^2\alpha - 1)\sin^2\theta}{2 - P[2\cos^2\theta\cos^2\alpha + \sin^2\alpha(1-\cos^2\alpha)]}. \tag{6.17}$$

Inal and Dubau (1989) assumed the pitch angle distribution in the following form

$$f(\alpha) = \frac{a}{4\pi} + (1-a)g(\alpha), \tag{6.18}$$

where a is a mixing coefficient ($0 \leq a \leq 1$) and

$$g(\alpha) = \frac{u+1}{2\pi}\cos^u\alpha\,\Theta(\tfrac{\pi}{2} - \alpha). \tag{6.19}$$

In eq.(6.19), $\Theta(x)$ is a step function and u is a constant parameter. Figure 6.9 shows the calculated polarization of the satellite lines j ($J = \frac{5}{2} \rightarrow J' = \frac{3}{2}$) and k ($\frac{3}{2} \rightarrow \frac{1}{2}$). These lines, for example, correspond to the $1s2p^2\ {}^2D_{\frac{5}{2}} \rightarrow 1s^22p\ {}^2P_{\frac{3}{2}}$ (j) and $1s2p^2\ {}^2D_{\frac{3}{2}} \rightarrow 1s^22p\ {}^2P_{\frac{1}{2}}$ (k) transitions of iron and calcium ions that are observed prominently from tokamak or solar plasmas.

Some satellite line emission can also be produced by inner-shell electron excitation. (For example, the 1s2s2p state can be produced by the excitation of the $1s^22s$ state.) In that case, we must consider both the effects due to the dielectronic recombination and due to the inner shell excitation in order to analyze the polarization of observed spectral lines. Inal and Dubau (1987) calculated the polarization of the line emission $1s2s2p \rightarrow 1s^22s$ of Fe^{23+} produced by the inner-shell electron excitation.

When the resonances overlap each other, the satellite lines are blended and the interference effect may be important. Such an example is seen in the satellite lines $1s2pnl \rightarrow 1s^2nl$ ($n \geq 4$) of an iron ion. The expression of the polarization in this case becomes complicated and furthermore the polarization depends on the collision cross section and on the probabilities of autoionization and radiative emission. Inal and Dubau (1989) also studied the polarization of the satellite lines for the overlapping resonances. They found that the interference effect makes an enhancement of the polarization.

The satellite lines emitted from the ion $A^{(z-1)+}$ in a high Rydberg resonance state are actually indistinguishable from the resonance line emitted from the ion A^{z+}. These satellite lines make an apparent increase in the resonance line intensity (Bely-Dubau *et al.* 1979, Dubau *et al.* 1981). They may also cause an apparent change of the polarization of the resonance line.

References

Bely-Dubau F., Gabriel A.H. and Volonté S.,1979, Mon. Not. Roy. Astr. Soc. **189**, 801

Dielectronic satellite spectra for highly charged helium-like ions.

V. Effect of total satellite contribution on the solar flare iron spectra

Cooper J. and Zare R.N., 1968 *Lectures in Teoretical Physics –Atomic Collision Processes*, Ed. by S. Geltmann, K.T. Mahanthappa and W.E. Brittin (Gordon and Breach, N.Y.) p.317.

Photoelectron angular distributions

Dubau J., Gabriel A.H., Loulergue M., Steeman-Clark L. and Volonté S., 1981, Mon. Not. Roy. Astr. Soc. **195**, 705.

Dielectronic satellite spectra for hydrogen-like iron in low density plasmas

Eidmann K., 1975, Plasma Phys. **17**, 121.

Calculation of free-free radiation from plasmas with non-Maxwellian isotropic or anisotropic electron velocity distributions

Gluckstern R.L. and Hull Jr., M.H., 1953, Phys. Rev. **90**, 1030.

Polarisation dependence recombination of the integrated bremsstrahlung cross section

Inal M.K. and Dubau J., 1987, J. Phys. B **20**, 4221,

Theory of excitation of He-like and Li-like atomic sublevels by directive electrons: application to x-ray line polarization

Inal M.K. and Dubau J., 1989, J. Phys. B **22**, 3329.

Polarization of dielectronic satellite lines

Kirkpatrick P. and Wiedmann L., 1945, Phys. Rev. **67**, 321.

Theoretical continuous x-ray energy and polarization

Lamoureux M., Jacquet L. and Pratt R.H., 1989, Phys. Rev. A **39**, 6323.

Angular distribution and polarization of the continuum emission in anisotropic plasmas

Milchberg H.M. and Weisheit J.C., 1982, Phys. Rev. A **26**, 1023.

Polarization of recombination radiation from nonequilibrium plasmas

Scofield J.H., 1989, Phys. Rev. A **40**, 3054.

Angular and polarization correlations in photoionization and radiative recombination

Scofield J.H., 1991, Phys. Rev. A **44**, 139.

Angular distribution of cascade x rays following radiative recombination from a beam

Table 6.1 Hydrogenic asymmetry parameters. $\hbar\omega$ is the photon energy and $\hbar\omega_2$ is the binding energy of the electron in level n = 2. (Milchberg and Weisheit 1982)

ω/ω_2	β_{2p}	β_L
1.00	0.484 85	0.888 89
1.02	0.491 86	0.899 77
1.04	0.498 80	0.910 47
1.06	0.505 66	0.921 01
1.08	0.512 46	0.931 38
1.10	0.519 17	0.941 60
1.15	0.535 66	0.966 46
1.20	0.551 72	0.990 38
1.25	0.567 38	1.013 4
1.30	0.582 63	0.035 6
1.40	0.612 02	1.077 7
1.50	0.640 00	1.116 9
1.75	0.704 40	1.203 9
2.00	0.761 90	1.277 8
2.50	0.860 22	1.396 0
2.90	0.926 15	1.469 6
3.00	0.941 18	1.485 7
3.10	0.924 86	1.486 3
3.50	0.864 86	1.490 9
4.00	0.800 00	1.500 00

Table 6.2 Polarization of dielectronic satellite lines (Inal and Dubau 1989)

J'	J=3/2	J=5/2	J=7/2
1/2	3/5	—	—
3/2	−3/4	1/2	—
5/2	1/7	−8/9	5/11

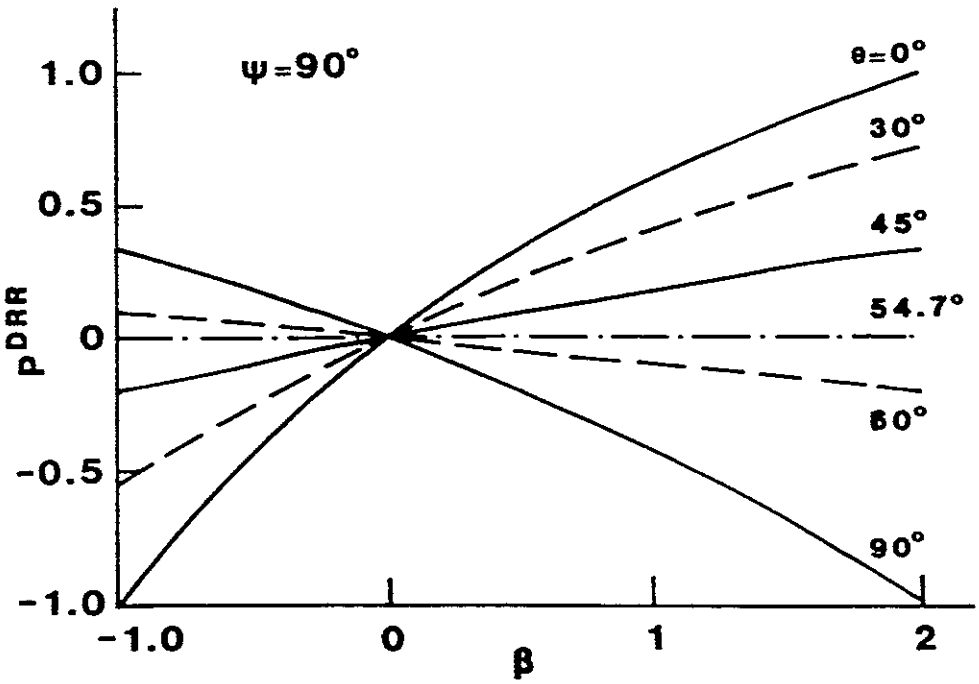

Fig.6.1 Degree of polarization of Direct radiative recombination emission obtained from eq.(6.8) for various values of the pitch angle θ vs the asymmetry parameter β, for the perpendicular direction of observation $\Psi = 90°$. (Lamoureux et al. 1989)

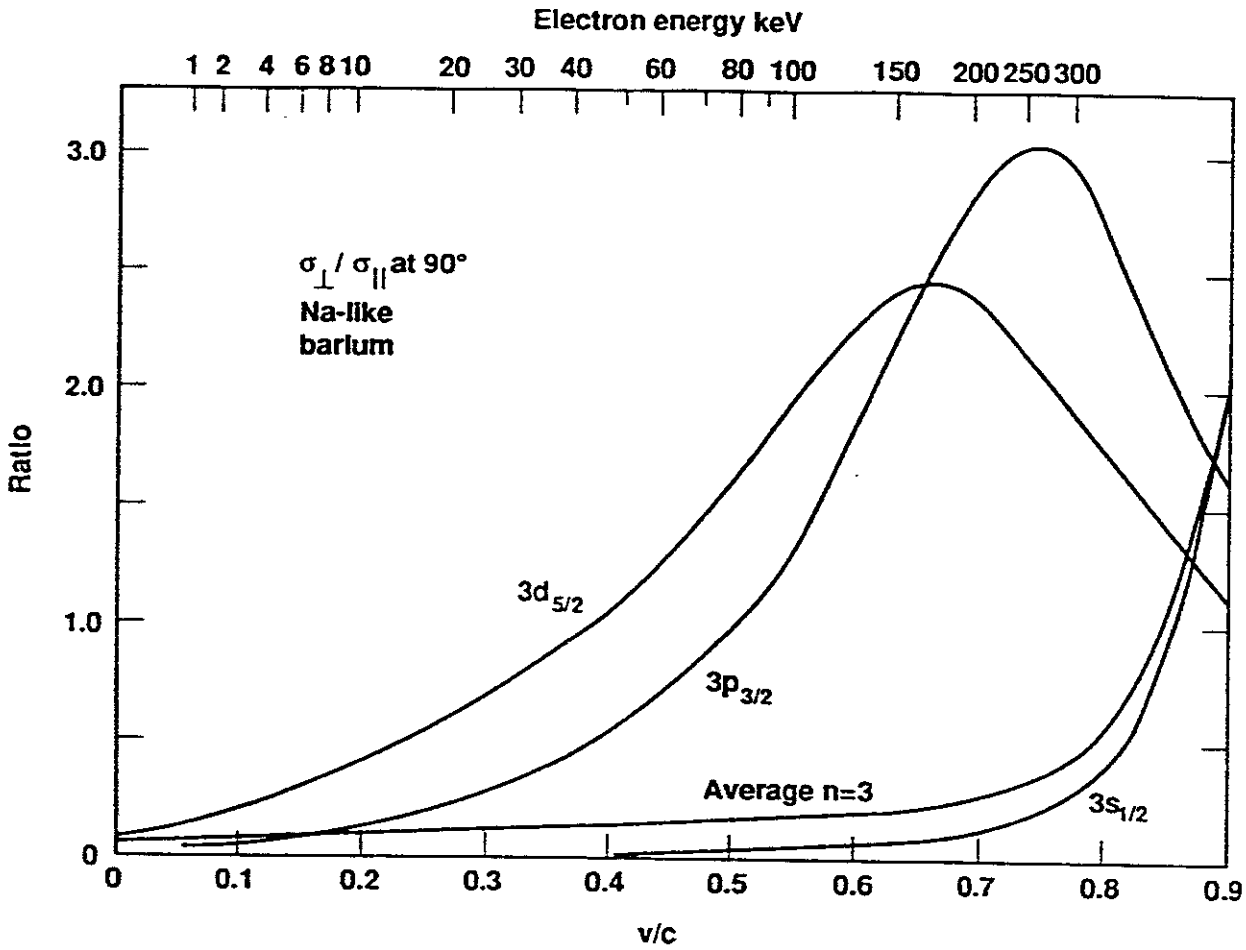

Fig.6.2 The ratio of emission of x rays at $\psi = 90°$ polarized perpendicular to the plane defined by the electron and photon momenta to that parallel to the plane. (Scofield 1989)

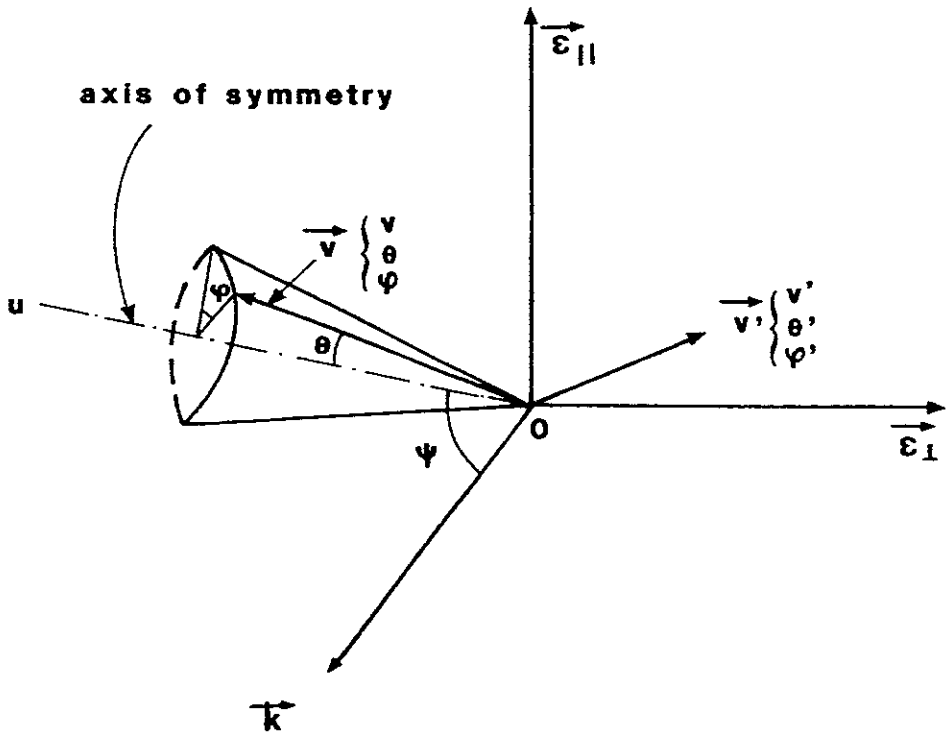

Fig.6.3 Geometry of observation of continuum emission. The axis of symmetry of the toroidal plasma lies in the ($\mathbf{k}$, $\mathbf{e}_{//}$) plane.

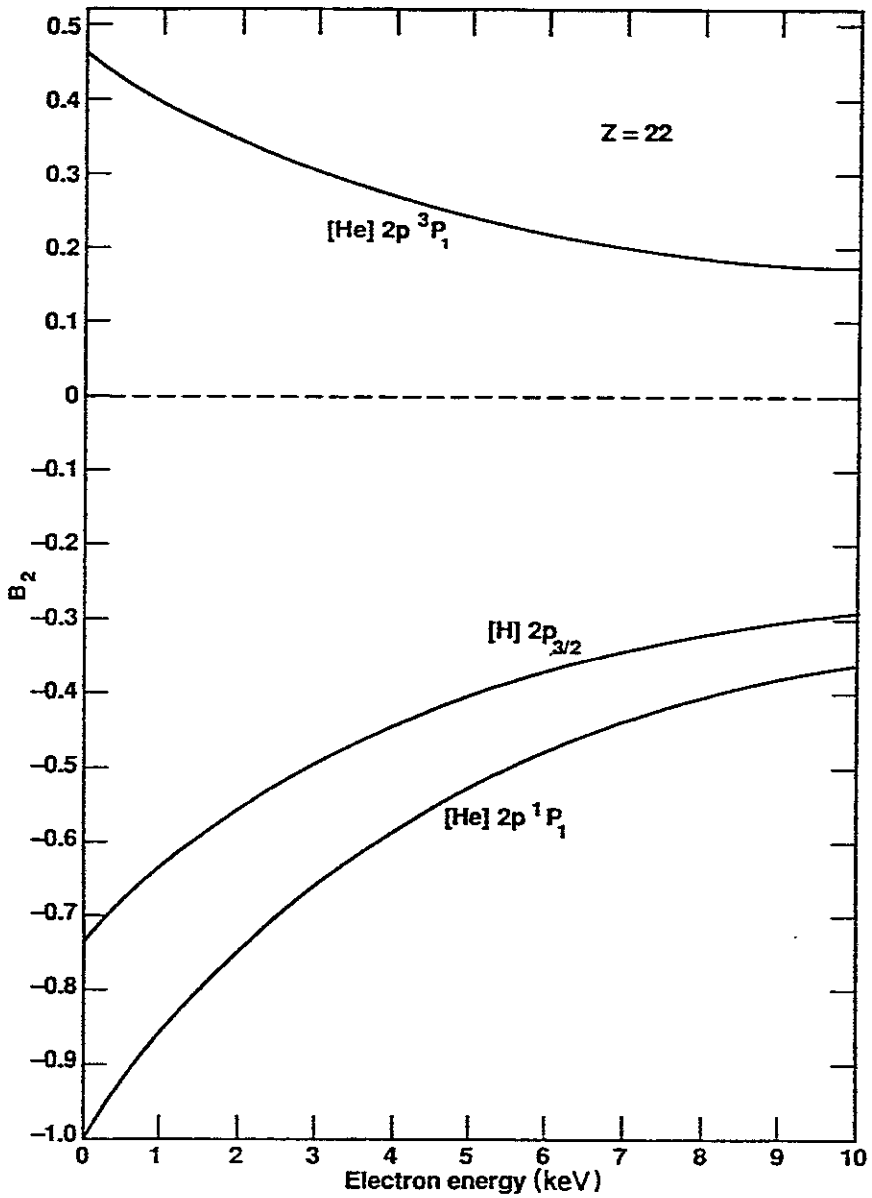

Fig.6.4 Longitudinal alignment parameter ρ_0^2 / ρ_0^0 of hydrogen and heliumlike states of titanium populated by radiative recombination as afunction of incoming electron energy. (Scofield 1991)

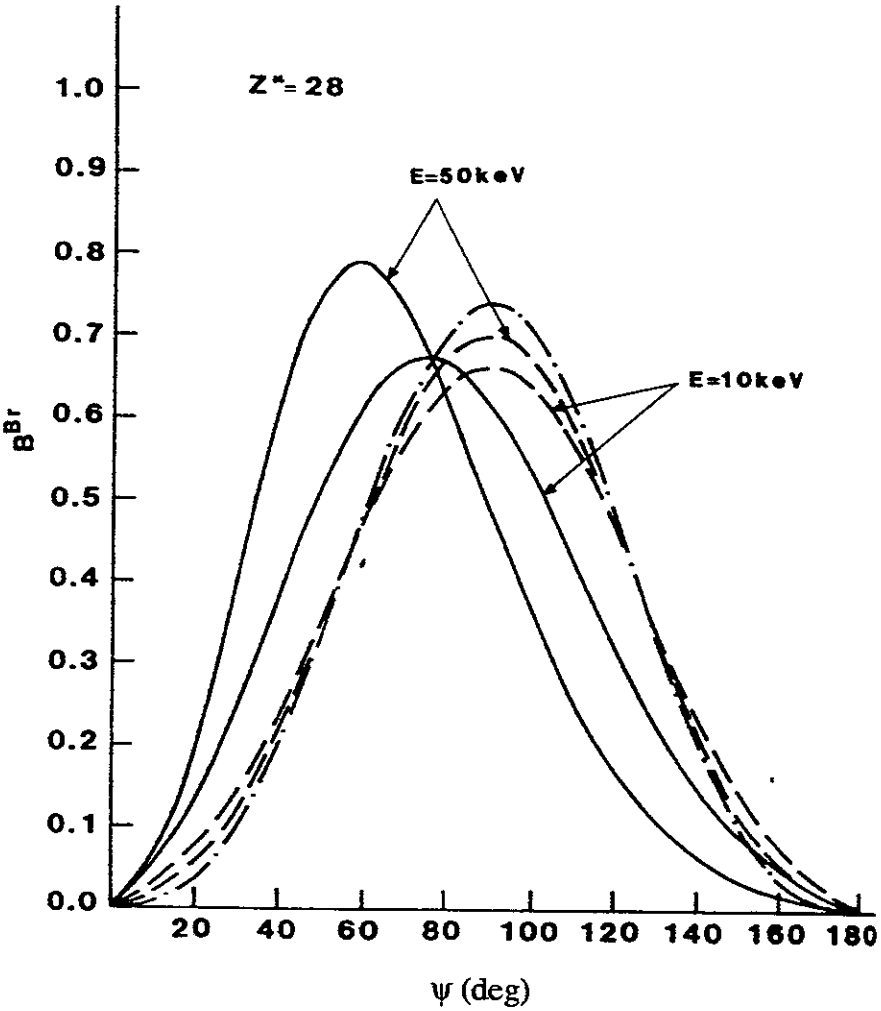

Fig.6.5 Angular distributions $B(\psi)$ for the bremsstrahlung collision, as a function of ψ, the angle of the photon emission with respect to the direction of the incident electron. The incident electron energies are E = 10 and 50 keV, the proportion of energy radiated is $h\nu / E = 95\ \%$. —, relativistic numerical results ; ---, dipole Sommerfeld theory ; and — · —, nonrelativistic Born approximation.
(Lamoureux et al. 1989)

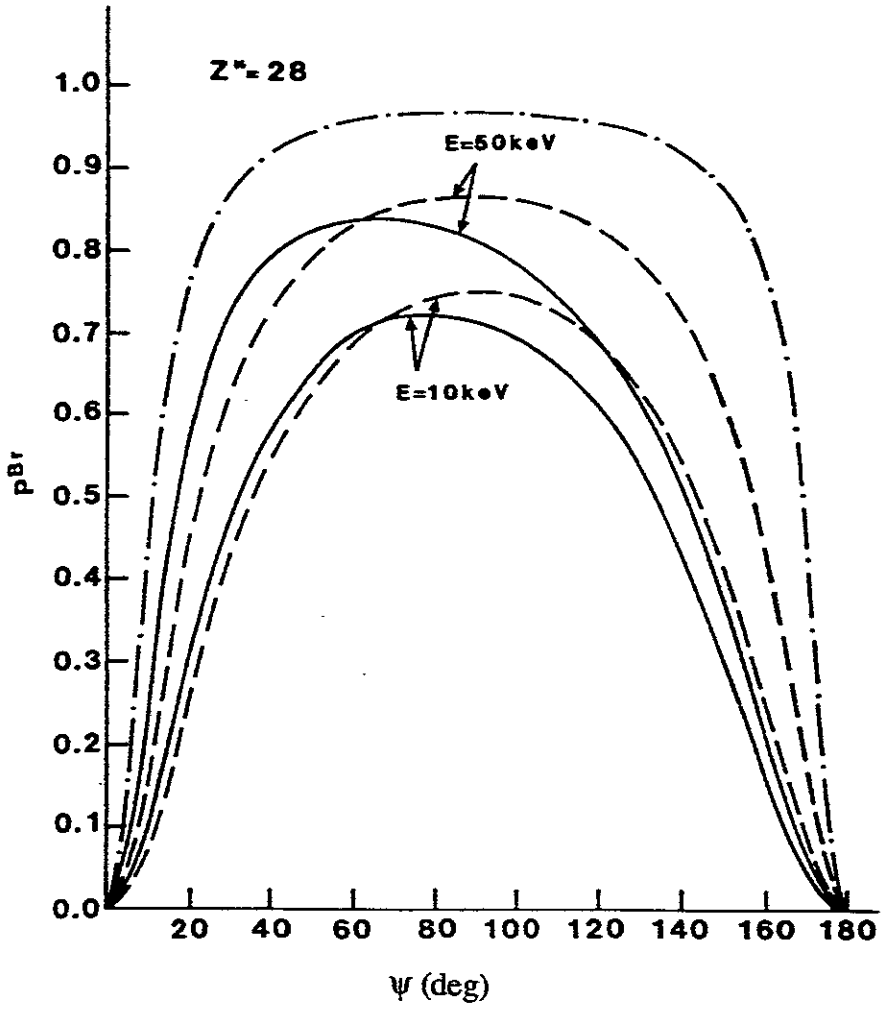

Fig.6.6 Same as in Fig.6.5 but for the degree of polarization. (Laumoureux et al. 1989)

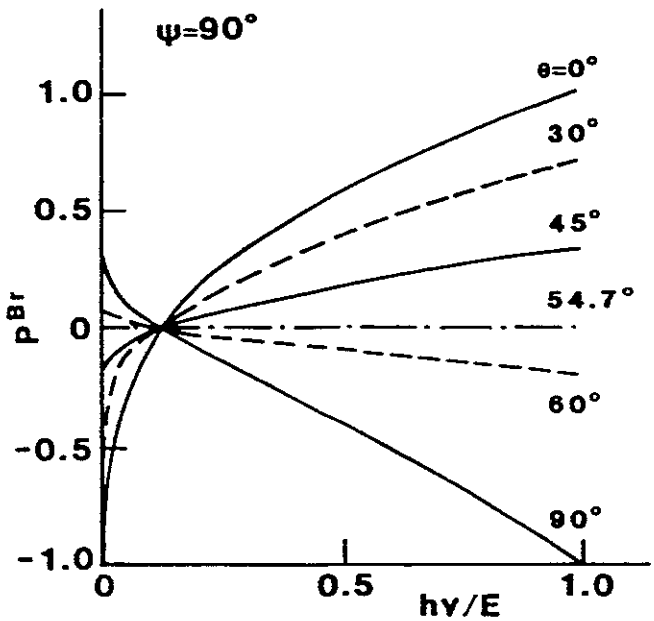

Fig.6.7 Degree of polarization of the Br emission obtained from eq.(6.14) as a function of the energy radiated hν / E for various values of the pitch angle θ, for the perpendicular direction of observation ψ = 90°. (Lamoureux et al. 1989)

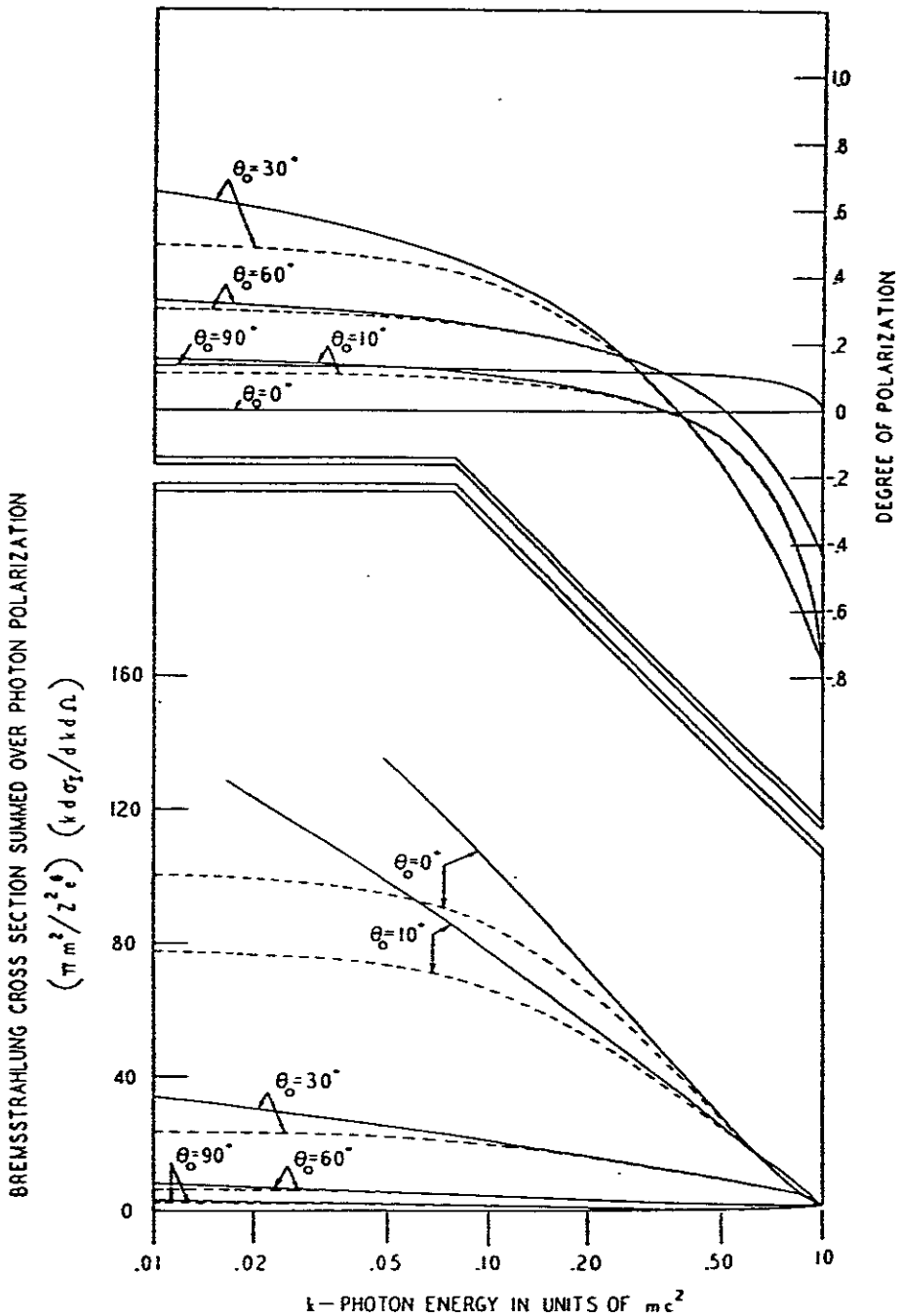

Fig.6.8 Bremsstrahlung cross section (lower half of figure) and degree of polarization (upper half of figure, sign reversed) for incident electrons with $E_0 = 2\ mc^2$ (≈ 0.5 MeV) vs photon energy for photon angles $\theta_0 = 0°, 10°, 30°, 60°, 90°$. The solid curves are without shielding and the dashed curves are with shielding for $Z = 13$.
(Gluckstern and Hull 1953)

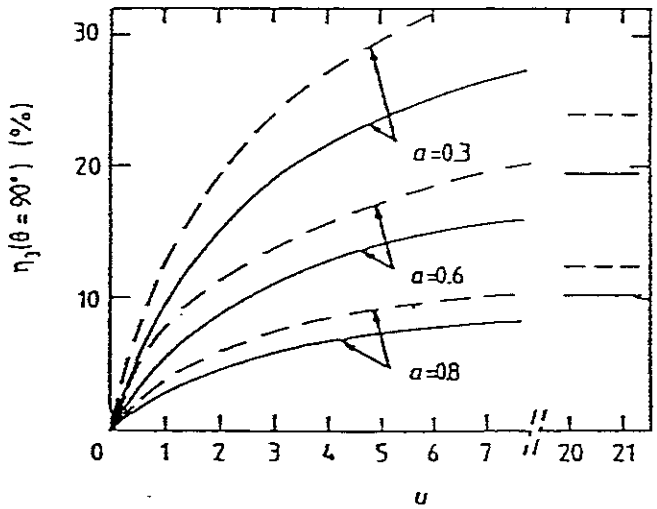

Fig.6.9 Polarization of the satellite lines
j ($J = \frac{5}{2} \rightarrow J' = \frac{3}{2}$) (—) and k ($\frac{3}{2} \rightarrow \frac{1}{2}$) (- - -)
as a function of the parameters a and u given in eqs.(6.18) and (6.19) (Inal and Dubau 1989).

VII. RELAXATION

7.1. Introduction

The multipole moments of the polarized atoms and ions (population, orientation and alignment) are relaxed in plasma by various processes. In this section, we review the relaxation phenomena brought about by isotropic collisional and radiative processes. The relaxation of a multipole moment is described by the rate equation involving a diagonal matrix, or a scalar quantity (We remember that ρ^k_q's are unnormalized.)

$$d\rho^k_q / dt = -g^k \rho^k_q \qquad (7.1)$$

where g^k is the relaxation rate of the multipole and is independent of q. The traditional experimental method to determine the relaxation rate is the Hanle effect (zero-field level crossing) experiment. A plasma or a vapor is illuminated by resonance radiation having a particular polarization from a particular direction, and orientation or alignment is created in the excited atoms. Direct fluorescence radiation is observed, where a variable magnetic field is applied and the intensity of a polarized component is recorded. Depending on the geometry of the arrangement, the observed intensity shows a Lorenzian profile or a dispersion profile as a function of the magnetic field strength. The half width of the Lorenzian profile corresponds to the relaxation rate of the orientation or the alignment, g^1 or g^2. The quantity g^1 is called the orientation destruction rate and g^2 the alignment destruction rate. The value of g^1 or g^2 is plotted as a function of the atom density. From the intercept of the fitted line at the low-pressure limit the natural lifetime is determined with the aid of the Landé g-factor. From the slope the collisional rate coefficient for destruction of orientation or alignment is determined. The collisional depopulation rate g^0 cannot be determined by this method.

Another method which is very similar to the above is the self-alignment method. (Kallas and Chaika 1969. Carrignton and Corney 1969) As will be discussed in §8.2 this method is based on the alignment created in excited atoms by the anisotropy of the plasma itself. The origin of the alignment may be the anisotropic velocity distribution of electrons which excite the atoms. Sometimes the degree of optical thickness of a transition line strongly depends on the direction in the plasma owing to the anisotropic plasma geometry, and this anisotropy results in the aligned excited atoms. Upon application of a variable magnetic field the Hanle signal is observed. The experimental procedure is the same as the above.

The laser-induced-fluorescence spectroscopy (LIFS) method is also applied to the study of relaxation of multipoles of excited atoms in plasma. Polarized pulsed laser

radiation, the pulse duration of which is shorter than the atomic lifetime, excites the atoms, and the subsequent time dependent direct fluorescence radiation is observed with its two polarization components separately. We now consider the example of Fig. 5.3; we excite atoms in level l with $J_l = 0$ by the π - light to a level with $J_u = 1$, and we observe the direct fluorescence with its π - and σ - polarized components, separately. The depolarization coefficient or the lognitudinal alignment defined by eq. (5.10) or (5.11) should be 1 for this excitation-observation scheme. From Fig. 5.3a we calculate the longitudinal alignment according to eq. (5.10), and this quantity is plotted in Fig. 5.3b. It is seen that this quantity decays exponentially with time starting from this value.

The temporal decay of the longitudinal alignment, which we call disalignment, is the decay of ρ_0^2 / ρ_0^0 . See eq. (5.11). Its rate is given as

$$h^2 = g^2 - g^0 \qquad (7.2)$$

and we call this quantity the disalignment rate.

In the present example, the observed disalignment rate is plotted against the filling gas pressure as shown in Fig. 7.1. (Fujimoto et al. 1983) Two different sets of the experimental data are fitted to lines having the same slope and different intercepts. From the slope the disalignment rate coefficient for atomic collisions is determined. The significance of the intercept is discussed in §7.5.

Recently, a comparison was made between the result of the relaxation rates determined by the self-alignment method and those by the LIFS method (Fujimoto and Matsumoto 1988); by the former method the alignment destruction rate g^2 due to atomic collisions is determined, and by the latter method the disalignment rate h^2 and the depopulation rate g^0 are determined separately. It was found that the alignment destruction rates determined by these two methods were not consistent within the experimental uncertainties. These authors argue as follows; The LIFS method is simple in its principle and straightforward in the interpretation of the observation. On the other hand, the self-alignment method is based on the assumption that the rate of creation of alignment is independent of the strength of the applied magnetic field. However, the mechanism of the creation of the alignment is not fully understood, and this assumption has yet to be justified. Thus, they raise a question on the validity of the self-alignment phenomenon as a reliable method for the observation of the alignment relaxation.

In the following we review the present status of our knowledge about the relaxation of polarized atoms and ions by various mechanisms. We put some emphasis

on the disalignment because, in plasma spectroscopy, alignment is more likely to be important than orientation.

7.2. Atomic collisions

There is a large body of experimental data on the destruction of orientation and alignment of excited state atoms due to atomic collisions as determined by the Hanle effect method and also by the self-alignment method. The cross section data are summarized in review articles by Baylis (1979) and by Kazantsev (1983). As noted above, however, the alignment destruction rate coefficients determined by the latter method should be treated with caution. The number of the rate coefficients determined by the pulsed LIFS method (e.g., Fig. 7.1) is very limited.

All the experimental data is concerned with the rate coefficient for thermal collisions, and the energy dependence of the cross section has not been observed.

7.3. Electron impacts

Orientation and alignment are understood as the population imbalance among the magnetic sublevels or the imbalance in the magnitudes of the diagonal elements of the density matrix. Thus, disorientation and disalignment are understood as the population transfer among these sublevels. If we look at the same polarized atoms with the quantization axis rotated by a certain angle, the orientation and the alignment are expressed as the existence of the off-diagonal elements of the density matrix, or the Zeeman coherence among the magnetic sublevels. In this case, these relaxation processes may be understood as the decay of the Zeeman coherence, or the destruction of the phase correlation among the wavefunctions of the magnetic sublevels.

Stark broadening of a spectral line is, in the impact approximation, the result of the destruction of the optical coherence, which is the phase correlation between the wavefunctions of the upper and lower levels of the transition. Therefore, we may expect that the Stark broadening is closely related with the disorientation or the disalignment.

Recently, an experiment has been performed by Hirabayashi et al. (1988) with the aim of examininig the validity of the above assumption. By the pulsed laser-induced fluorescence (LIFS) method, disalignment of excited neon atoms was observed in an afterglow plasma and its rate due to electron collisions was determined. It was found that the rate coefficient was actually close to that for the Stark broadening.

There is a large body of experimental and theoretical data of Stark broadening, and these data may be used for an estimate of the disalignment rate coefficient.

7.4. Ion collisions — Effect of electric field

The alignment in the atomic ensemble "rotates" under the influence of an electric field. The direction of the rotation axis depends on the orientation of the alignment relative to the field direction, and the rotation frequency depends on the field strength and the scalar and tensor polarizabilities of the atoms. (Querdane et al. 1986, Angel and Sandard 1968) The effect of a uniform electric field has been studied in the beam-foil spectroscopy.

In plasma we have an electric field, called the microfield, exerted by the plasma electrons and ions. The normal field strength (in SI units)

$$F_0 = (ze / 4\pi\varepsilon_0) (4\pi n_i / 3)^{2/3} \qquad (7.3)$$

gives the typical magnutude of the field. Here e is the unit charge, ε_0 is the dielectric constant of vacuum and z and n_i are the charge and the density of the ions. The direction of the microfield is random and its strengths are distributed. The Holtsmark field is an example of the distribution. The effect of this randomly distributed field on the alignment has been examined by Hirabayashi et al. (1988), and it was found that the magnitude of the alignment decreased with time and finally reached a constant value. (Fig. 7.2)

7.5. Trapped radiation

In the Hanle effect experiment, the effect of a finite optical thickness, or the opacity effect, has long been recognized as an origin of an apparent reduction in the width of the Lorentzian profile of the Hanle signal. This phenomenon is called the coherence narrowing and has been a subject of many studies. In the context of the present study, reabsorption of the radiation may bring about disalignment; this is because the population is conserved by reabsorption of a photon, but the alignment is only partly conserved. This phenomenon is understood from the following argument given by D'Yakonov and Perel' (1965).

We consider a classical atom with its dipole in the z-direction. The dipole radiation, averaged over the direction, has its components $E_z^2 : E_x^2 : E_y^2 = 8 : 1 : 1$. We consider a large number of identical atoms and assume that the optical thickness is so high that the radiation is reabsorbed completely. The rate equation for the energy of the z-dipoles is

$$dI_z / dt = -A I_z + 0.8 A I_z + 0.1 A I_x + 0.1 A I_y \qquad (7.4)$$

where A is the spontaneous transition probability. We now introduce the quantity

$$I = I_z - (1/3)(I_x + I_y + I_z) \qquad (7.5)$$

which characterizes the preferential polarization of the atoms in the z-direction. If we note that the total energy of the dipoles does not change with time, it is straightforward to show

$$dI/dt = - (3/10)A\,I \qquad (7.6)$$

This process is nothing but disalignment by the trapped radiation.

The actual disalignment rate depends on the combination of the angular momenta of the upper and the lower levels of the transition line and also on the magnitude of the optical thickness of this line. Saloman and Happer (1966) give the depolarization factor, which corresoponds to the coefficient (1 − 3/10) in eq. (7.8). Tables 7.1 and 7.2 reproduce the result.

Figure 7.1 (Fujimoto et al. 1983) shows the two sets of the experimental data. These sets are different in the degree of the optical thickness of the four lines terminating on the $2p^5\,3s$ configuration levels. The intercept is interpreted as due to the disalignment by the trapped radiation, and its magnitude is found to be consistent with the estimate based on the observed optical thickness and Table 7.2.

Appendix. Geometry for experiment free from higher multipole moments and their relaxation

Suppose, in our experiment, we want to determine the atomic population n(u) or $\rho^0_0(J_u\,J_u)$ from our observation of an emission line intensity. Determination of atomic lifetime and determination of atomic transition probability are examples of such experiments. If the excitation of the upper level atoms is spatially isotropic, the irreducible components of the density matrix higher than ρ^0_0 are absent, and the emission line intensity is given by the first term of the r.h.s. of eqs. (2.13a), (2.19a,b), (5.6), (5.12) or (5.18).

In many cases, the excitation is anisotropic. For instance, we may use an electron beam to excite the atoms, or in the laser-induced-fluorescence spectroscopy (LIFS) experiment the laser light, even if it is unpolarized, is highly anisotropic. Even the excitation in plasma, alignment is indued. (See §8.2.) In these cases, the second and third terms in the above equations may contribute to our observed intensity. From now on, we base our discussion mainly on eq. (5.6).

Sometimes we are interested only in the rate of temporal decay of the population following pulsed excitation, e.g., the determination of atomic lifetime. In this case, if

the quantities ρ_q^1 */ ρ_0^0 and ρ_q^2 */ ρ_0^0 are independent of time, it is obvious from eq. (5.6) that the observed intensity from any direction by any detector gives the correct temporal decay of the population. However, if ρ_q^1 */ ρ_0^0 or ρ_q^2*/ ρ_0^0 changes with time the decay time constant of the observed line intensity can be different from that of the population. This could happen when there is an appreciable electric or magnetic field or these atoms are subjected to disalignment, eq. (7.2), or disorientation which is similar to the disalignment, by collisions or by radiation reabsorption (Fujimoto et al. 1982, 1983).

Sometimes we want to determine the population n(u) without being affected by the presence of the orientation or the alignment, and especially, by their relaxation. We discuss the experimental configuration for this purpose. Strictly speaking, there is no straighforward answer to this question. This is because, besides ρ_q^1*/ ρ_0^0 and ρ_q^2 */ ρ_0^0 created by the excitation which we apply, another ρ_q^1 */ ρ_0^0 and ρ_q^2 */ ρ_0^0 could be produced owing to spatially anisotropic relaxation. Furthermore, the plasma itself induces alignment, called the self-alignment which will be discussed in §8.2. The directions of symmetry of these spatial anisotropies may be different, and no simple configuration can eliminate the effect of these anisotropies. In the subsequent discussions we neglect the latter two anisotropies; this is equivalent to assuming that the plasma itself is spatially isotropic and no electric or magnetic field affects ρ_q^1 */ ρ_0^0 and ρ_q^2 */ ρ_0^0 .

Cylindrical symmetry along the quantization axis is assumed. We start with eq. (5.18). Originally this equation has been derived for linearly polarized weak light excitation. However, we have seen that, with appropriate modifications to W_2, this equation is valid for strong light excitation as well as for unpolarized light excitation. This equation is also valid even for collisional excitation by a beam-like particles. In all the cases, W_2 is understood to be the longitudinal alignment defined by eq. (5.10) or (5.11).

1. A straightforward consequence of eq. (5.18) is a configuration in which $f_0^2(\mathbf{e}_l) = 0$, or $\theta = 35.26°$, and we observe the linearly polarized light with the polarization vector $\mathbf{e}_l$. This is the magic angle configuration, in which the angle between the quantization axis and the direction of the transmission axis of the polarizer for observation is the magic angle, 54.74°.
2. From the direction $\theta = 90°$ we measure the intensities of the two polarized components for $\mathbf{e}_r$ and $\mathbf{e}_l$; or the σ light and the π light respectively. The quantity $(I_\pi + 2\, I_\sigma)$ is proportional to the population n(u). This quantity is the denominator of the longitudinal alignment, eq. (5.10), and is plotted in Fig. 5.3b.

3. If our detector does not have a polarization selectivity, as is the case with a combination of a head-on photomultiplier and a filter, we may choose $\theta = 54.74°$, then the observed intensity $(I(\mathbf{e}_r) + I(\mathbf{e}_l))$ gives directly the population. See also eq.(5.12).

3a. In many cases our detector has a polarization selectivity, as is the case with a monochromator. We may still choose $\theta = 54.74°$ and tilt our detector around the line of sight by 45° so that $I(\mathbf{e}_r)$ and $I(\mathbf{e}_l)$ are detected with an equal efficiency.

3b. In the above configuration, instead of tilting our detector, we apply a magnetic field in the direction of observation so as to effectively eliminate the polarization selectivity of our ditector. The magnitude of the magnetic field should be strong to have a Larmor frequancy high enough to average the observed intensity over the resolution time of our detector, and still weak enough not to affect the dynamics of the atoms concerned. (Fujimoto et al. 1982). In Fig. 5.2, the traces "55°" are the results obtained by this method.

References

Angel J.R.P. and Sandard P.G.H., 1968, Proc. R. Soc. London Ser. A **305**, 125.
The hyperfine structure Stark effect
I. Theory

Balyis W.E., 1979, *Progress in Atomic Spectroscopy* Part B, eds., W. Hanle and H. Kleinpoppen (Plenum), New York p.1227.
Collisional depolarization in the excited state

Carrington C.G. and Corney A., 1969, Opt. Comm. **1**, 115.
Hanle effect in a neon discharge

D'Yakonov M.I. and Perel' V.I., 1965, Sov. Phys.— JETP **20**, 997.
Coherence relaxation during diffusion of resonance radiation

Fujimoto T., Goto C. and Fukuda K., 1982, Phys. Scr. **26**, 443.
Determination of atomic lifetime by the laser-induced fluorescence method— Application to neon $2p^53p$ levels

Fujimoto T., Goto C., Uetani Y. and Fukuda K., 1983, Phys. Scr. **28**, 617.
Effect of radiative relaxation of excitation anisotropy on the measurement of atomic lifetime. Demonstration on argon $2p_4$ level.

Fujimoto T. and Matsumoto S.,1988, J. Phys. B **21**, L267.
Comments on the self-alignment method for observing excited atoms in a discharge plasma

Hirabayashi A., Nambu Y., Hasuo M. and Fujimoto T., 1988, Phys. Rev. A **37**, 83.
Disalignment of excited neon atoms due to electron and ion collisions

Kallas Kh. and Chaika M.,1969, Opt. Spectrosc. **27**, 376.
Alignment of excited states of neon in a direct current discharge

Kazantsev S.A., 1983, Sov. Phys. — Usp. **26**, 328.
Astrophysical and laboratory applications of self-alignment

Ouerdane Y., Denis A. and Désesquelles J., 1986, Phys. Rev. A **34**, 1966.
Time evolution of alignment and orientation in an electric field for the n $^1D_2$ He I levels ($3 \leq n \leq 5$)

Saloman E.B. and Happer W., 1966, Phys. Rev. **144**, 7.
Lifetime, coherence narrowing, and hyperfine structure of the ($6s^2$ 6p7s) $^3P_1^0$ state in lead

Table 7.1 Depolarization factor of multipolarity 1 by trapped radiation. (Saloman and Happer 1966)

J \ J'	0	1	2	3	4
0	0	1/2	0	0	0
1	0	1/8	3/8	0	0
2	0	1/8	1/24	1/3	0
3	0	0	1/6	1/48	5/16
4	0	0	0	3/16	1/80

J \ J'	1/2	3/2	5/2	7/2
1/2	1/3	5/12	0	0
3/2	1/12	1/15	7/20	0
5/2	0	3/20	1/35	9/28
7/2	0	0	5/28	1/63

Table 7.2 Depolarization factor of multipolarity 2 by trapped radiation. (Salomon and Happer 1966)

J \ J'	0	1	2	3	4
0	0	7/10	0	0	0
1	0	7/40	147/600	0	0
2	0	7/1000	147/600	21/125	0
3	0	0	1/50	21/80	11/80
4	0	0	0	7/240	539/2000

J \ J'	1/2	3/2	5/2	7/2
1/2	0	7/20	0	0
3/2	0	28/125	49/250	0
5/2	0	7/500	32/125	3/20
7/2	0	0	1/40	4/15

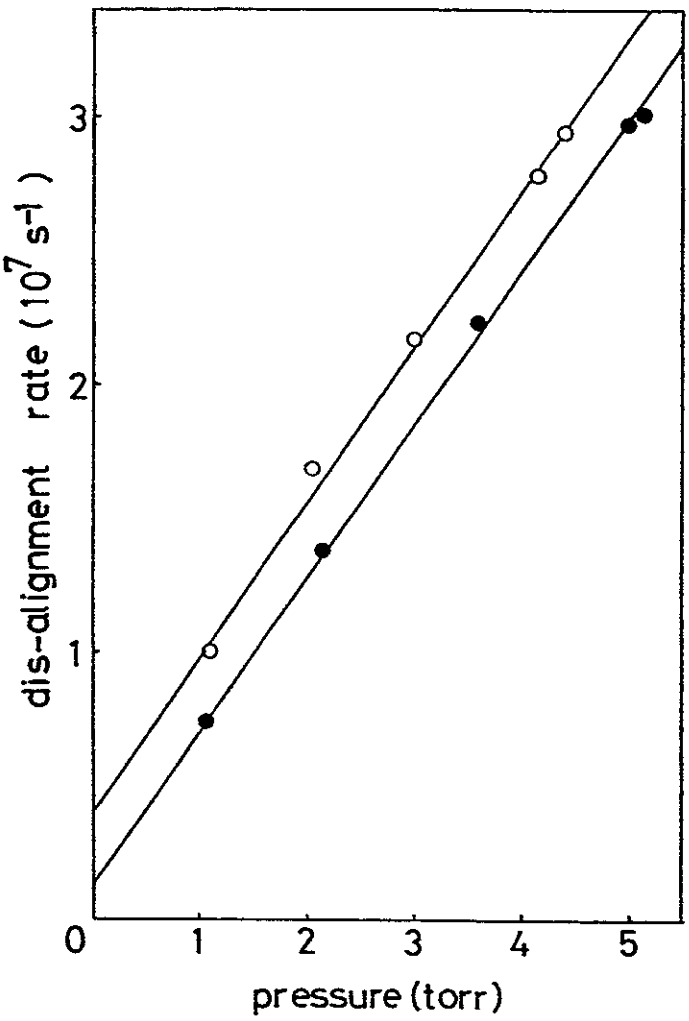

Fig.7.1 The disalignment rate of the neon $2p_2$ level as a function of pressure. The two sets of the experimental data correspond to different rates of disalignment by the trapped radiations $2p_2 \longrightarrow 1s_k$ ($\kappa = 2 - 5$). The intercept gives the radiative disalignment rate. See text for further detail. (Fujimoto et al. 1983)

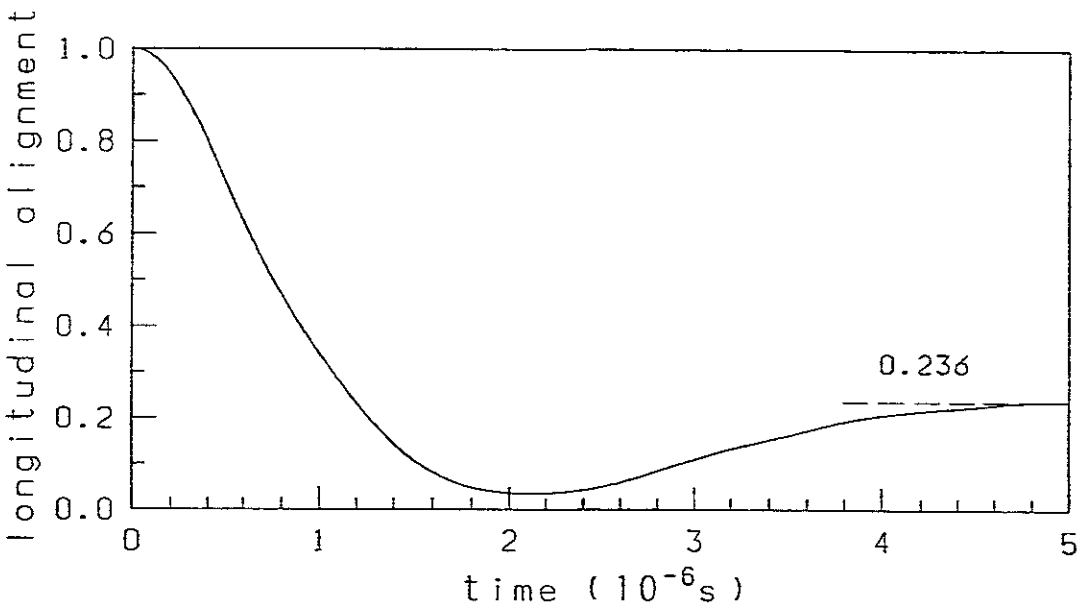

Fig.7.2 Temporal development of the longitudinal alignment of the aligned neon $2p_2$ atoms due to the Holtsmark field. $n_e = 5 \times 10^{19}$ m^{-3}. (Hirabayashi et al. 1986)

VIII. OTHER ASPECTS OF POLARIZATION PHENOMENA

8.1. Forbidden line emission due to electric field

An electric field causes Stark mixing among the electronic states of an atom, and a forbidden transition under the field free condition becomes partially allowed owing to the admixture of the allowed line component. In this case, the emission line is polarized. The emission intensity and the degree of polarization depend on the field strength. In the following, the basic formulation and its application to the lithium atom system are given (Kawawsaki et al. 1988).

8.1.1. Stark mixing and transition probabilities

Suppose an electric field (strength F) in the z-direction is present. The Hamiltonian for an atom is

$$H = H_0 + ezF \tag{8.1.1}$$

where H_0 is the Hamiltonian for the free atom. Let $|\gamma_j>$ be the eigenfunction for H_0 with its eigenvalue E_0. It is understood that γ_j represents the quantum numbers L_j, J_j, S_j, M_j and other parameters necessary to specify the state j. The eigenfunction of eq. (8.1.1) is expressed as

$$|\gamma_j\ (F)> = \sum_i C(\gamma_j\ \gamma_i)\ |\gamma_i> \tag{8.1.2}$$

where the expansion coefficient is normalized. It is noted that the coefficient is non-zero only for the states with $S_j = S_i = S$ and $M_j = M_i = M$. The coefficient is calculated from the coupled equation

$$\{E_0(\gamma_k) - E(\gamma_j)\}\ C(\gamma_j\ \gamma_k) + eF\sum_i <\gamma_k\ |z|\ \gamma_i>\ C(\gamma_j\gamma_i) = 0 \tag{8.1.3}$$

We note $z = r\cos\theta$. The radial matrix element is evaluated in the Coulomb approximation. The angular part is given by (Kollath and Standage 1979)

$$<\gamma_k|\cos\theta|\gamma_i> = (-1)^{Jk-M+Ji+3/2}\{(2J_k+1)(2J_i+1)(2L_k+1)(2L_i+1)\}^{1/2}$$
$$\times \begin{pmatrix} J_k & 1 & J_i \\ -M & 0 & M \end{pmatrix} \begin{Bmatrix} L_k & 1 & L_i \\ 0 & 0 & 0 \end{Bmatrix} \begin{Bmatrix} L_k & J_k & S \\ J_i & L_i & 1 \end{Bmatrix} \tag{8.1.4}$$

where ( ) and { } are Wigner's 3j- and 6j-symbols, respectively.

Suppose we excite atoms in level l by radiation to level i. The relative population among the magnetic substates $g(M_i)$ is proportional to the relative transition probability which is given by the 3j-symbol (Sobelman 1979), i.e.,

$$g(M_i) \propto \begin{pmatrix} J_i & 1 & J_l \\ -M_i & \sigma & M_l \end{pmatrix}^2 \tag{8.1.5}$$

with $\sigma = 0$ for linearly polarized light with its polarization vector along the z direction and $\sigma = \pm 1$ for circularly polarized light. In the case of the two step excitation via the intermediate level h the relative population in level i is given as

$$g(M_i) \propto \begin{pmatrix} J_i & 1 & J_h \\ -M_i & \sigma_2 & M_h \end{pmatrix}^2 \begin{pmatrix} J_h & 1 & J_l \\ -M_h & \sigma_1 & M_l \end{pmatrix}^2 \tag{8.1.6}$$

Suppose state i and state j are Stark mixed, and we observe the fluorescence from j to k. The relative transition probability for the fluorescence emission is given by a similar formula to eq. (8.1.5) with i and l replaced by j and k, respectively. By combining the relative population, eq. (8.1.5) or (8.1.6), the expansion coefficient, eq. (8.1.3), and the relative transition probability, we readily calculate the intensity of the polarized components of the fluorescence light.

8.1.2. Example ——— Application to lithium

We consider the excitation-observation geometry as shown in Fig. 8.1.1. The electric field is applied in the z direction and the atoms are excited by the laser light coming from the x direction with its linear polarization directed in the z direction (parallel polarized) or the y direction (perpendicularly polarized). The fluorescence light is observed from the y direction with its linearly polarized components resolved: the π–light which is polarized in the z direction and σ–light in the x direction.

The first example is the excitation-observation scheme shown in Fig. 8.1.2 (a): The ground state atoms in the 2^2S level are excited to 4^2P, and the 463.6 nm line ($4^2P \longrightarrow 2^2P$) is observed together with the direct fluorescence of $4^2P \longrightarrow 2^2S$ (allowed transition). In the caluculation of the expansion coefficient, eq.(8.1.3), we include only the levels having the principal quantum number n = 4. We assume the equal populations in the magnetic sublevels of the ground state atoms before laser excitation.

We calculate the relative population for three modes of excitation: 1) parallel excitation, 2) perpendicular excitation and 3) the isotropic excitation by which the relative population $g(M_i)$ is independent of M_i. Table 8.1.1 gives examples of the relative populations among the magnetic sublevels for the three cases. For the

fluorescence the degree of polarization $P = (I_\pi - I_\sigma)/(I_\pi + I_\sigma)$ is calculated. Under the conditions of practical interest the degree of Stark mixing increases almost linearly with F, and P is almost independent of F. Table 8.1.2 gives P at F = 5 kV/cm for the cases corresponding to Table 8.1.1.

The intensity ratio of the forbidden line to the allowed line is readily calculated from the expansion coefficient. Figure 8.1.2(b) gives the ratio; here the intensitiy is understood as $(I_\pi + I_\sigma)$ and it is expressed as the number of emitted photons. It is seen the intensity ratio is virtually independent of polarization of the laser light.

The second example is the scheme shown in Fig. 8.1.3(a): we employ the two step excitation to 4^2D via the intermediate 2^2P state, and the forbidden line is 1873 nm ($4^2D \longrightarrow 3^2D$). We assume that the polarization directions of the laser light are both parallel or perpendicular. Table 8.1.1 gives the relative populations and table 8.1.2 gives the polarization. Figure 8.1.3(b) gives the intensity ratio.

From the experimental view point, instead of observing the infrared forbidden line in the above experiment, it is more practical to observe the subsequent fluorescence 610.4 nm ($3^2D \longrightarrow 2^2P$) line (Fig. 8.1.3(a)). Since virtually all the atoms in the 3^2D level radiatively decay to the 2^2P level the intensity ratio in Fig. 8.1.3(b) applies also to this case, where the intensity is understood as the integrated intensity over the duration of the fluorescence pulse. Table 8.1.2 contains P for the 610.4 nm line.

The third example is depicted in Fig. 8.1.4(a); absorption of the forbidden transition of 460.2 nm ($2^2P \longrightarrow 4^2F$) and observation of the 1871 nm ($4^2F \longrightarrow 3^2D$) line or the 610.4 nm line. Again the polarization directions of the laser light for the two step excitation are assumed both parallel or perpendicular. Figure 8.1.4(b) gives the effective absorption probability (s^{-1}) for the spectral intensity of the laser light of 1 erg/cm^2.

So far the electric field has been assumed static. In the case of a time varying field this approximation is justified if the following condition is satisfied; viz,

$$\omega_p << \omega_{ji} = | E_0(\gamma_j) - E_0(\gamma_i) | /h \qquad (8.1.7)$$

where ω_p stands for the angular frequancy of the electric field. In our example (Lindgård and Nielsen 1977), $\omega_{ji} = 9.3 \times 10^{11}$ s^{-1} for the 4^2D–4^2F mixing case, and 2.9×10^{13} s^{-1} for the 4^2P–4^2D case.

We have neglected the presence of the nuclear spin. Lithium has the nuclear spin 1 for ^{6}Li and 3/2 for ^{7}Li. The level splitting due to the hyperfine interaction is estimated to be less than 1.4 MHz for 4^2D (Radzig and Smirnov 1985). When we compare this with the decay probability of 2×10^7 s^{-1} of this level, the effect of the splitting is well neglected.

References

Kawasaki K, Takiyama K, and Oda T., 1988, Jpn. J. Appl. Phys. **27**, 83.
Forbidden transitions of LiI in laser-induced fluorescence spectroscopy for the measurement of low-frequency electric fields in plasmas

Kollath K.J. and Standage M.C., 1979, Progress in Atomic Spectroscopy, Part B (Plenum Press, New York) p. 963.
Stark Effect

Lindgård A. and Nielsen S.E., 1977, At. Data Nucl. Data Tables **19**, 533.
Transition probabilities for the alkali isoelectronic sequences LiI, NaI, KI, RbI, CsI, FrI.

Radzig A.A. and Smirnov B.M., 1985, Reference Data on Atoms, Molecules, and Ions (Springer-Verlag, Heiderberg) p. 101.

Sobelmann I.I., 1979, Atomic Spectra and Radiative Transitions (Springer-Verlag, Heiderberg) p. 203.

Table 8.1.1 The relative population of g(M)

	n = 4			The exciting laser(s)		
	L_i	J_i	M_i	parallel polarized	perpendicular polarized	isotropic
From 2^2S	1	1/2	$\pm 1/2$	1/6	1/6	1/6
	1	3/2	$\pm 3/2$	0	1/4	1/6
	1	3/2	$\pm 1/2$	1/3	1/12	1/6
From 2^2S via 2^2P	2	3/2	$\pm 3/2$	0	39/305	1/10
	2	3/2	$\pm 1/2$	13/80	19/305	1/10
	2	5/2	$\pm 5/2$	0	27/122	1/10
	2	5/2	$\pm 3/2$	0	27/610	1/10
	2	5/2	$\pm 1/2$	27/80	27/610	1/10

Table 8.1.2 Degree of polarization at F = 5 kV/cm

The exciting laser(s)	Transition		
	$4^2P \rightarrow 2^2P$ 463.6 nm	$4^2D \rightarrow 3^2D$ 1873 nm	$3^2D \rightarrow 2^2P$ 610.4 nm
parallel polarized	0.467	0.448	0.439
perpendicular polarized	0.0	0.170	0.099
isotropic	0.215 (0.447)*	0.291 (0.321)*	0.250

*with neglect of the effect of the electron spin

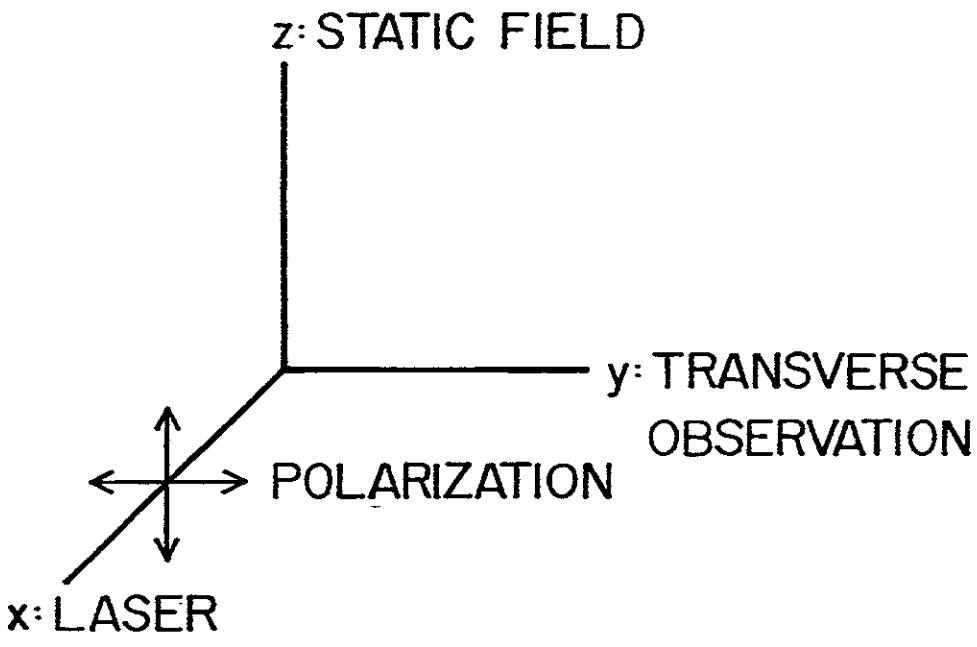

Fig.8.1.1 Excitation-observation geometry. (Kawasaki et al. 1988)

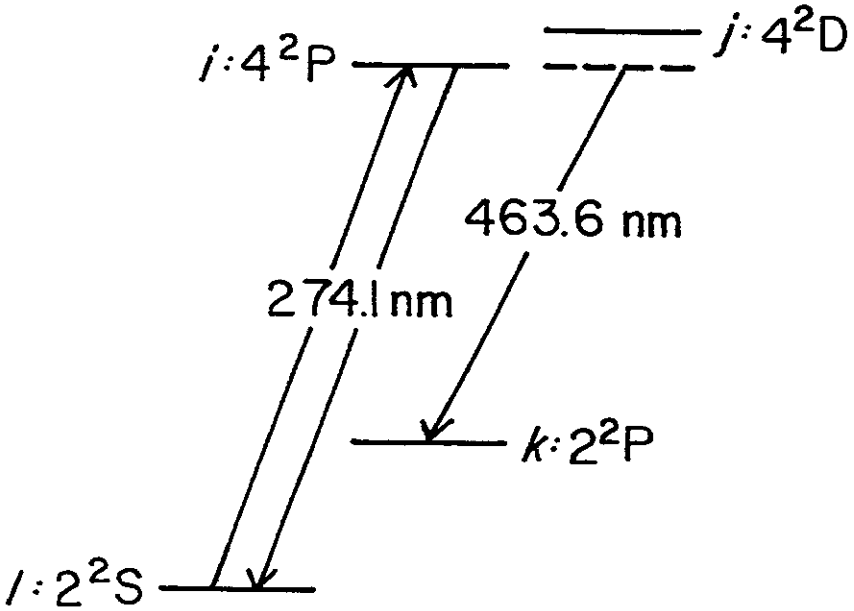

Fig.8.1.2 (a) Excitation-observation scheme.

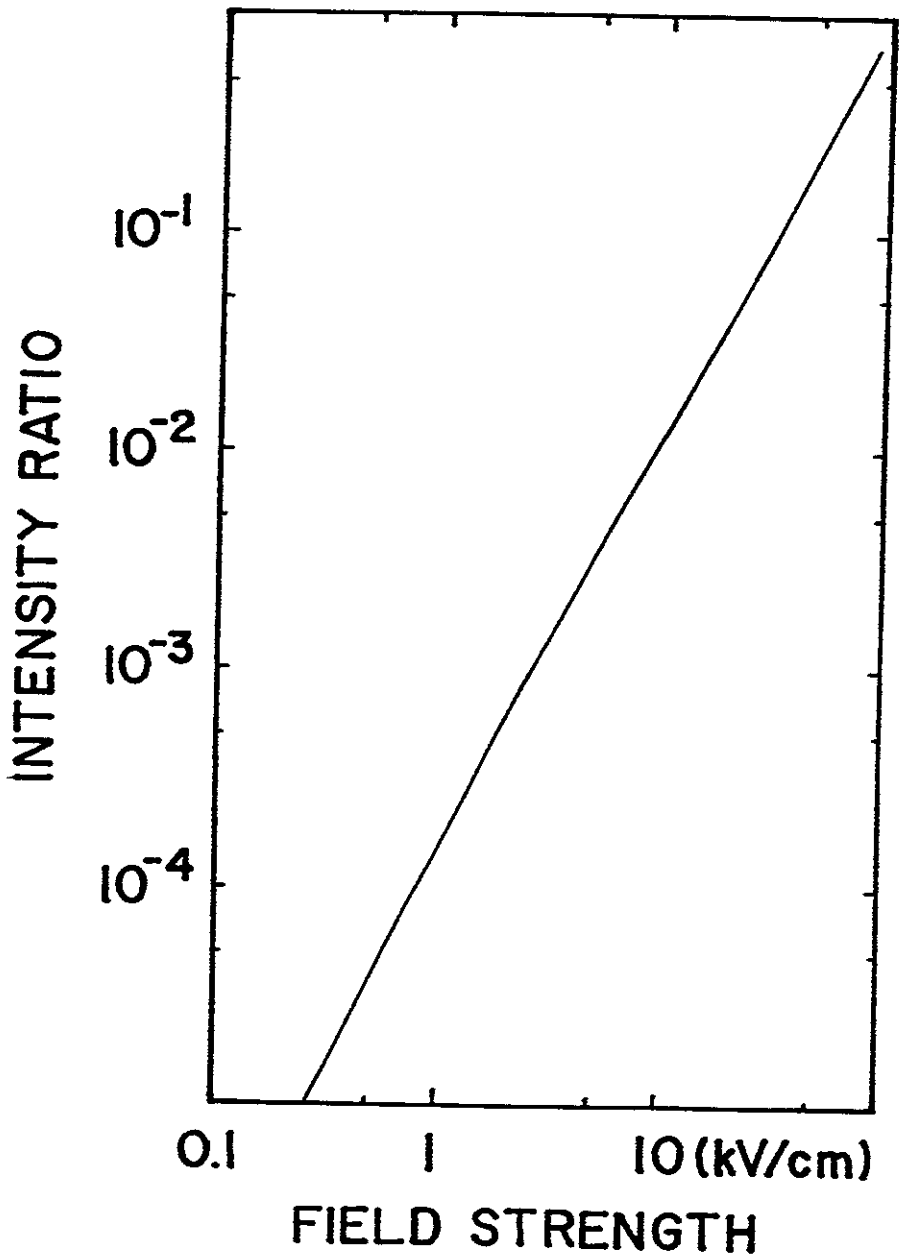

Fig.8.1.2 (b) Intensity ratio of the forbidden line to the allowed line against the electric field strength. Both the parallel excitation and the perpendicular excitation apply to the curve. (Kawasaki et al. 1988)

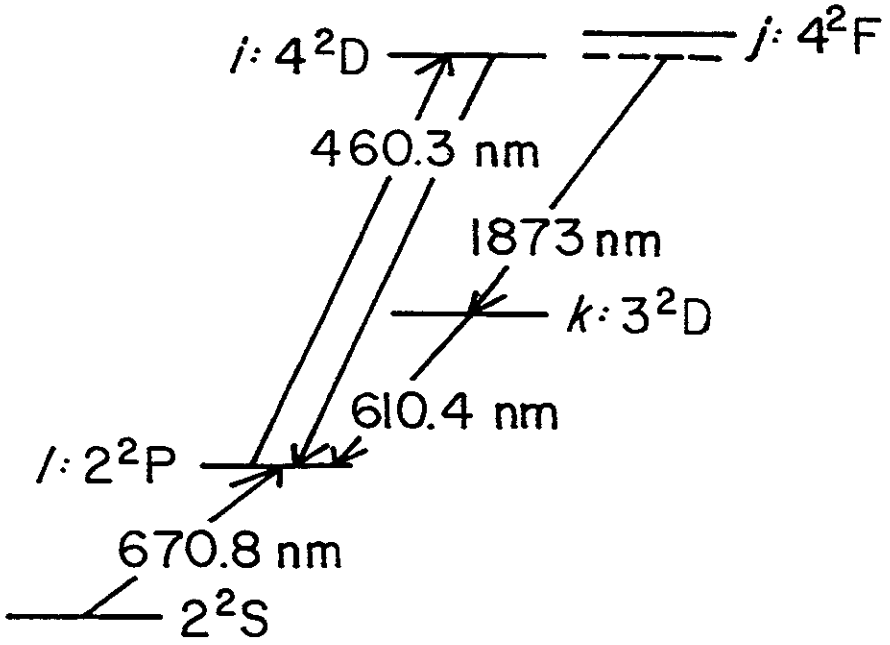

Fig.8.1.3 (a) Excitation-observation scheme.

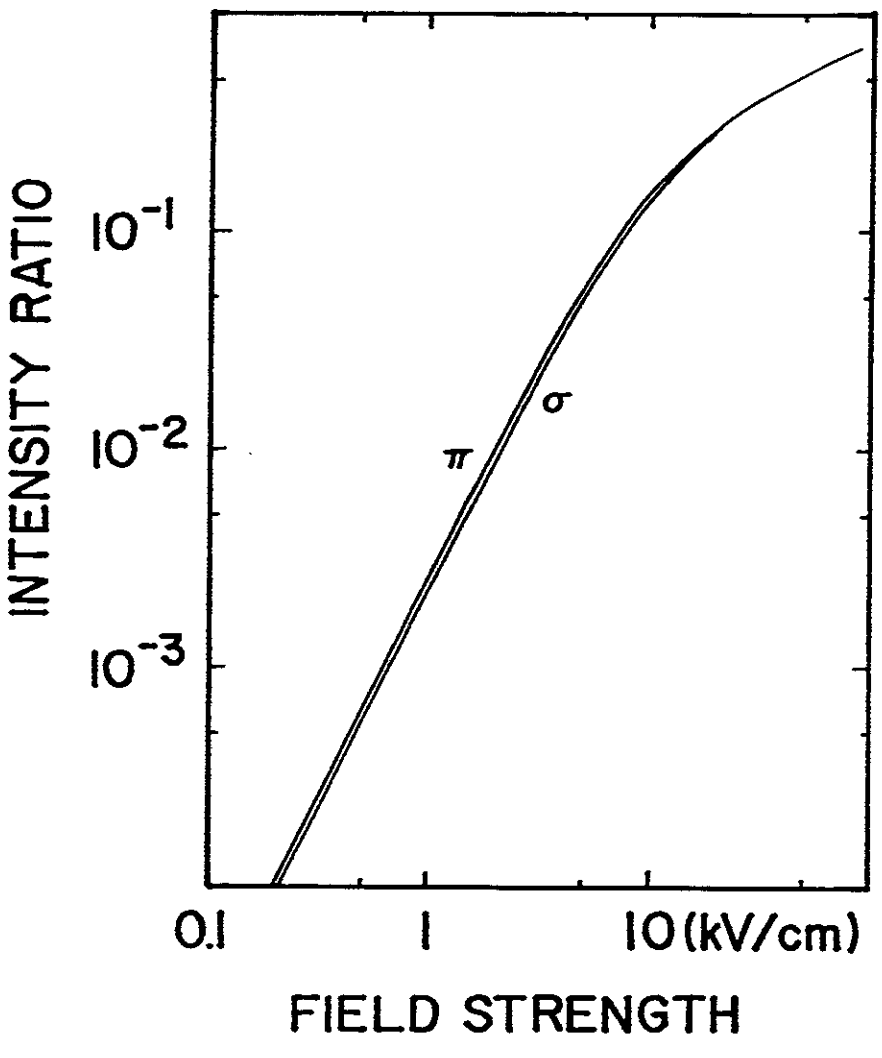

Fig.8.1.3.(b) Intensity ratio of the forbidden line to the allowed line. "π" means the parallel excitation and "σ" the perpendicular excitation. (Kawasaki et al. 1988)

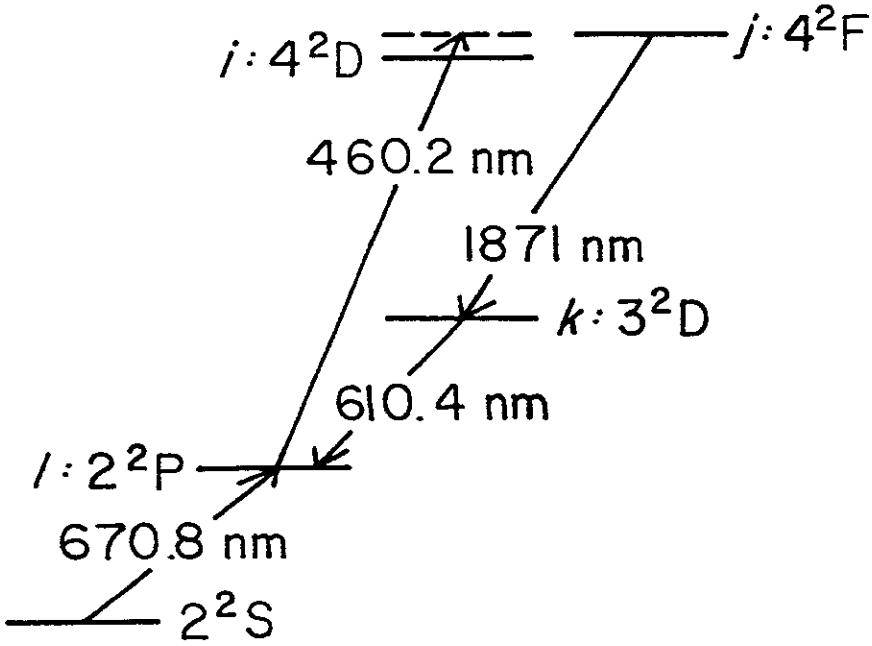

Fig.8.1.4 (a) Absorption by the 2^2P atoms of the forbidden transition of the 460.2 nm line.

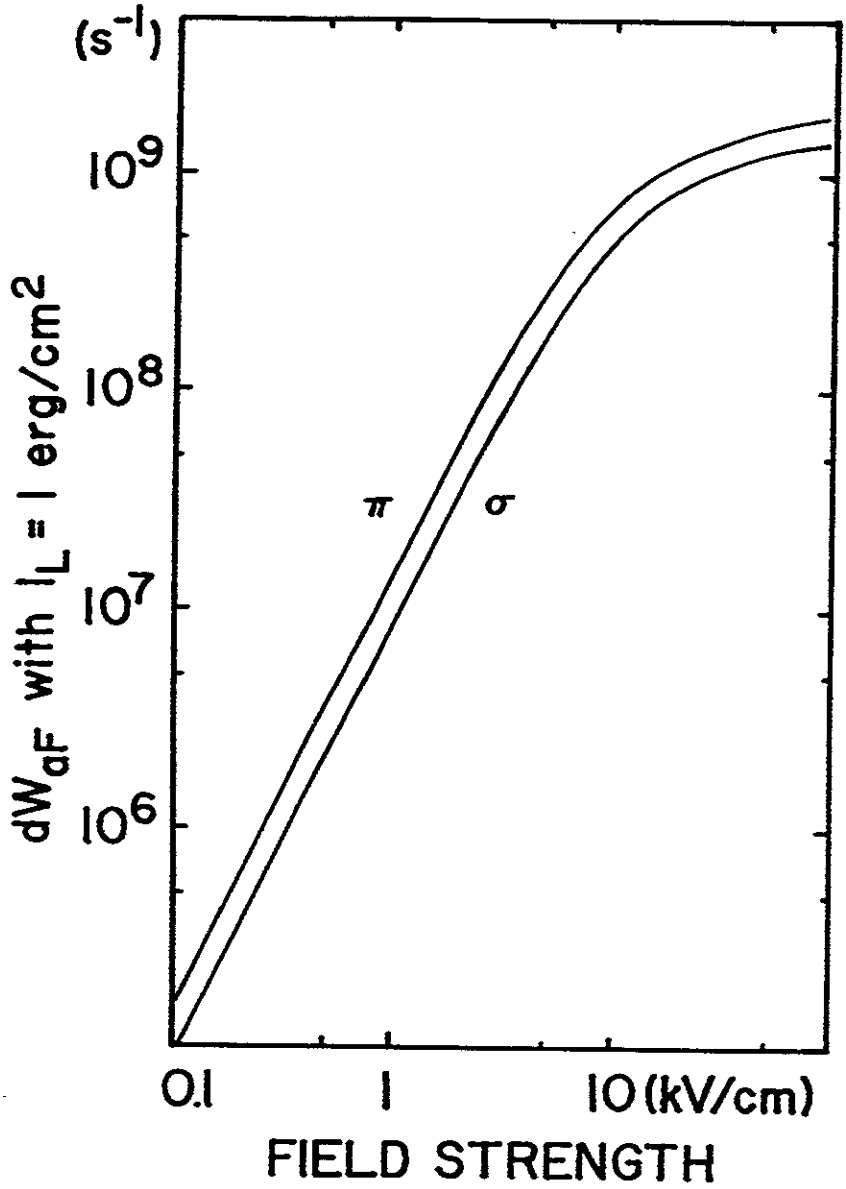

Fig.8.1.4 (b) Effective absorption probability (s^{-1}).
(Kawasaki et al. 1988)

8.2. Self alignment

Lombardi and Pebay-Peyroula (1965), Kallas and Chaika (1969) and Carrington and Corney (1969) independently discovered that the emission lines from an rf discharge plasma or a glow discharge plasma are polarized, where the polarization was detected as a Hanle signal when a variable magnetic field was applied. This means that the excited atoms in these plasmas are polarized (aligned) without any external anisotropic excitation, in the case of a glow discharge, in the direction of the tube axis. This phenomenon is called the self alignment. The self alignment produced in a glow discharge plasma was ascribed to the effect of radiation trapping which was spatially anisotropic owing to the cylindrical geometry of the plasma.

An interesting finding by Kallas and Chaika (1969) was that a neon level with the angular momentum $J = 0$, which is free from any anisotropy, showed a change in its emission line intensity similar to the Hanle signal. They proposed as its possible origin the latent (concealed or hidden) alignment (Chaika 1971a, b). Owing to the non-uniform spectral line profile (e.g., a gaussian profile) of the radiation field of the resonance line in the plasma, the group of the ground-state atoms having no velocity component in the propagation direction of the absorbed photon is more strongly excited to the resonance level, resulting in alignment in this group of the excited atoms. Subsequent photo-excitation from this level to the higher-lying $J = 0$ level may result in a dependence of the population on the applied magnetic field.

The radiation trapping theory was extended so as to include the spatial anisotropy (orientation and alignment) of excited atoms. On the basis of the general formulation developed for an infinite volume, Perel' and Rogova (1974) obtained the spatial distribution of the self aligned atoms for a simple geometry. The inclusion of the self alignment lead to the modification to the escape factor by Holstein (1947, 1951) for the resonance radiation, or the effective lifetime of the resonance atoms. Rogova (1974) studied further photoexcitation of these self-aligned atoms by another radiation field which produces higher-lying excited atoms. Owing to the presence of the self alignment a change in magnitude and profile of the absorption coefficient was obtained, giving an explanation to the observation on the $J = 0$ level population.

In a glow discharge plasma, high-lying excited atoms of rare gases were also found to be aligned, and this was ascribed to the anisotropic velocity distribution of electrons which excited these atoms (Kazantsev and Eiduk 1978, Kazantsev et al. 1979, Kazantsev et al. 1983). Alignment of a similar origin was observed in a hollow-cathode discharge plasma for excited helium and neon atoms (Zhechev and Chaika 1977, 1978). Again, the magnetic-field dependence of the line intensity was observed for the ($J=0 \longrightarrow J=1$) line. Determination of the quadrupole moment of the velocity distribution function of electrons was reported (Kazantsev 1983a).

An experimental verification of the latent alignment was reported by Lukomskii et al. (1985) and by Govyrin et al. (1988).

A review paper summarized the studies of the self alignment, including the polarization studies of the solar prominence (Kazantsev 1983b, See also §8.4.). This review includes a large number of the experimental data on the lifetime and the alignment destruction cross section, which have been determined by the self alignment method on discharge plasmas. As mentioned in Chapter 7, however, this method is questioned as a reliable method for determination of these quantities (Fujimoto and Matsumoto 1988).

For an atmospheric arc plasma, it was found that some of the argon-ion lines are strongly polarized, up to 10 % (Fig. 8.2.1, Margolin et al. 1984). This was also ascribed to the alignment due to the anisotropic velocity distribution of electrons. By estimating the energy dependent alignment production cross section and the quadrupole moment of the velocity distribution function of electrons in the plasma, these authors reproduced approximately the observed polarization degree of several emission lines (Fig. 8.2.1).

Self alignment in a high frequency discharge was also found and ascribed to the anisotropic electron impact excitation. From the observed alignment and using the transport cross section values, the electric field strength was determined (Kazantsev et al. 1985). Kazantsev and Subbotenko(1987) studied a high frequency discharge plasma. Figure 8.2.2 is reproduced from their paper showing the spatial dependence of polarization of a neutral helium line for a capacitive discharge plasma. They discussed the polarization against the position in terms of the electron velocity distribution. They also reported spatial dependence of the polarization of emission lines along the line perpendicular to the discharge axis (Fig. 8.2.3). In the region close to the glass boundary the emission lines starting from high-lying excited levels show large polarization, whereas those from low-lying levels show polarization simply decreasing toward the glass wall. They discussed these findings in terms of the structure of the sheath and the electron velocity distribution in this region.

Self alignment of excited ions due to their drift motion was predicted (Petrashen et al. 1985). Alignment in excited ions was actually found in a hollow-cathode discharge and was ascribed to the proposed mechanism (Kazantsev et al. 1987a, b).

By coupling the neon $2p_4$ and $3s_2$ atoms by the 632.8 nm laser line, Ducroy et al. (1973) observed a higher multipole moment (hexadecapole moment) in the $2p_4$ atoms.

References

Carrington C.G. and Corney A., 1969, Opt. Comm. **1**, 115.
Hanle effect in a neon discharge

Chaika M.P., 1971a, Opt. Spectrosc. **30**, 443.
Latent alignment of excited states of gas atoms due to isotropic irradiation

Chaika M., 1971b, Opt. Spectrosc. **31**, 356.
Light absorption by vapor with hidden alignment

Ducloy M., Gorza M.P. and Decomps B., 1973, Opt. Comm. **8**, 21.
High-order nonlinear effects in a gas laser: creation and detection of an hexadecapole moment in the neon $2p_4$ level

Fujimoto T. and Matsumoto S., 1988, J. Phys. B: At. Mol. Opt. Phys. **21**, L267.
Comments on the self-alignment method for observing excited atoms in a discharge plasma

Govyrin V.I., Markov V.P., Mashek I.Ch. and Chaika M.P., 1988, Opt. Spectrosc. **64**, 138.
Effect of latent alignment on the intensity of spectral lines emitted by a low-temperature plasma

Holstein T, 1947, Phys. Rev. **72**, 1212.
Imprisonment of resonance radiation in gases

Holstein T. 1951, Phys. Rev. **83**, 1159.
Imprisonment of resonance radiation in gases. II.

Kallas Kh. and Chaika M., 1969, Opt. Spectrosc. **27**, 376.
Alignment of excited states of neon in a direct current discharge

Kazantsev S.A., 1983a, Letters **37**, 158.
Determination of the quadrupole moment of the electron distribution function in a plasma

Kazantsev S.A., 1983b, Sov. Phys. —— Usp. **26**, 328.
Astrophysical and laboratory applications of self-alignment

Kazantsev S.A. and Eiduk V.I., 1978, Opt. Spectrosc. **45**, 735.
Hanle effect on highly excited atomic levels of inert gases in a discharge

Kazantsev S.A. and Subbotenko A.V., 1987, J. Phys. D: Appl. Phys. **20**, 741.
Polarization spectroscopy of a high-frequency discharge plasma

Kazantsev S.A., Markov V.P., Morozova S.L. and Chaika M.P., 1979, Opt. Spectrosc. **46**, 619.
Alignment of xenon atoms in a gas discharge

Kazantsev S.A., Rys A.G. and Chaika M.P., 1983, Opt. Spectrosc. **54**, 124.
Alignment of excited atoms by electron collision in a discharge

Kazantsev S.A., Polynovskaya N.Ya., Pyatnitskii L.N. and Edelman S.A., 1985, Opt. Spectrosc. **58**, 28.

Polarization-spectroscopy study of the anisotropic properties of a low-temperature plasma

Kazantsev S.A., Polezhaeva N.T. and Rebane V.N., 1987a, Opt. Spectrosc. **63**, 15.

Self-alignment of ions due to their drift

Kazantsev S.A., Petrashen A.G., Polezhaeva N.T., Rebane V.N. and Rebane T.K., 1987b, JETP Letters **45**, 17.

Drift self-alignment of ions in a plasma

Lombardi M. and Pebay-Peyroula J.C., 1965, C. R. Acad. Sci. **261**, 1485.

Polarisation de la lumière émise par une vapeur atomique lors d'une décharge haute fréquence

Lukomskii N.G., Plishchuk V.A., and Chaika M.P., 1985, Opt. Spectrosc. **58**, 284.

Hidden anisotropy of collisions in a low-temperature plasma

Margolin L.Ya., Polynovskaya N.Ya., Pyatnitskii L.N., Timergaliev R.Sh. and Édel'man S.A., 1984, High Temperature **22**. 149.

Polarization of the emission lines of an arc plasma at atmospheric pressure

Perel' V.I. and Rogova I.V., 1974, Sov. Phys. —— JETP **38**, 501.

Alignment of excited atoms in a gas discharge

Petrashen A.G., Rebane V.N. and Rebane T.K., 1985, Opt. Spectrosc. **58**, 22.

Self-alignment of excited atoms in a gas discharge under the action of ion drift

Rogova I.V., 1974, Opt. Spectrosc. **37**, 4.

Influence of alignment of excited atoms on the light absorption coefficient in a gaseous medium

Zhechev D.Z. and Chaika M.P., 1977, Opt. Spectrosc. **43**, 352.

Radiation from a hollow-cathode discharge in a weak magnetic field

Zhechev D.Z. and Chaika M.P., 1978, Opt. Spectrosc. **45**, 229.

The generation of alignment signals in a hollow-cathod discharge

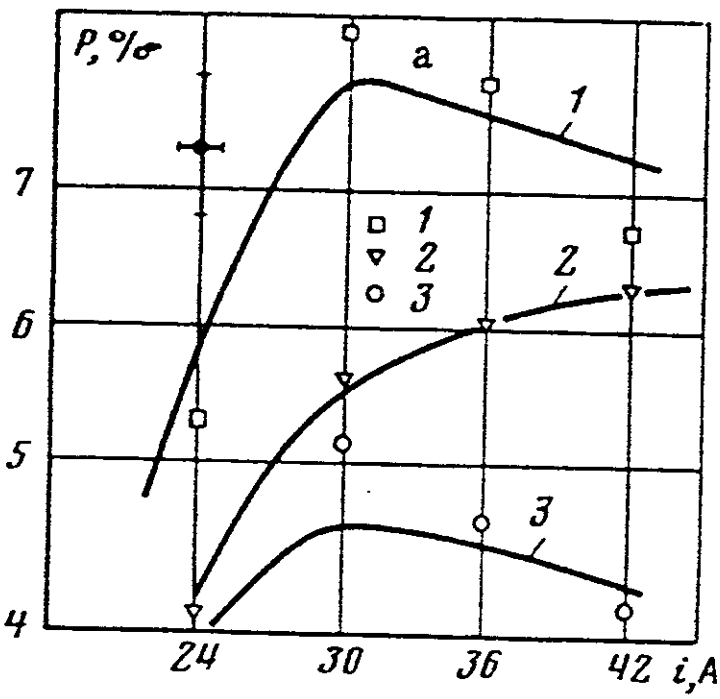

Fig.8.2.1 Dependences of the degree of polarization near the axis of the plasma on the discharge current. 1) ArII 488.0 nm, 2) ArII 480.6 nm, 3) ArII 454.5 nm. The statistical errors are indicated in the upper left. The solid curves show the calculated results. (Margolin et al. 1984)

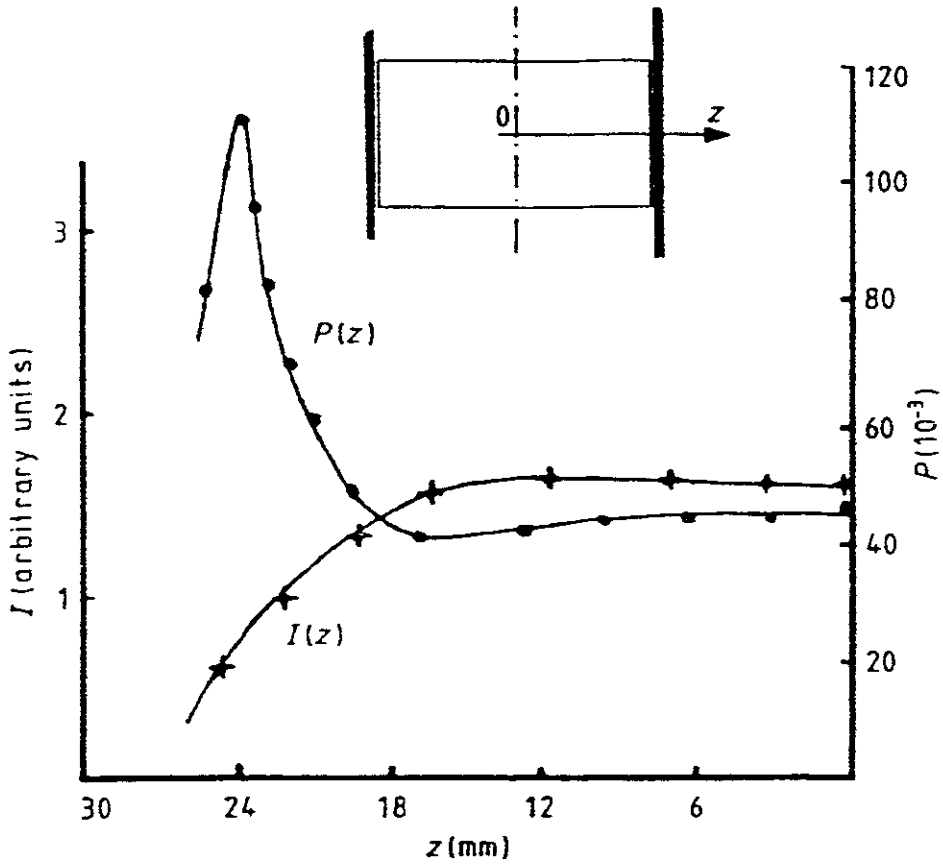

Fig.8.2.2 Polarization and intensity variations along the OZ axis of the cylindrical capacitive discharge on the line HeI 499.2 nm ($2^1P - 4^1D$) at pressure of 18 mTorr. (Kazantsev and Subbotenko, 1987)

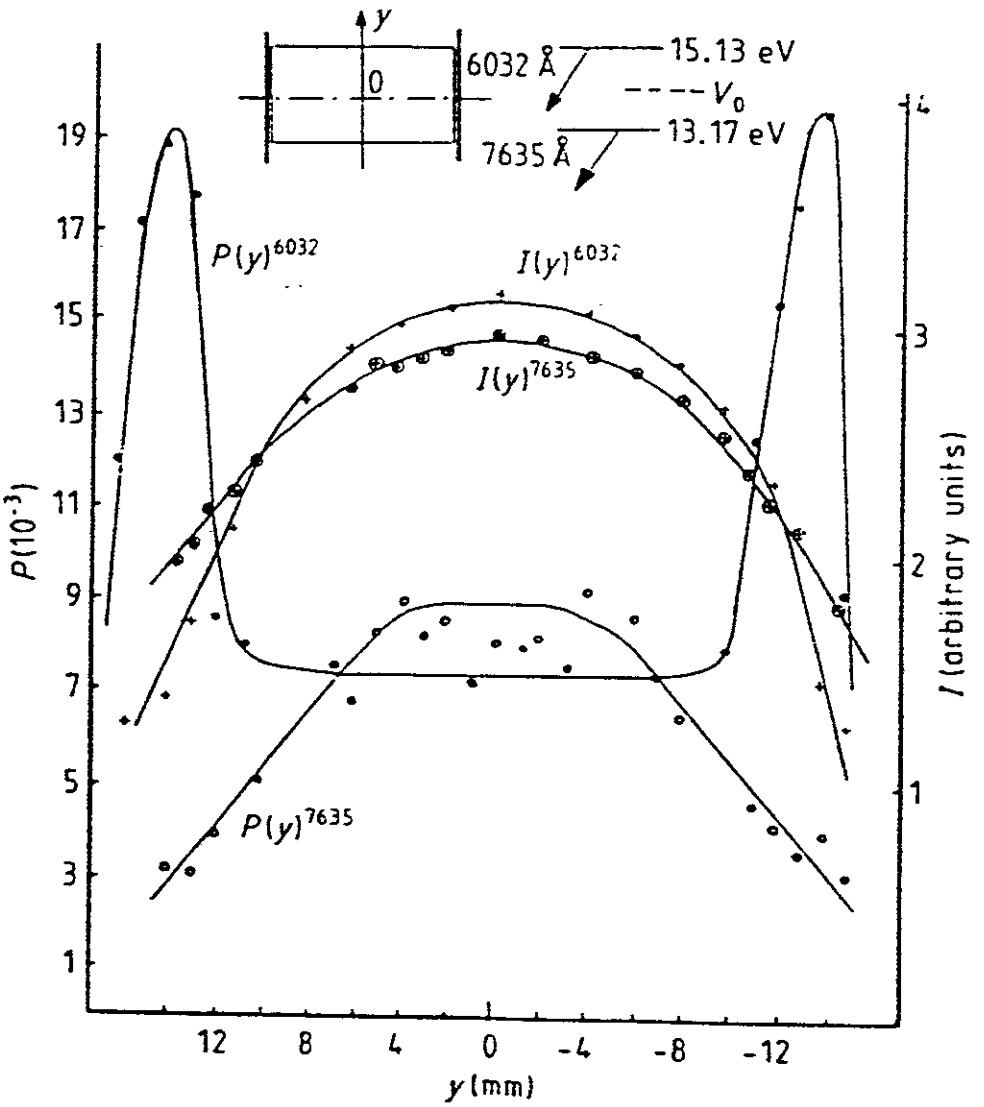

Fig.8.2.3 Polarization and intensity variations along the line pertendiculr to the cyrinder axis of the capacitive discharge in argon for the spectral lines with different excitation potentials of the upper level. (Kazantsev and Subbotenko, 1987)

8.3. Lyman doublet intensity ratio

We consider the situation in which hydrogenlike ions in the ground level are excited to an np level by collisions with electrons having an anisotropic velocity distribution. We first consider the limiting cases.

We assume that the L-S coupling scheme is valid, and the collisional excitation does not involve the elctronic spin. Furthermore, we neglect the nuclear spin. One extreme case would be the collisional excitation which corresponds to the π-light excitation of the photo-excitation. Then, in the decoupled representation, only the $m_l = 0$ sublevel in the np level is populated. For the sake of convenience we call this case the "π- excitation". The spin angular momentum is then coupled, and we obtain the population distribution among the M_J substates in the $J = 1/2$ and $3/2$ doublet levels. The result is shown in the Kastler diagram in Fig. 8.3.1(a). The population distribution in the case of the "σ-excitation" is similarly calculated. (Fig. 8.3.1(b)) It would be interesting to note that these population distributions are identical to the photo-excitation by the linearly polarized light.

Suppose we observe the Lyman doublet radiation from a direction making angle θ to the quantization axis. We present in Table 8.3.1 the relative intensities of this doublet lines with their π- and σ-components separately for the case of $\theta = \pi/2$ and those for $\theta = 0$.

Polarization of the Lyman lines from a non-thermal plasma was first treated by Haug (1980). Recently, the cross sections for excitation to the $m_l = 0$ and $m_l = \pm 1$ sublevels of the 2p level of hydrogenlike ions has been calculated (Itikawa et al., 1991) in the distorted wave method. Figure 8.3.2 shows the quantity $(Q_0 - Q_1)/(Q_0 + Q_1)$ for the hydrogenlike ions. For the π- and σ-light excitation this quantity is 1 and -1, respectively. It is seen that for very low energies the excitation is rather close to the π-excitation, and for higher energies it would tend to the σ-excitation, as expected from the discussion in Chapter 3, eq. (3.22).

References

Haug E., 1981, Solar Phys. **71**, 77.
Electron impact polarization of x-ray lines from hydrogen-like ions during solar flares

Itikawa Y., Srivastava R. and Sakimoto K., 1991, Phys. Rev. A **44** 7195.
Polarization of line radiation emitted from He-like and H-like ions following electron impact

Table 8.3.1.

Relative intensities of Lyman doublet in the limits of anisotropic excitation. In the isotropic excitation the relative intensities (α_1, α_2) should be (1, 2).

excitation	observation			
	$\theta = 0$	$\theta = \pi/2$		
		π -comp.	σ -comp.	total
" π -excitation"	(2, 2)	(1, 4)	(1, 1)	(2, 5)
" σ -excitation"	(4, 10)	(2, 2)	(2, 5)	(4, 7)

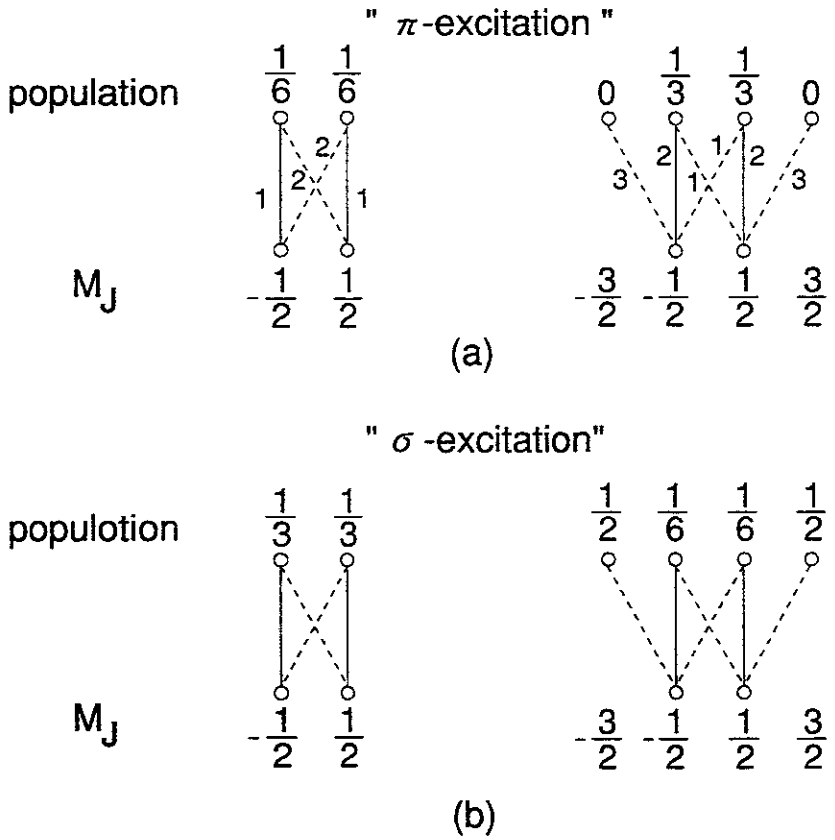

Fig.8.3.1 The relative populations in the magnetic substates of the 2p $^2P_{1/2}$ and $^2P_{3/2}$ levels for the "π-excitation" (a), and for the "σ-excitation".

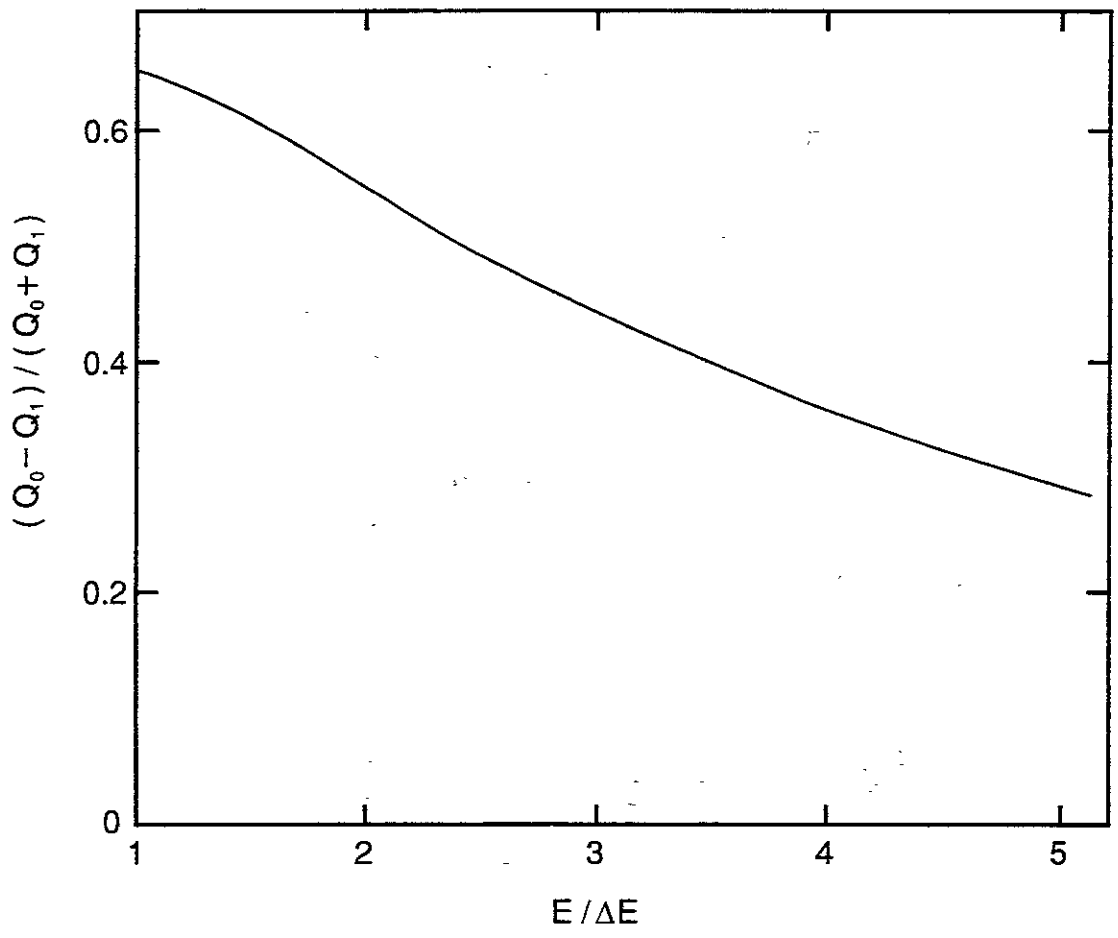

Fig.8.3.2 Difference of the cross sections of excitation to the $m_J = 0$ and $m_J = 1$ magnetic substates (in the uncoupled representation) of the 2p level of the hydrogenlike ions. (Itikawa et al. 1991)

8.4. Hanle effect - Observation of solar prominences

8.4.1 Introduction

Hanle(1924) observed a rotation of the plane of polarization of the emitted lines from an illuminated mercury vapor in a weak magnetic field. The Hanle effect is the modification of the linear polarization parameters of a spectral line by a local magnetic field: It is described by the combination of the damping of the atomic state with its lifetime τ and the rotation of the atomic polarization around the magnetic field with the Larmor frequency of the order of $\omega = (e/2m_e c)B \simeq 8 \text{ x } 10^6 B(\text{Gauss}) \text{ s}^{-1}$ (cgs units). The typical value of the field strength B for the Hanle effect to be sensitive is given by $0.2 \leq \omega\tau \leq 10$. Under this condition, the splittings of the sublevels due to the Zeeman effect are of the same order with the natural width of the levels and they overlap each other. Table 8.4.1 gives the typical values of magnetic field for selected lines of astrophysical and solar interest (Sahal-Bréchot 1981).

8.4.2 Magnetic fields in solar prominences

Clouds of material which emit visible lines (mainly Hα) above the solar surface owing to excitations by the photospheric radiation field are called prominences. According to Rayleigh scattering the direction of polarization of the lines is parallel to the limb and the degree of polarization increase with height above the limb, in zero magnetic field. The polarization of these scatterd lines are modified by magnetic fields in the prominence. The effect of the magnetic field is to rotate the angle φ (rotation of the orientation of polarization) and to decrease the polarization degree p. In fact measured polarization degree is smaller than that predicted for radiative scattering, and the polarization direction is rotated from the limb direction. The maximum polarization p_{max} is calculated as a function of the height above the limb. The depolarization and the rotation of the polarization direction by the Hanle effect depend both on the strength and direction of the field in a non-linear manner. They can be calculated by taking into account the coherence effects in radiative scattering caused by interference in the wave functions of the partially overlapping sublevles. A formalism for the quantum theory of the Hanle effect is developed by Bommier and Sahal-Bréchot (1978) and Bommier (1980). This formalism has been applied to obtain the Stokes parameters of the lines of solar quiescent prominences. The three components of the magnetic field can be determined by interpreting the Hanle effect for the spectral lines which are already linearly polarized. In Fig.8.4.1, the calculation reference frame (0XYZ) and the solar reference frame (0xyz) are shown (Bommier 1981). From the observed values p (degree

Table8.4.1.

Domain of sensitivity to the Hanle effect of selected lines of astrophysical interest. B_{typ} is the 'typical' magnetic field defined by $\omega\tau = 1$, and p_{lim} the maximum theoretical value of the polarization degree obtained for an infinite height above the solar limb.(Sahal- Bréchot 1981)

Spectrum	λ (Å)	Transition	A	B_{typ} (G)	P_{lim}
Fe XIV	5303	$3p\ ^2P_{3/2} \rightarrow 3p\ ^2P_{1/2}$		5×10^{-6}	0.43
C III	1909	$2s2p\ ^3P_1 \rightarrow 2s^2\ ^1S_0$		1.1×10^{-5}	1
He I	10 830	$2p\ ^3P_{2,1,0} \rightarrow 2s\ ^3S_1$		0.83	
He I (D_3)	5875	$3d\ ^3D_{3,2,1} \rightarrow 2p\ ^3P_{2,1,0}$		6	
He I (D_3)	major comp.	$3d\ ^3D_{3,2,1} \rightarrow 2p\ ^3P_{2,1}$		6	
He I (D_3)	minor comp.	$3d\ ^3D_1 \rightarrow 2p\ ^3P_0$		16	1
C IV	1548	$2p\ ^2P_{3/2} \rightarrow 2s\ ^2S_{1/2}$		22.5	0.43
N V	1239	$2p\ ^2P_{3/2} \rightarrow 2s\ ^2S_{1/2}$		28.7	0.43
O VI	1032	$2p\ ^2P_{3/2} \rightarrow 2s\ ^2S_{1/2}$		34.7	0.43
Si IV	1394	$3p\ ^2P_{3/2} \rightarrow 3s\ ^2S_{1/2}$		78.2	0.43
Si III	1206	$3s3p\ ^1P_1 \rightarrow 3s^2\ ^1S_0$		295.	1
Lα	1216			53.2	0.27
Lβ, Hα	1026, 6563			16	
Lγ, Hβ	992, 4861			7	

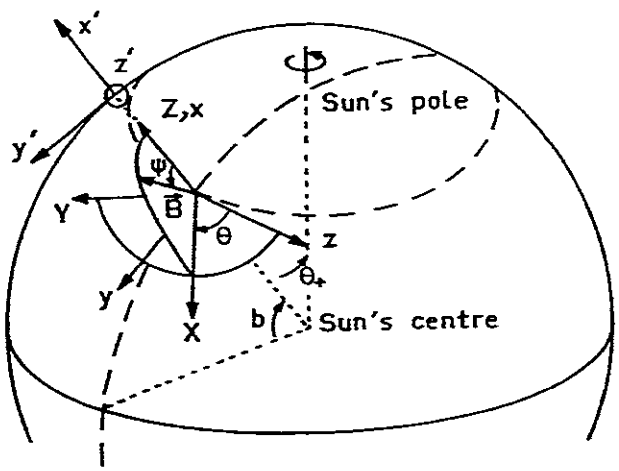

Fig.8.4.1 The calculation reference frame (0XYZ) and the solar reference frame(0xyz). The angle ψ is the angle between the magnetic field and the solar radius(0Z, 0x). θ is the angle between the line of sight(0z) and the projection of the field in the horizontal plane(0X) in the solar refernce frame.(Bommier 1981)

of polarization) and φ , the two sets of B(ψ), $\theta(\psi)$ are obtained, where θ is the angle between the projection of the magnetic field **B** on the horizontal plane (0X) and a reference direction that is usually the line of sight(0z), and ψ is the angle between the magnetic field **B** and the the solar radius. φ is the angle between the direction of linear polarization and the 0x axis.

The theory of statistical equilibrium of the density matrix in a directive incident radiation field and in a weak magnetic field has been established by Bommier (1977), Bommier and Sahal-Bréchot (1978) and Landi Degl'Innocenti (1982). The optically thin lines, the HeI D_3 and Hβ, from solar prominences have been studied (Leroy et al. 1977, Leroy et al. 1983, 1984, Querfeld et al. 1985, Athay et al. 1983). The theoretical results are generally given in diagrams in which a group of curves showing linear polarization p/p_{max} as functions of the magnetic field strength B and direction(ψ, θ). The results for the case of the D_3 line is shown in Fig.8.4.2 as an example. From the observed values p/p_{max} and φ, the magnetic field B and the angle θ can be obtained for a specified value of ψ ($\psi = 90°$ in Fig.8.4.2). The diagram has been completed for stronger fields by Bommier (1980) for HeI D_3 line, unresolved and resolved in its two main components taking into account the fine structure splitting between $^3D_3$ and $^3D_2$. In the case of one line observations, the magnetic field cannot be determined uniquely, because three coordinates of the magnetic field vector have to be determined but only the two parameters are observed for the linear polarization parameters of the line. The complete determination of the field vector requires a multi-line diagnostics. Bommier, Leroy and Sahal-Bréchot (1981) have shown that 2 lines with different sensitivity to the magnetic field strength are sufficient to determine completely the field vector. In this case, two components of HeI D_3 line, $3d\ ^3D_1 - 2p\ ^3P_0$ and $3d\ ^3D_{3,2,1} - 2p\ ^3P_{2,1}$, or the total D_3 line and the λ 10830A infrared line $2p\ ^3P_{2,1,0} - 2s\ ^3S_1$ were used. Superposition of $(B(\psi), \theta(\psi))$ interpretation curves of polarization measurements in the two components D_3 line is shown in Fig.8.4.3. Curves (1) (thick line) and (2) (thin line) show the $(B(\psi), \theta(\psi))$ solutions as a function of ψ for the minor component $3d\ ^3D_1 - 2p\ ^3P_0$ and the major component $3d\ ^3D_{3,2,1} - 2p\ ^3P_{2,1}$, respectively. The observed polarization parameters are $p = 6.2$ %, $\varphi = 11$ ° for the minor component, p = 1.7 %, φ =18 ° for the major component, for the height h=0.75 min. The result of B and θ is given from the overlapping of the two curves.

Simultaneous analysis of the longitudinal Zeeman effect and the Hanle effect in one single line can also give a complete set of parameters of the field vector although the accuracy is worse than that by the previous method. It is also possible to use only one line together with additional information; i.e., the horizontality of the field which is considered very likely for quiescent prominences or the direction of the observed matter motions which follow the line of force in the case of active objects. In all these

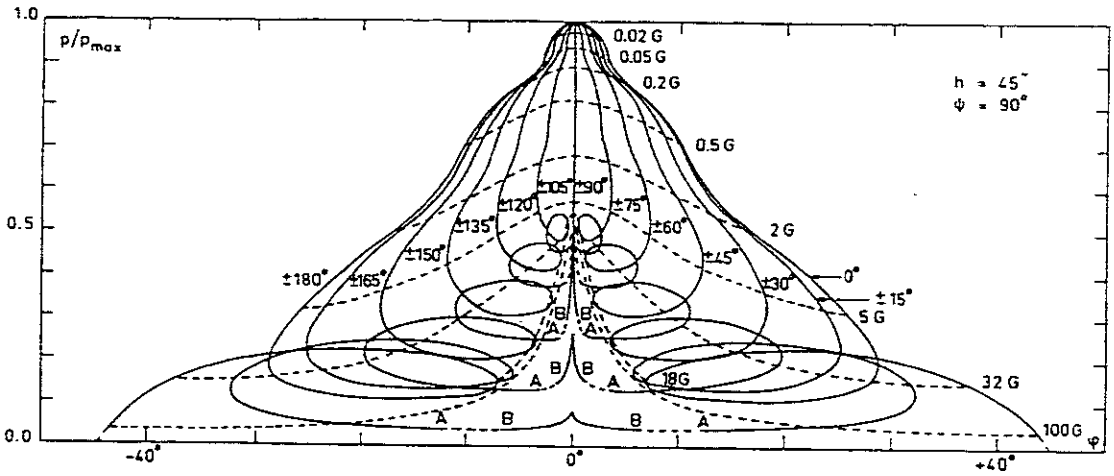

Fig.8.4.2 Hanle effect diagram. p/p_{max} as a function of φ for various values of the magnetic field B(B, θ, ψ). The height above the limb h = 45 arc min. and the magnetic field is horizontal(ψ = 90 °). The full curves correspond to constant θ values. The dashed curves correspond to constant B values. (Bommier 1980)

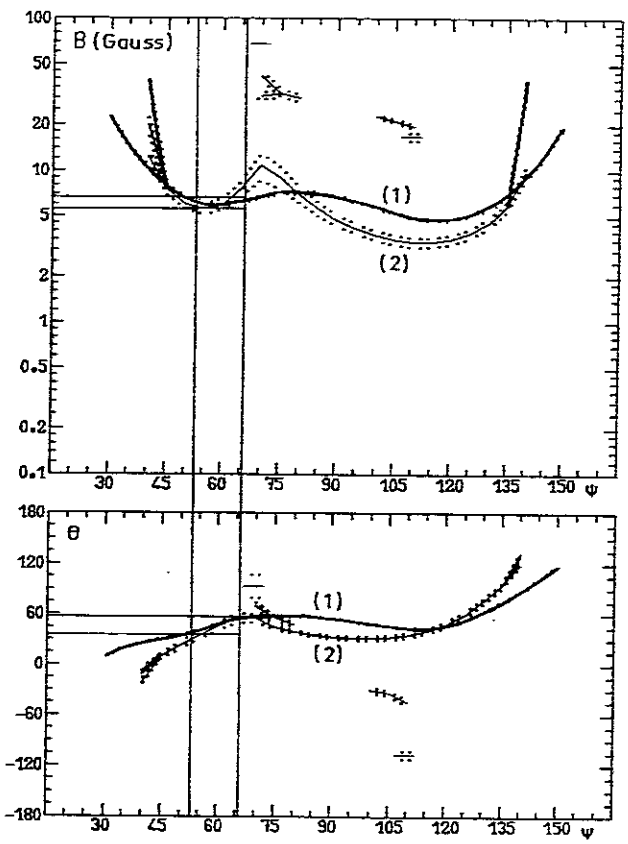

Fig.8.4.3 Two series of $(B(\psi), \theta(\psi))$ solutions which can be derived from the polarization diagrams of the two He D_3 lines. Curve (1) (thick line) is for the minor component and (2) (thin line) for the major component. The level crossings mean the multiple solutions. (Bommier et al. 1981)

cases, however, an ambiguity, called fundamental ambiguity remains; that is, the two field vectors symmetrical with respect to the line of sight can not be distinguished.

The interpretation of the data of HeI D_3 and Hβ has provided another multi-line diagnostics (Bommier et al. 1986). Hβ is depolarized by collisions with the electrons and protons of the medium. In this case in addition to the 3 coordinates of the magnetic field, another parameter, the electron density, is determined through the depolarization effect of collisions of electrons and protons with the hydrogen atoms. The depolarization and alignment transfer cross srction are very large among the close but not degenerate levels (n, ℓ, j) to $(n, \ell \pm 1, j \pm 1)$. The Hanle effect of the coronal Lα line was studied by Bommier and Sahal-Bréchot (1982) taking into account the hyperfine structure, and the results were given in analytical formulae.

The depolarization by multiple scattering in optically thick prominences was found from the simultanous polarization measurements of Hα and D_3 lines (Leroy 1981) and the calculation of the linear polarization in optically thick lines has been done for the Hα line. By using the four observed polarization parameters of D_3 and Hα, a method has been proposed of determination of the electron density together with the the magnetic field. This is a coupled problem of the polarized radiation entering the statistical equilibrium equations for the atomic densty-matrix, and the density-matrix elements entering the radiative transfer equations for polarized radiation, as described by Landi Degl'Innocenti (1983). The solution of this coupled problem can be obtained either by an iterative method (Landi Degl'Innocent et al. 1987, Bommier et al. 1989) or by a "global" method which is a kind of the integral method (Landi Degl'Innocenti et al. 1990).

8.4.3 Discussion

Compared to usual Zeeman studies with a magnetograph, the three component of the magnetic field can be completely determined by the Hanle effect. Generally speaking the Hanle studies are more useful in weak fields, whereas the Zeeman studies are better for higher fields. Since the Hanle effect affects the whole line profile in the same way, the integrated profiles can be used for faint lines, whereas in the Zeeman studies high spectral resolution is required. For the Zeeman studies, the sublevel separation should be large compared to the Doppler width. This implies that Zeeman studies of UV and X-ray lines in high temperature plasmas are very difficult.

In laboratory plasmas for fusion research such as tokamaks, the magnetic field is very strong to be the order of 10^4 Gauss. From the condition $\omega\tau \simeq 1$ for the Hanle

effect to be sensitive, τ is calculated to be the order of 10^{-11} s. This value corresponds to the soft x-ray regions, $\sim 100\mathring{A}$. The polarization measurements in short wavelength ranges might be useful for future plasma diagnostics.

References

Athay, R.G., Querfeld, C.W., Smartt, R.N., Landi Degl'Innocenti, E., Bommier, V., 1983, Solar Phys. **89**, 3

Vector magnetic fields in prominences. III. HeI D_3 Stokes profile analysis for quiescent and eruptive prominences

Bommier, V., 1977, These de 3eme cycle, Paris VII University

Bommier, V. and Sahal-Bréchot, S., 1978, Astron. Astrophy., **69**, 57

Quantum theory of the Hanle effect: calculation of the Stokes parameters of the D_3 helium line for quiescent prominences

Bommier, V and Sahal-Bréchot, S., 1982, Solar Phys., **78**, 157

The Hanle effect of the coronal Lα line of hydrogen: Theoretical investigation

Bommier, V., 1980, Astron. Astrophy., **87**, 109

Quantum theory of the Hanle effect

Bommier, V., Landi Degl'Innocenti, E. and Sahal-Bréchot, S. 1989, Astrono. Astrophy. **211** 230

Linear polarization of the hydrogen Hα line in filaments. I. Theoretical investigation

Bommier V., Leroy, J.L. and Sahal-Bréchot, S., 1986, Astron. Astrophy., **156** 79, 90

The linear polarization of hydrogen Hβ radiation and the joint diagnostics of magnetic field vector and electron density in quiescent prominences I., II.

Bommier, V., Leroy, J.L. and Sahal-Bréchot, S., 1981, Astron. Astrophy. , **100** 231

Dermination of the complete vector magnetic field in solar prominences, using the hanle effect

Hanle, W. 1924, Z. Phys., **30**, 93

Uber magnetishe Beeinflussung der Polarisation der resonanzfluoreszenz

Landi Degl'Innocenti E., 1982, Solar Phys., **79**, 291

The determination of vector magnetic fields in prominences from the observations of the Stokes profiles in the D_3 line of helium

Landi Degl'Innocenti E., 1983, Solar Phys., **85**, 33

Polarization in spectral lines. II. A classification scheme for solar observations

Landi Degl'Innocenti E., Bommier, V. and Sahal-Bréchot, S., 1987, Astron. Astrophy. **186**, 335

Linear polarization of hydrogen Balmer lines in optically thick quiescent prominences. I. Theoretical inestigation

Landi Degl'Innocenti E., Bommier, V. and Sahal-Bréchot, S., 1990, Astron. Astrophy. **235**, 459

Resonane line polarization and the Hanle effect in optically thick media, I. Formulation for the two-level atom

Leroy, J.L., 1981, Solar Phys., **71**, 285

Simultaneous measurements of the polarization in Hα and D_3 prominence emissions

Leroy, J.L. Ratier, G., Bommier, V. 1977, Astron. Astrophy., **54**, 811

The polarization of the D_3 emission line in prominences

Leroy, J.L., Bommier, V. and Sahal-Bréchot, S., 1984, Astron. Astrophy., **131**, 33

New data on the magnetic structure of quiescent prominences

Leroy, J.L., Bommier, V. and Sahal-Bréchot, S., 1983, Solar Phys., **83** 135

The magnetic field in the prominences of the polar crown

Querfeld, C.W., Smartt, R.N., Bommier, V., Landi Degl'Innocenti, E., House, L.L., 1985, Solar Phys. **96**, 277

Vector magnetic fields in prominences. II. HeI D_3 Stokes profiles analysis for two quiescent prominences

Sahal-Bréchot, S., 1981, Space Science Reviews, **29**, 391

The hanle effect applied to magnetic field diagnostics

Acknowledgement

The authors would like to thank Ms. Mari Asai for typing the manuscript.

Recent Issues of NIFS Series

NIFS-DATA-1 Y. Yamamura, T. Takiguchi and H. Tawara, *Data Compilation of Angular Distributions of Sputtered Atoms* ; Jan. 1990

NIFS-DATA-2 T. Kato, J. Lang and K. E. Berrington, *Intensity Ratios ofEmission Lines from OV Ions for Temperature and Density Diagnostics* ; Mar. 1990 [At Date and Nucl Data Tables 44(1990)133]

NIFS-DATA-3 T. Kaneko, *Partial Electronic Straggling Cross Sections of Atoms for Protons* ; Mar. 1990

NIFS-DATA-4 T. Fujimoto, K. Sawada and K. Takahata, *Cross Section for Production of Excited Hydrogen Atoms Following Dissociative Excitation of Molecular Hydrogen by Electron Impact* ; Mar. 1990

NIFS-DATA-5 H. Tawara, *Some Electron Detachment Data for H^- Ions in Collisions with Electrons, Ions, Atoms and Molecules –an Alternative Approach to High Energy Neutral Beam Production for Plasma Heating–* ; Apr. 1990

NIFS-DATA-6 H. Tawara, Y. Itikawa, H. Nishimura, H. Tanaka and Y. Nakamura, *Collision Data Involving Hydro-Carbon Molecules*; July 1990

NIFS-DATA-7 H.Tawara, *Bibliography on Electron Transfer Processes in Ion-Ion/Atom/Molecule Collisions –Updated 1990–*; Oct. 1990

NIFS-DATA-8 U.I.Safronova, T.Kato, K.Masai, L.A.Vainshtein and A.S.Shlyapzeva, *Excitation Collision Strengths, Cross Sections and Rate Coefficients for OV, SiXI, FeXXIII, MoXXXIX by Electron Impact($1s^22s^2$ -$1s^22s2p$-$1s^22p^2$ Transitions)* Dec.1990

NIFS-DATA-9 T.Kaneko, *Partial and Total Electronic Stopping Cross Sections of Atoms and Solids for Protons;* Dec. 1990

NIFS-DATA-10 K.Shima, N.Kuno, M.Yamanouchi and H.Tawara, *Equilibrium Charge Fraction of Ions of Z=4-92 (0.02-6 MeV/u) and Z=4-20 (Up to 40 MeV/u) Emerging from a Carbon Foil;* Jan.1991

NIFS-DATA-11 T. Kaneko, T. Nishihara, T. Taguchi, K. Nakagawa, M.

Murakami, M. Hosono, S. Matsushita, K. Hayase, M.Moriya, Y.Matsukuma,K.Miura and Hiro Tawara; *Partial and Total Electronic StoppingCross Sections of Atoms for a Singly Charged Helium Ion: Part I*;Mar. 1991

NIFS-DATA-12 Hiro Tawara, *Total and Partial Cross Sections of Electron Transfer Processes for Be^{q+} and B^{q+} Ions in Collisions with H, H_2 and He Gas Targets -Status in 1991-;* Jun. 1991

NIFS-DATA-13 T. Kaneko, M. Nishikori, N. Yamato, T. Fukushima, T. Fujikawa, S. Fujita, K. Miki, Y. Mitsunobu, K. Yasuhara, H. Yoshida andHiro Tawara, *Partial and Total Electronic Stopping Cross Sections of Atoms for a Singly Charged Helium Ion : Part II;* Aug. 1991

NIFS-DATA-14 T. Kato, K. Masai and M. Arnaud, *Comparison of Ionization Rate Coefficients of Ions from Hydrogen through Nickel ;* Sep. 1991

NIFS-DATA-15 T. Kato, Y. Itikawa and K. Sakimoto, *Compilation of Excitation Cross Sections for He Atomic by Electron Impact;* Mar. 1992